DYNAMIC RESPONSE OF A PARTIALLY EMBEDDED BAR
UNDER TRANSVERSE EXCITATIONS

Thesis by

Ronald Y.S. Pak

In Partial Fulfillment of the Requirements
for the Degree of
Doctor of Philosophy

California Institute of Technology
Pasadena, California

1985

(Submitted May 14, 1985)

ACKNOWLEDGMENTS

ABSTRACT

This dissertation is concerned with the dynamic response of a finite flexible bar partially embedded in a half-space, under transverse loadings. The loadings are applied at the unembedded end of the bar and may, in general, be a combination of time-harmonic shear and moment. The problem is intended to serve as a fundamental idealization for the dynamic analysis of piles or other embedded foundations whose flexibilities are not negligible.

By treating the bar as a one-dimensional structure and the half-space as a three-dimensional elastic continuum, the interaction problem is formulated as a Fredholm integral equation of the second kind. The essential tool required in the formulation is a group of Green's functions which describe the response of an elastic half-space to a finite, distributed, buried source which acts in the lateral direction. By means of a technique developed for a class of three-dimensional asymmetric wave propagation problems, the Green's functions are derived as integral representations. A numerical procedure for the computation of the semi-infinite Hankel-type integrals involved is presented which is free of the basic difficulties commonly encountered in such problems. Owing to the special nature of the kernel function, a numerical scheme which contains the essence of quadrature and collocation techniques is developed for the solution of the governing integral equation. Selected results for the interaction problem are presented to illustrate various

basic features of the solution. In addition to furnishing the compliance functions commonly used in soil-structure interaction studies, the solution should prove useful in providing a basis for the assessment and improvement of approximate and numerical models currently employed for such analyses.

TABLE OF CONTENTS

CHAPTER I

INTRODUCTION

In soil-structure interaction studies, an important phase is the analysis of the interaction between the foundation and the underlying soil. At present, there are three approaches to this class of problems. One approach attempts to solve the corresponding wave propagation problems by strictly numerical techniques, e.g., the finite element methods. As only a finite region of the soil medium can be included in a numerical model, special treatment of the boundary is usually necessary to prevent erroneous results [10]. A second line of attack can be termed as semi-analytical and a representative example is the boundary element method [48]. Although this group of techniques is still primarily numerical in nature, some analytical information, such as the singular solutions for a half-space, are usually incorporated. The third group of efforts attempts to solve the problem analytically; some common techniques are the method of integral transforms and the theory of singular and regular integral equations.

In general, numerical approaches permit easy handling of complex foundation geometries and material behaviors. However, they often suffer in their basic inability to model media of semi-infinite extent. The semi-analytical methods are attempts to remedy such a problem but other typical numerical approximations, such as continuum discretiza-tion, are still inherent in this approach. In contrast to these two groups of techniques, analytical approaches are usually feasible only

for problems with simple geometric configurations and material behaviors. The main advantage of this line of attack is, however, that it can often lead to exact or asymptotic results while furnishing more physical insight into the problem. In addition to their direct applicability to various practical situations, analytical solutions are usually considered as the fundamental check on the accuracy and reliability of approximate and numerical models. The present study belongs to this third group of efforts.

1.1 BACKGROUND

The problem under consideration is concerned with the dynamic response of a finite flexible cylindrical bar embedded in a half-space, under transverse loadings. The loadings are applied at the unembedded end of the bar and may, in general, be a combination of time-harmonic lateral shear and moment. For applications in soil-structure interaction, the problem serves well as an idealization for the dynamic analysis of piles or other embedded foundations whose flexibilities are not negligible.

Despite their theoretical and practical significance, analytical works for embedded foundations are, in comparison with those for surface foundations, rather limited [27]. Of the problems that have been considered, the geometric dimensions are usually reduced by the assumptions of (a) plane strain, e.g., Thau and Umek [45], and Dravinsky and Thau [11] or (b) anti-plane shear, e.g., Luco [24], Thau [43], Thau and Umek [44], and Wong and Trifunac [51]. Problems that are axially

symmetric have also been attempted as in Luco [26], Apsel and Luco [4], and Fowler and Sinclair [14]. With the exception of the last, all the aforementioned studies have taken the embedded structures to be rigid and thus have totally ignored the deformability of the foundation. Attempts to account for foundation deformability exist, but they are mostly approximate in nature. The best known among them are, perhaps, the works of Baranov [7], Tajimi [42] and Novak et al. [35,36,37]. In these analyses, the embedding soil medium is approximated by a stratum of independent infinitesimally thin elastic layers overlying an independent half-space. As a consequence of the approximations involved, solutions obtained in this manner do not satisfy all of the basic governing equations in elasticity, nor do they meet all of the boundary conditions such as those on the free surface. Owing to a lack of more rigorous solutions for comparison thus far, the validity and accuracy of these approximate approaches are difficult to assess.

1.2 OUTLINE OF PRESENT WORK

Following the treatment by Muki and Sternberg [33,34] of a class of static load-transfer problems for embedded rods, the embedded bar in the problem under consideration is regarded essentially as a one-dimensional structure while the embedding medium is taken to be a three-dimensional elastic half-space. A mathematical formulation of the problem is presented in Chapter II which culminates in a derivation of the governing Fredholm integral equation. An essential tool required in the development is a group of Green's functions which describe the response

of an elastic half-space to a finite, distributed, buried source which
acts in the lateral direction. The derivation and evaluation of the
solution to this three-dimensional asymmetric wave propagation problem
are described in Chapters III and IV, respectively. Chapter V is
devoted to the development of the solution scheme for the governing
integral equation. Illustrative numerical results are presented in
Chapter VI. In Chapter VII, a summary of this investigation is pro-
vided.

CHAPTER II

FORMULATION OF THE PROBLEM

In this chapter a mathematical formulation is presented for the three-dimensional interaction problem of a partially embedded bar in an elastic half-space, under transverse excitations. To this end, a rectangular Cartesian coordinate frame $\{0; x_1, x_2, x_3\}$ is used that spans the three-dimensional Euclidean space E. The position vector of points in E is denoted by $\underset{\sim}{x} = (x_1, x_2, x_3)$ and the unit base vectors in the x_1, x_2, x_3 directions are designated by $\hat{e}_1$, $\hat{e}_2$, and $\hat{e}_3$, respectively.

Formally, one considers a finite cylindrical elastic bar of length ℓ with its longitudinal centroidal axis coincident with the x_3-axis. For clarity of presentation and convenience of referencing, the open cross-sectional region of the bar and its boundary are denoted by Π and $\partial\Pi$, respectively. The open half-space is defined by

$$H = \{\underset{\sim}{x} \mid \underset{\sim}{x} \in E \ , \ x_3 > 0\} \qquad ;$$

The cylindrical subdomain of H occupied by the bar is designated by

$$D = \{\underset{\sim}{x} \mid (x_1, x_2) \in \Pi \ , \ 0 < x_3 < \ell\} \qquad ;$$

and the open cross section of $\overline{D}$ located at $x_3 = z$ is denoted by

$$\Pi_z = \{\underset{\sim}{x} \mid (x_1, x_2) \in \Pi \ , \ x_3 = z\} \qquad (0 \leq z \leq \ell) \qquad .$$

According to these definitions, the embedding medium would occupy the region $H-\bar{D}$ (see Figure 2.1). It should be noted that the interface between the bar and the embedding medium consists of the bar's circumferential and bottom surfaces only. With the notations above, it can be simply written as $\partial D - \Pi_0$ where ∂D denotes the boundary of D. Finally, it is assumed that the loading is applied at the top of the bar and that it may, in general, be a combination of time-harmonic lateral shear force and moment acting in the same plane. The present investigation is concerned with the response of the bar under the action of lateral loads on the assumption that the embedding medium can be considered as a homogeneous, isotropic, linear elastic solid and that the bar can be adequately modeled by an appropriate engineering beam theory.

2.1 MECHANICS OF INTERACTION

The present treatment of the problem aims at a bar whose diameter or lateral dimension is suitably small compared to the length of the embedded segment. As in the classical treatment by Muki and Sternberg on this class of problems [34], the embedding medium is extended throughout the half-space $\bar{H}$ and an elastic body S with the same material properties as the original material is assumed to occupy this extended region. Next, a fictitious reinforcement B_* is introduced throughout the bar region D such that the "composite solid" occupying D is "equivalent" to the actual embedded bar segment. For the problem under consideration, "equivalence" is taken to mean that the reinforced region
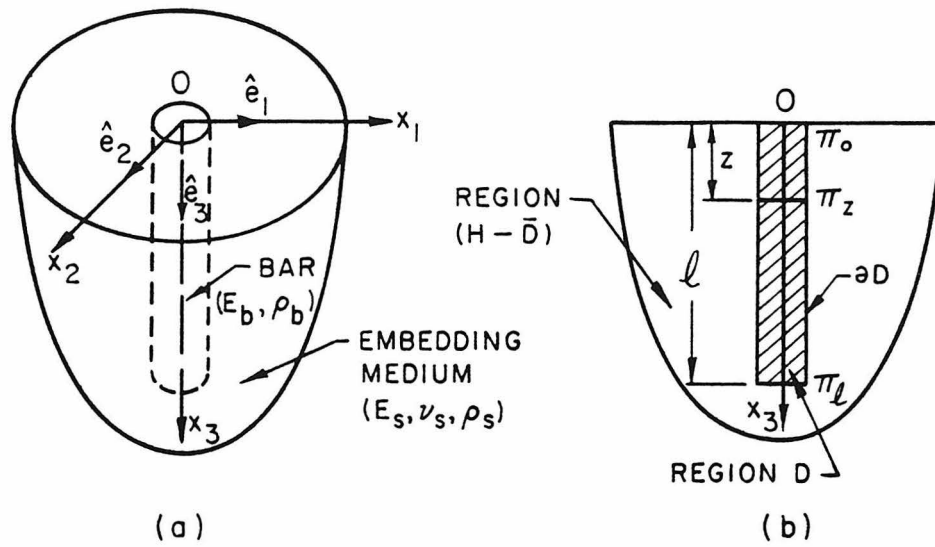
Figure 2.1   Geometry of Bar and Medium

(a) Extended Half-space S

(b) Fictitious Reinforcement B*
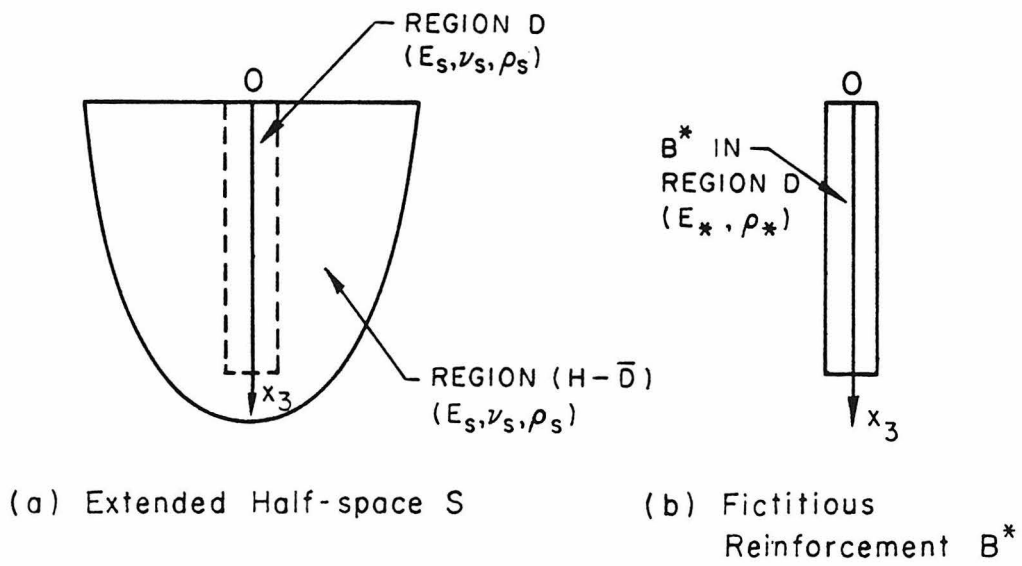
Figure 2.2   Decomposition of the Problem

will have the same inertial and flexural properties as the actual bar. Typically, for a solid bar the reinforcement B_* is assigned a Young's modulus of

$$E_* = E_b - E_s > 0 \qquad (2.1.1)$$

and a mass density of

$$\rho_* = \rho_b - \rho_s \geq 0 \qquad (2.1.2)$$

where the subscripts b and s denote the corresponding quantities of the bar and of the embedding medium, respectively (see Figure 2.2).

In what follows, the extended medium is treated as a three-dimensional continuum within the framework of classical elastodynamics. In contrast, the reinforcement B_* is regarded as a one-dimensional elastic structure. Since most engineering interests for this problem lie in the low-frequency range, it is considered adequate to adopt the Bernoulli-Euler bending beam theory for B_*. Accordingly, B_* is governed by the constitutive law

$$E_* I \frac{\partial^2 u_*}{\partial z^2} (z,t) = M_*(z,t) \qquad (2.1.3)$$

and the dynamic equilibrium conditions

$$\frac{\partial M_*}{\partial z} (z,t) = V_*(z,t) \quad , \qquad (2.1.4)$$
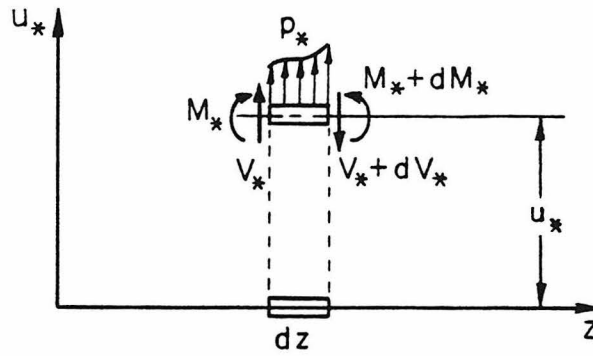
Figure 2.3   Beam Theory for B_*
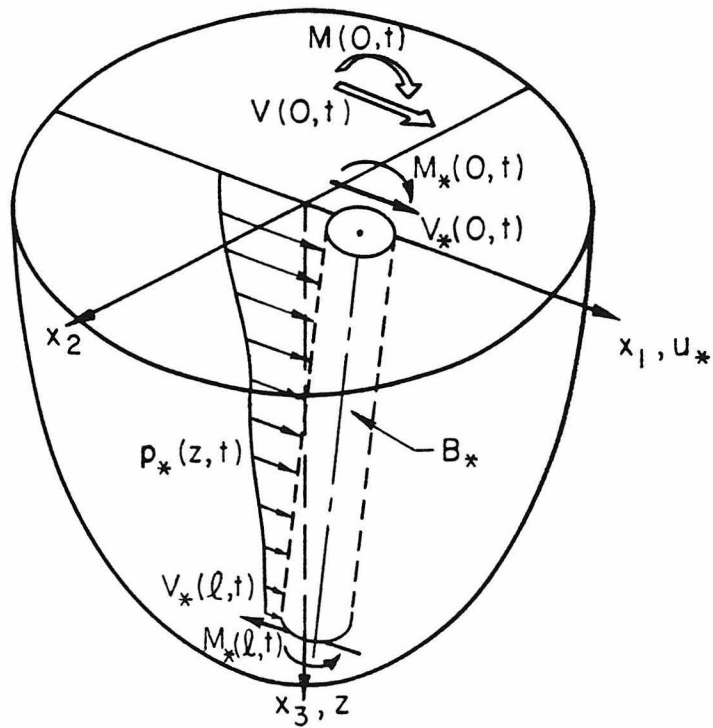
Figure 2.4   Forces acting on B_* and
their Sign Conventions

$$p_*(z,t) - \frac{\partial V_*}{\partial z}(z,t) = \rho_* A \frac{\partial^2 u_*}{\partial t^2}(z,t) \quad , \qquad (2.1.5)$$

where the notation and sign conventions are explained in Figure 2.3.

As to the interaction forces between the embedded bar and the medium, it is known that on occasion it is possible to have direct load transfers at both the top and the bottom of the bar [32]. This is mathematically and physically plausible as one might expect the stresses at the ends to exhibit some singular behavior. Allowing for this possibility and assuming without loss of generality that the lateral loads are acting in the $x_1 - x_3$ plane as shown in Figure 2.4, the external forces acting on B_* consist of

(i) $p_*(z,t)\hat{e}_1$, the distributed normal forces per unit length exerted by S on B_*;

(ii) $V_*(0^+,t)\hat{e}_1$, the resultant shear force at the top end of the bar after a possible direct load transfer;

(iii) $M_*(0^+,t)(-\hat{e}_2)$, the resultant bending moment at the top end of the bar after a possible direct moment transfer;

(iv) $V_*(\ell,t)(-\hat{e}_1)$, the end shear force at the bottom of the bar; and

(v) $M_*(\ell,t)\hat{e}_2$, the end moment at the bottom of the bar.

As for the forces acting on the half-space, they consist of

(i) $\quad -p_*(z,t)\hat{e}_1$;

(ii) $\quad [V(0,t)-V_*(0^+,t)]\hat{e}_1$, the direct shear load transfer at the top of the bar;

(iii) $\quad [M(0,t)-M_*(0^+,t)](-\hat{e}_2)$, the direct moment transfer at the top of the bar;

(iv) $\quad V_*(\ell,t)\hat{e}_1$, the end shear transfer from B_*; and

(v) $\quad M_*(\ell,t)(-\hat{e}_2)$, the end moment transfer from B_*.

It should be noted that the effects of shear stresses acting on the circumferential surface of the bar have been neglected. This is equivalent to permitting slippage along the shaft of the bar. If the additional assumption of small cross-sectional rotation of the bar is made, the analysis can be simplified further as the effects of direct moment transfers become negligible. It follows, then, that one may take as a reasonable first approximation for many applications

$$M_*(\ell,t) = 0 \qquad\qquad (2.1.6)$$

and

$$M(0,t) - M_*(0^+,t) = 0. \qquad\qquad (2.1.7)$$

2.2 STEADY-STATE CONDITION

If the applied loads are taken to be harmonic in time with frequency ω, they can be represented as

$$V(0,t) = V_0 e^{i\omega t} \quad , \tag{2.2.1}$$

$$M(0,t) = M_0 e^{i\omega t} \quad , \tag{2.2.2}$$

where V_0 and M_0 are, in general, complex constants. Under this condition, the solution is expected to be of the form

$$\underset{\sim}{u}(\underset{\sim}{x},t) = \underset{\sim}{u}(\underset{\sim}{x}) e^{i\omega t} \quad , \tag{2.2.3}$$

$$u_*(z,t) = u_*(z) e^{i\omega t} \quad ,$$

$$p_*(z,t) = p_*(z) e^{i\omega t} \quad ,$$

etc.

Omitting the time factor $e^{i\omega t}$ from here on for brevity, the constitutive law and the dynamic equilibrium conditions for B_* become

$$E_* I \frac{d^2 u_*}{dz^2}(z) = M_*(z) \quad , \tag{2.2.4}$$

$$\frac{dM_*}{dz}(z) = V_*(z) \quad , \tag{2.2.5}$$

$$p_*(z) - \frac{dV_*}{dz}(z) + \omega^2 \rho_* A u_*(z) = 0 \quad . \tag{2.2.6}$$

For the description of the response of the extended medium to the interaction forces, it is convenient to first determine an influence function (commonly called Green's function) $\overset{\wedge}{\underset{\sim}{u}}(\underset{\sim}{x},s)$ which is defined as the displacement at a point $\underset{\sim}{x}$ in S due to a harmonic body-force field

distributed across the disc Π_s, acting in the x_1-direction, with unit resultant (see Fig. 2.5). On the supposition that $\hat{\underset{\sim}{u}}(\underset{\sim}{x},s)$ can be found, the time independent part of the displacement in the half space can be written as

$$\underset{\sim}{u}(\underset{\sim}{x}) = [V_0 - V_*(0^+)]\hat{\underset{\sim}{u}}(\underset{\sim}{x},0) + V_*(l)\hat{\underset{\sim}{u}}(\underset{\sim}{x},l) - \int_0^l p_*(s)\hat{\underset{\sim}{u}}(\underset{\sim}{x},s)ds \quad ,$$

$$\underset{\sim}{x} \in S \quad . \qquad (2.2.7)$$

In particular, along the centroidal axis of the bar where $\underset{\sim}{x} = (0,0,x_3)$, the displacement in the x_1-direction can be represented as

$$u_1(x_3) = [V_0 - V_*(0^+)]\hat{u}_1(x_3,0) + V_*(l)\hat{u}_1(x_3,l) - \int_0^l p_*(s)\hat{u}_1(x_3,s)ds \quad ,$$

$$0 \leq x_3 < \infty \quad . \qquad (2.2.8)$$

To render the motion of B_* compatible with that of S, the imposition of a suitable bond condition is necessary. For this purpose, the requirement is adopted that the lateral displacement of the bar and the half-space be equal along the centroidal axis of the bar over the length of embedment; i.e.,

$$u_*(x_3) = u_1(x_3) \qquad \text{for} \quad 0 \leq x_3 \leq l \quad . \qquad (2.2.9)$$
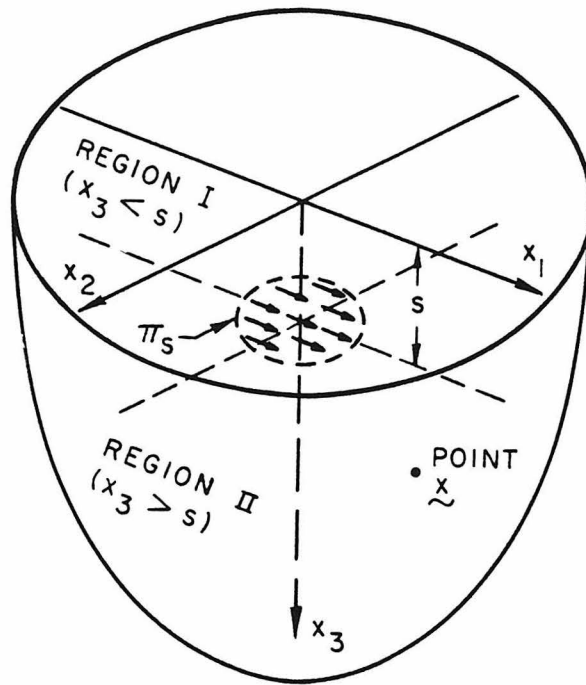
Figure 2.5   Problem Configuration for Green's Function
$\hat{\underset{\sim}{u}}(\underset{\sim}{x},s)$

There are other possible choices of bond conditions, but it is believed that the one proposed above has the most intuitive appeal. It also represents a generalization of one of the two successful schemes employed by Muki and Sternberg in their treatment of two-dimensional load transfer problems [32]. More importantly, this scheme provides a governing equation with many attractive analytical properties, which are helpful in the final solution process.

With the aid of (2.2.8), the bond condition (2.29) can be written as

$$u_*(z) = [V_0 - V_*(0^+)]\hat{u}_1(z,0) + V_*(\ell)\hat{u}_1(z,\ell) - \int_0^\ell p_*(s)\hat{u}_1(z,s)ds$$

$$\text{for } 0 \leq z \leq \ell \quad . \qquad (2.2.10)$$

Equation (2.2.10) represents the primary governing equation for the interaction problem under consideration.

2.3 REDUCTION TO A FREDHOLM INTEGRAL EQUATION

By virtue of (2.2.6), (2.2.10) can be written as

$$u_*(z) = [V_0 - V_*(0^+)]\hat{u}_1(z,0) + V_*(\ell)\hat{u}_1(z,\ell)$$

$$- \int_0^\ell \left[\frac{dV_*(s)}{ds} - \omega^2\rho_* A \, u_*(s)\right]\hat{u}_1(z,s)ds \quad . \qquad (2.2.11)$$

Integrating by parts and taking into account the possible discontinuity of the integrand, (2.2.11) becomes, upon application of (2.1.6) and (2.1.7),

$$u_*(z) = V_0 \hat{u}_1(z,0) - M_0 \frac{\partial \hat{u}_1}{\partial s}(z,0) - M_*(z) \left[\frac{\partial \hat{u}_1}{\partial s}(z,s) \right]_{z^-}^{z^+}$$

$$- \int_0^{\ell} M_*(s) \frac{\partial^2 \hat{u}_1}{\partial s^2}(z,s)ds + \omega^2 \rho_* A \int_0^{\ell} u_*(s) \hat{u}_1(z,s)ds$$

$$\text{for } 0 < z < \ell \quad . \quad (2.2.12)$$

At z=0 and ℓ, (2.2.11) can be reduced to

$$u_*(0) = V_0 \hat{u}_1(0,0) - M_0 \frac{\partial \hat{u}_1}{\partial s}(0,0) - \int_0^{\ell} M_*(s) \frac{\partial^2 \hat{u}_1}{\partial s^2}(0,s)ds$$

$$+ \omega^2 \rho_* A \int_0^{\ell} u_*(s) \hat{u}_1(0,s)ds \quad (2.2.13)$$

and

$$u_*(\ell) = V_0 \hat{u}_1(\ell,0) - M_0 \frac{\partial \hat{u}_1}{\partial \xi}(\ell,0) - \int_0^{\ell} M_*(s) \frac{\partial^2 \hat{u}_1}{\partial s^2}(\ell,s)ds$$

$$+ \omega^2 \rho_* A \int_0^{\ell} u_*(s) \hat{u}_1(\ell,s)d\xi \quad , \quad (2.2.14)$$

respectively. At a later stage when the influence function $\hat{u}_1(z,s)$ is studied more fully, one can show that (2.2.12) can actually be reduced to (2.2.13) and (2.2.14) through an analytical limiting process.

In equation (2.2.12), there are still two unknowns $u_*(z)$ and $M_*(z)$. With the constitutive law for a beam (2.2.4), M_* can be expressed in terms of u_* and vice versa. In the present study, $M_*(z)$ is chosen as the prime unknown because $u_*(z)$ can be obtained from M_* by integration which is more accurate numerically than differentiation. To this end, it can be shown that

$$u_*(z) \;=\; -\int_0^{\ell} G(z,s) M_*(s)\,ds \;+\; u_*(0)\left(1 - \frac{s}{\ell}\right) \;+\; u_*(\ell)\left(\frac{z}{\ell}\right) \qquad (2.2.15)$$

where

$$G(z,s) \;=\; \frac{1}{E_* I}\begin{cases}\left(1 - \frac{s}{\ell}\right)z & , \quad z < s \\[2ex] \left(1 - \frac{z}{\ell}\right)s & , \quad z > s \end{cases} .$$

Substitution of (2.2.15) into (2.2.12) finally reduces the interaction equation to:

$$A(z)M_*(z) \;+\; B(z)u_*(0) \;+\; C(z)u_*(\ell) \;+\; \int_0^{\ell} K(z,s)M_*(s)\,ds$$

$$= \; V_0\hat{u}_1(z,0) \;-\; M_0\frac{\partial \hat{u}_1}{\partial s}(z,0) \qquad \text{for} \quad 0 \le z \le \ell \qquad (2.2.16)$$

where

$$A(z) = \left[\frac{\partial \hat{u}_1}{\partial s}(z,s)\right]^{z^+}_{s=z^-}$$

$$B(z) = (1 - \frac{z}{\ell}) - \omega^2 \rho_* A \int_0^\ell (1 - \frac{s}{\ell})\hat{u}_1(z,s)ds$$

$$C(z) = (\frac{z}{\ell}) - \omega^2 \rho_* A \int_0^\ell (\frac{s}{\ell})\hat{u}_1(z,s)ds \qquad (2.2.17)$$

$$G(z,s) = \frac{1}{E_* I} \begin{cases} (1 - \frac{s}{\ell})z & , \quad z < s \\ (1 - \frac{z}{\ell})s & , \quad z > s \end{cases}$$

$$K(z,s) = \frac{\partial^2 \hat{u}_1}{\partial s^2}(z,s) - G(z,s) + \omega^2 \rho_* A \int_0^\ell G(\eta,s)\hat{u}_1(z,\eta)d\eta \quad .$$

Equation (2.2.16) is a Fredholm integral equation of the second kind, as it can be put into the standard form

$$a(z)y(z) - \int_a^b k(z,s)y(s)ds = g(z) \quad . \qquad (2.2.18)$$

The solution of (2.2.16) furnishes the bending moment $M_*(z)$, which in turn will render the response of the whole system fully determinate with the aid of (2.2.7). It should be noted, however, that the formulation thus far has relied on the availability of the Green's functions $\hat{u}_1(z,s)$, $\frac{\partial \hat{u}_1}{\partial s}(z,s)$ and $\frac{\partial^2 \hat{u}_1}{\partial s^2}(z,s)$. Unfortunately, these functions are

not available in the current literature and must be derived. The following chapter is devoted to this phase of the analysis.

CHAPTER III

DERIVATION OF THE GREEN'S FUNCTIONS

To solve the integral equation (2.2.16), it is first necessary to determine the Green's functions $\hat{u}_1(z,s)$, $\frac{\partial \hat{u}_1}{\partial s}(z,s)$, and $\frac{\partial^2 \hat{u}_1}{\partial s^2}(z,s)$. This is a three-dimensional asymmetric wave propagation problem concerning the dynamic response of an elastic half-space to a finite, distributed, buried source acting in the lateral direction.

The extensive literature on wave propagation in an elastic half-space dates back to the pioneering work of Lamb [21]. Many authors since then have studied elastic waves produced by point and line loads, but only a few investigations were concerned with asymmetric source problems. Among them may be mentioned the works of Pekeris and Longman [38], Chao [8], Johnson [20], and Israel and Kovach [19]. However, none of these studies have considered sources that are finite in extent. Of those that do, they are mostly concerned with surface loading only, e.g., Thiruvenkatachar [46], Arnold, Bycroft and Warburton [3], Thomson and Kobori [47], Gladwell [16], Luco and Westmann [25], Maiti and Mitra [28], and Wong and Luco [50]. The work of Fowler and Sinclair [14] represents a rare exception where a finite, buried source problem is addressed. Their method of analysis is, however, only applicable to axisymmetric situations.

In this chapter, a technique for the derivation of $\hat{u}_1(z,s)$ and its derivatives is presented. The procedure is of sufficient generality to

be useful in both axisymmetric and asymmetric wave propagation problems.

3.1 HALF-SPACE PROBLEMS IN ELASTICITY

In both static and dynamic elasticity, the method of potentials is a very powerful tool for the treatment of complicated boundary-value problems. For static half-space problems, the work of Harding and Sneddon [18], later generalized by Muki [31], is of classical importance as they have shown how the powerful technique of integral transforms can be combined with the method of potentials for the solution of this class of problems.

For dynamic half-space problems, the use of Lamé potentials together with Hankel transforms has been very successful in simplifying cases in the presence of axial symmetries. Similar attempts to date for asymmetric problems have, however, not met with equal success. One of the undesirable features of those attempts is that they do not reduce Navier's equations to a set of simple real wave equations as in the axisymmetric situations [28]. They also involve complicated transformed stress-potential and displacement-potential relations that make the imposition of boundary conditions difficult for buried-source problems. These are perhaps some of the reasons why, despite complicated manipulations, many researchers still choose to operate directly on Navier's equations in tackling asymmetric problems. In what follows, a method of potentials is developed which does not have the drawbacks mentioned above and thus furnishes an efficient means to approach asymmetric wave propagation problems in general.

3.2   A METHOD OF POTENTIALS

3.2.1   Displacement Potentials

Important to the development of the technique is a theorem due to Helmholtz on the decomposition of a vector field. In short, the theorem states that subject to some regularity conditions [29] on the vector field $\underset{\sim}{u}$, there exists a scalar field ϕ and a vector field with components ψ_i, i=1,2,3 such that

$$\underset{\sim}{u} = \nabla\phi + \nabla\times\underset{\sim}{\psi} \quad . \qquad (3.2.1)$$

Lamé has shown subsequently that such representation of a displacement vector field satisfies the displacement equations of motion in elasticity with zero body-force fields

$$(\lambda+\mu)\nabla(\nabla\cdot\underset{\sim}{u}) + \mu\nabla^2\underset{\sim}{u} = \rho\frac{\partial^2}{\partial t^2}\underset{\sim}{u} \qquad (3.2.2)$$

identically, provided that $\phi(\underset{\sim}{x},t)$ and $\underset{\sim}{\psi}(\underset{\sim}{x},t)$ are solutions of

$$\nabla^2\phi = \frac{1}{c_d^2}\frac{\partial^2\phi}{\partial t^2} \quad , \qquad (3.2.3)$$

$$\nabla^2\underset{\sim}{\psi} = \frac{1}{c_s^2}\frac{\partial^2\underset{\sim}{\psi}}{\partial t^2} \quad . \qquad (3.2.4)$$

Here, λ and μ are the Lamé constants, and C_d and C_s are the dilatational and equivoluminal wave speeds, respectively. However, it is apparent that the representation (3.2.1) contains some arbitrariness as it

relates the three components of displacement to four scalar functions: ϕ and ψ_i, i=1,2,3. To reduce the degree of arbitrariness, an extra constraint, which is commonly called the "gauge condition," is usually imposed. To this end, the requirement is adopted that

$$\left(\nabla^2 - \frac{1}{c_s^2}\frac{\partial^2}{\partial t^2}\right)(\nabla \cdot \underset{\sim}{\psi}) = 0 \qquad (3.2.5)$$

which states that either $\nabla \cdot \underset{\sim}{\psi} = 0$, which is the trivial solution, or that $\nabla \cdot \underset{\sim}{\psi}$ is a non-vanishing solution of (3.2.5).

Although the imposition of the gauge condition renders the representation determinate, it would be more convenient to have three potentials to determine at the outset instead of four. As shown in Morse and Feshbach [30], the vector wave equation (3.2.4) in $\underset{\sim}{\psi}$ is satisfied in general cylindrical coordinates by

$$\underset{\sim}{\psi} = (\chi\hat{z}) + \nabla x(\eta\hat{z}) \qquad (3.2.6)$$

where $\hat{z}$ is the unit vector along the axial cylindrical coordinate z, provided the scalar functions χ,η satisfy the wave equations

$$\nabla^2\chi = \frac{1}{c_s^2}\frac{\partial^2\chi}{\partial t^2} \quad , \qquad (3.2.7a)$$

$$\nabla^2\eta = \frac{1}{c_s^2}\frac{\partial^2\eta}{\partial t^2} \quad . \qquad (3.2.7b)$$

As can be easily shown, $\underset{\sim}{\psi}$ in (3.2.6) satisfies the gauge condition (3.2.5) identically. Thus with (3.2.1) and (3.2.6), the problem reduces

to the determination of three scalar functions ϕ, χ, and η which are governed by the wave equations (3.2.3), (3.2.7a) and (3.2.7b), respectively. In circular cylindrical coordinates (r,θ,z), this representation leads to the displacement-potential relations:

$$
u_r = \frac{\partial \phi}{\partial r} + \frac{1}{r}\frac{\partial \chi}{\partial \theta} + \frac{\partial^2 \eta}{\partial z \partial r} \quad ,
$$

$$
u_\theta = \frac{1}{r}\frac{\partial \phi}{\partial \theta} - \frac{\partial \chi}{\partial r} + \frac{1}{r}\frac{\partial^2 \eta}{\partial z \partial \theta} \quad , \qquad (3.2.8)
$$

$$
u_z = \frac{\partial \phi}{\partial z} - \frac{1}{r}\frac{\partial}{\partial r}\left(r\frac{\partial \eta}{\partial r}\right) - \frac{1}{r^2}\frac{\partial^2 \eta}{\partial \theta^2} \quad ,
$$

where u_r, u_θ and u_z are the displacements in the r, θ, and z directions, respectively. The strain-displacement relations are given as

$$
\varepsilon_{rr} = \frac{\partial u_r}{\partial r} \quad , \qquad \varepsilon_{\theta\theta} = \frac{1}{r}\left(\frac{\partial u_\theta}{\partial \theta} + u_r\right) \quad , \qquad \varepsilon_{zz} = \frac{\partial u_z}{\partial z} \quad ,
$$

$$
\varepsilon_{r\theta} = \frac{1}{r}\frac{\partial u_r}{\partial \theta} + r\frac{\partial}{\partial r}\left(\frac{u_\theta}{r}\right) \quad , \qquad \varepsilon_{z\theta} = \frac{1}{r}\frac{\partial u_z}{\partial \theta} + \frac{\partial u_\theta}{\partial z} \quad , \qquad (3.2.9)
$$

$$
\varepsilon_{rz} = \frac{\partial u_r}{\partial z} + \frac{\partial u_z}{\partial r} \quad .
$$

The stress-strain laws for a linearly elastic medium are used in the

form

$$\tau_{rr} = \lambda\Delta + 2\mu\varepsilon_{rr} \quad , \quad \tau_{\theta\theta} = \lambda\Delta + 2\mu\varepsilon_{\theta\theta} \quad ,$$

$$\tau_{zz} = \lambda\Delta + 2\mu\varepsilon_{zz} \quad , \qquad\qquad (3.2.10)$$

$$\tau_{r\theta} = \mu\varepsilon_{r\theta} \quad , \quad \tau_{z\theta} = \mu\varepsilon_{z\theta} \quad , \quad \tau_{rz} = \mu\varepsilon_{rz} \quad ,$$

where $\Delta = \nabla^2\phi$. The strain-potential relations can be obtained by substituting (3.2.8) into (3.2.9). Substitution of the strain-potential relations into (3.2.10) gives the stress-potential relations.

To complete the formulation of the boundary-value problem, it remains to specify the boundary conditions. Although body-force fields have been ruled out in the analysis, the effects of a distributed body-force field oriented in an arbitrary direction over the disc Π_s can be simulated by artificially viewing the half-space as composed of an upper and a lower region (region I and II in Fig. 2.5) divided by the plane z=s, and inserting a discontinuity in stresses over Π_s across that plane, e.g.,

$$\tau_{zr}(r,\theta,s^-,t) - \tau_{zr}(r,\theta,s^+,t) = \begin{cases} P(r,\theta,t) & , (r,\theta)\in\Pi \\ 0 & , (r,\theta)\notin\Pi \end{cases} ,$$

$$\tau_{z\theta}(r,\theta,s^-,t) - \tau_{z\theta}(r,\theta,s^+,t) = \begin{cases} Q(r,\theta,t) & , (r,\theta)\in\Pi \\ 0 & , (r,\theta)\notin\Pi \end{cases} , \quad (3.2.11)$$

$$\tau_{zz}(r,\theta,s^-,t) - \tau_{zz}(r,\theta,s^+,t) = \begin{cases} R(r,\theta,t) & , (r,\theta) \in \Pi \\ 0 & , (r,\theta) \notin \Pi \end{cases} ,$$

where $P(r,\theta,t)$, $Q(r,\theta,t)$ and $R(r,\theta,t)$ are specified body-force distributions. On requiring all displacements to be continuous across the plane z=s and the stresses to vanish on the free surface,

$$\tau_{zz}(r,\theta,0,t) = \tau_{zr}(r,\theta,0,t) = \tau_{z\theta}(r,\theta,0,t) = 0 , \quad (3.2.12)$$

it remains only to specify the condition at infinity, commonly called the "radiation condition." A consideration of the characteristics of a half-space suggests that the solution in region II be required to contain only outgoing waves and to be bounded as z approaches infinity. These conditions also ensure that the problem is mathematically well-posed.

3.2.2 Steady-State Solution

With the assumption of steady-state motion, one may express the potentials and other quantities of interest in the form

$$\phi(r,\theta,z,t) = \phi(r,\theta,z)e^{i\omega t} ,$$

$$\chi(r,\theta,z,t) = \chi(r,\theta,z)e^{i\omega t} , \quad (3.2.13)$$

$$\eta(r,\theta,z,t) = \eta(r,\theta,z)e^{i\omega t} , \text{ etc.}$$

With the time factor $e^{i\omega t}$ suppressed henceforth, Equations (3.2.3), (3.2.7a) and (3.2.7b) become

$$(\nabla^2 + k_d^2)\phi(r,\theta,z) = 0 \quad ,$$

$$(\nabla^2 + k_s^2)\chi(r,\theta,z) = 0 \quad , \qquad (3.2.14)$$

$$(\nabla^2 + k_s^2)\eta(r,\theta,z) = 0 \quad ,$$

where $k_d = \omega/C_d$, $k_s = \omega/C_s$, and $\nabla^2 = \dfrac{\partial^2}{\partial r^2} + \dfrac{1}{r}\dfrac{\partial}{\partial r} + \dfrac{1}{r^2}\dfrac{\partial^2}{\partial\theta^2} + \dfrac{\partial^2}{\partial z^2}$. In view of the completeness of the set of angular eigenfunctions $\{e^{im\theta}\}_{m=-\infty}^{+\infty}$, one may write

$$\phi(r,\theta,z) = \sum_{m=-\infty}^{\infty} \phi_m(r,z)e^{im\theta} \quad ,$$

$$\chi(r,\theta,z) = \sum_{m=-\infty}^{\infty} \chi_m(r,z)e^{im\theta} \quad , \qquad (3.2.15)$$

$$\eta(r,\theta,z) = \sum_{m=-\infty}^{\infty} \eta_m(r,z)e^{im\theta} \quad ,$$

and

$$u_r(r,\theta,z) = \sum_{m=-\infty}^{\infty} u_{r_m}(r,z)e^{im\theta} \quad ,$$

$$u_\theta(r,\theta,z) = \sum_{m=-\infty}^{\infty} u_{\theta_m}(r,z)e^{im\theta} \quad , \qquad (3.2.16)$$

$$u_z(r,\theta,z) = \sum_{m=-\infty}^{\infty} u_{z_m}(r,z)e^{im\theta} \quad .$$

Likewise, one may write (3.2.11) as

$$
\tau_{zr}(r,\theta,s^-) - \tau_{zr}(r,\theta,s^+) = \begin{cases} \displaystyle\sum_{m=-\infty}^{\infty} P_m(r)e^{im\theta} & , (r,\theta) \in \Pi \\ \\ 0 & , (r,\theta) \notin \Pi \end{cases}
$$

$$
\tau_{z\theta}(r,\theta,s^-) - \tau_{z\theta}(r,\theta,s^+) = \begin{cases} \displaystyle\sum_{m=-\infty}^{\infty} Q_m(r)e^{im\theta} & , (r,\theta) \in \Pi \\ \\ 0 & , (r,\theta) \notin \Pi \end{cases} \qquad (3.2.17)
$$

$$
\tau_{zz}(r,\theta,s^-) - \tau_{zz}(r,\theta,s^+) = \begin{cases} \displaystyle\sum_{m=-\infty}^{\infty} R_m(r)e^{im\theta} & , (r,\theta) \in \Pi \\ \\ 0 & , (r,\theta) \notin \Pi \end{cases} .
$$

Substituting (3.2.15) into (3.2.14) and invoking the orthogonality condition of the eigenfunctions $\{e^{im\theta}\}$, one is led to the conclusion that

$$
\frac{\partial^2 \phi_m}{\partial r^2} + \frac{1}{r}\frac{\partial \phi_m}{\partial r} + \left(k_d^2 - \frac{m^2}{r^2}\right)\phi_m + \frac{\partial^2}{\partial z^2}\phi_m = 0 \quad ,
$$

$$
\frac{\partial^2 \chi_m}{\partial r^2} + \frac{1}{r}\frac{\partial \chi_m}{\partial r} + \left(k_s^2 - \frac{m^2}{r^2}\right)\chi_m + \frac{\partial^2}{\partial z^2}\chi_m = 0 \quad , \qquad (3.2.18)
$$

$$
\frac{\partial^2 \eta_m}{\partial r^2} + \frac{1}{r}\frac{\partial \eta_m}{\partial r} + \left(k_s^2 - \frac{m^2}{r^2}\right)\eta_m + \frac{\partial^2}{\partial z^2}\eta_m = 0 \quad ,
$$

for m=0,±1,±2,...

In view of the geometry and the boundary conditions of the problem, it is natural to introduce the mth order Hankel transform

$$\tilde{f}^{m}(\xi,z) = \int_{0}^{\infty} f(r,z)\, r\, J_{m}(\xi r)dr \quad , \qquad (3.2.19)$$

with the inversion formula

$$f(r,z) = \int_{0}^{\infty} \tilde{f}^{m}(\xi,z)\, \xi\, J_{m}(\xi r)d\xi \quad , \qquad (3.2.20)$$

where J_{m} is the Bessel function of the first kind of order m. Application of (3.2.19) to Equations (3.2.18) reduces them to a set of ordinary differential equations in z:

$$\frac{d^{2}\tilde{\phi}_{m}^{m}}{dz^{2}}(\xi,z) + (k_{d}^{2} - \xi^{2})\, \tilde{\phi}_{m}^{m}(\xi,z) = 0 \quad ,$$

$$\frac{d^{2}\tilde{\chi}_{m}^{m}}{dz^{2}}(\xi,z) + (k_{s}^{2} - \xi^{2})\, \tilde{\chi}_{m}^{m}(\xi,z) = 0 \quad , \qquad (3.2.21)$$

$$\frac{d^{2}\tilde{\eta}_{m}^{m}}{dz^{2}}(\xi,z) + (k_{s}^{2} - \xi^{2})\, \tilde{\eta}_{m}^{m}(\xi,z) = 0 \quad ,$$

for m=0,±1,±2,... ,

where ξ is the transform parameter. The solutions of (3.2.21) are

easily found to be

$$\overset{m}{\tilde{\phi}}_{Im}(\xi,z) \;=\; A_m^I(\xi)e^{\alpha z} \;+\; B_m^I(\xi)e^{-\alpha z} \quad,$$

$$\overset{m}{\tilde{\chi}}_{Im}(\xi,z) \;=\; C_m^I(\xi)e^{\beta z} \;+\; D_m^I(\xi)e^{-\beta z} \quad, \tag{3.2.22}$$

$$\overset{m}{\tilde{\eta}}_{Im}(\xi,z) \;=\; E_m^I(\xi)e^{\beta z} \;+\; F_m^I(\xi)e^{-\beta z} \qquad \text{in region I} \ ,$$

and

$$\overset{m}{\tilde{\phi}}_{IIm}(\xi,z) \;=\; B_m^{II}(\xi)e^{-\alpha z} \quad,$$

$$\overset{m}{\tilde{\chi}}_{IIm}(\xi,z) \;=\; D_m^{II}(\xi)e^{-\beta z} \quad, \tag{3.2.23}$$

$$\overset{m}{\tilde{\eta}}_{IIm}(\xi,z) \;=\; F_m^{II}(\xi)e^{-\beta z} \qquad \text{in region II} \ ,$$

where $\alpha = (\xi^2 - k_d^2)^{1/2}$; $\beta = (\xi^2 - k_s^2)^{1/2}$; and $A_m^I, \ldots, F_m^I, B_m^{II}, \ldots, F_m^{II}$ are constants of integration to be determined from the boundary conditions. The radicals α and β are made single-valued by specifying the branch cuts emanating from the branch points $\xi = \pm k_d$ and $\xi = \pm k_s$, respectively. The branches are chosen such that the real parts of α and β are always nonnegative (see Fig. 3.1). This can be confirmed to be the physically correct choice if a small amount of material damping is introduced at the outset of the formulation. Under this choice of the branches, the $e^{\alpha z}$ and $e^{\beta z}$ terms in region II become inadmissible due to the radiation condition and are thus omitted in (3.2.23).
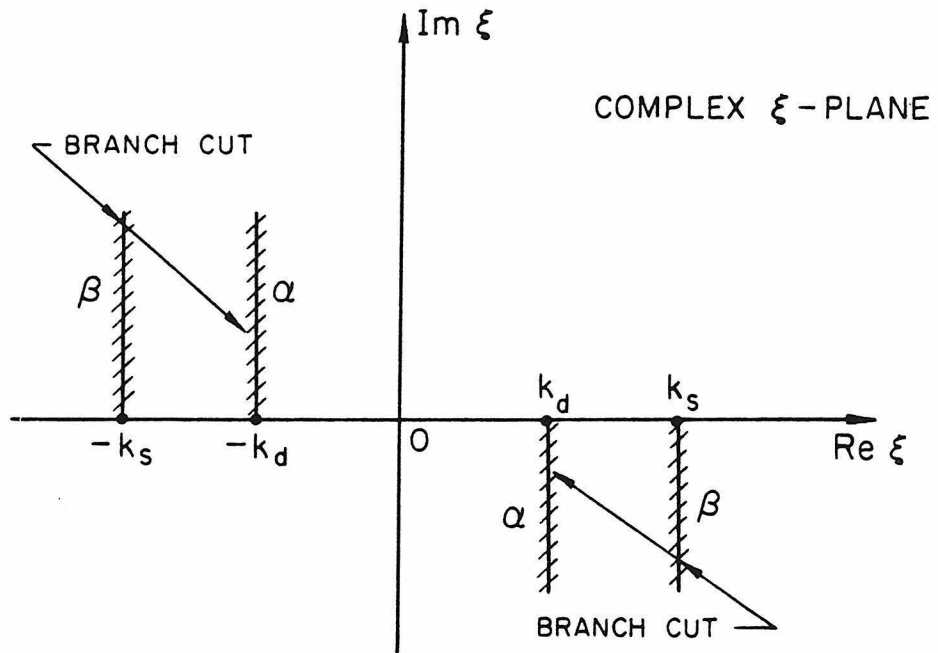
Figure 3.1   Branch Cuts for α and β

Despite the complicated expressions for the stress-potential and displacement-potential relations in (3.2.10) and (3.2.8), the transformed relations, in proper combinations, are relatively simple. It can be shown that the transformed displacement-potential relations are:

$$\tilde{u}_{z_m}^m = \frac{d}{dz}\tilde{\phi}_m^m + \xi^2\tilde{\eta}_m^m \quad,$$

$$\tilde{u}_{r_m}^{m-1} - i\tilde{u}_{\theta_m}^{m-1} = \xi\left[\tilde{\phi}_m^m + \frac{d}{dz}\tilde{\eta}_m^m + i\tilde{\chi}_m^m\right] \quad, \qquad (3.2.24)$$

$$\tilde{u}_{r_m}^{m+1} + i\tilde{u}_{\theta_m}^{m+1} = -\xi\left[\tilde{\phi}_m^m + \frac{d}{dz}\tilde{\eta}_m^m - i\tilde{\chi}_m^m\right] \quad.$$

The transformed stress-potential relations required for the analysis take the form

$$\tilde{\tau}_{zz_m}^m = -\lambda\xi^2\tilde{\phi}_m^m + (\lambda+2\mu)\frac{d^2}{dz^2}\tilde{\phi}_m^m + 2\mu\xi^2\frac{d}{dz}\tilde{\eta}_m^m \quad,$$

$$\tilde{\tau}_{zr_m}^{m-1} - i\tilde{\tau}_{z\theta_m}^{m-1} = \mu\xi\left[2\frac{d}{dz}\tilde{\phi}_m^m + \frac{d^2}{dz^2}\tilde{\eta}_m^m + \xi^2\tilde{\eta}_m^m + i\frac{d}{dz}\tilde{\chi}_m^m\right] \quad,(3.2.25)$$

$$\tilde{\tau}_{zr_m}^{m+1} + i\tilde{\tau}_{z\theta_m}^{m+1} = -\mu\xi\left[2\frac{d}{dz}\tilde{\phi}_m^m + \frac{d^2}{dz^2}\tilde{\eta}_m^m + \xi^2\tilde{\eta}_m^m - i\frac{d}{dz}\tilde{\chi}_m^m\right] \quad.$$

By the above relations, the imposition of (3.2.11), (3.2.12) and the displacement continuity condition at the plane z=s is greatly

facilitated; it provides the nine equations required for the solution of the nine unknowns $A_m^I \ldots F_m^{II}$. This set of equations can be solved explicitly in terms of the Fourier coefficients P_m, Q_m and R_m of the body-force field distributions. Substitution of them into (3.2.24) will give the transformed Fourier components of the displacements. For the special case where the distributed body-force field has no x_3-components, the transformed components of lateral displacements take the form:

$$
\tilde{u}_{r_m}^{m-1} - i\tilde{u}_{\theta_m}^{m-1} =
\begin{bmatrix}
\dfrac{\xi^2}{\alpha k_s^2} e^{-\alpha|z-s|} - \dfrac{\beta}{k_s^2} e^{-\beta|z-s|} \\[2ex]
-\dfrac{\xi^2}{\alpha k_s^2} \dfrac{R^+(\xi)}{R^-(\xi)} e^{-\alpha(z+s)} - \dfrac{\beta}{k_s^2} \dfrac{R^+(\xi)}{R^-(\xi)} e^{-\beta(z+s)} \\[2ex]
+\dfrac{4\xi^2 \alpha\beta (2\xi^2 - k_s^2)}{\alpha k_s^2 R^-(\xi)} e^{-(\beta s + \alpha z)} \\[2ex]
\dfrac{4\xi^2 \alpha\beta (2\xi^2 - k_s^2)}{\alpha k_s^2 R^-(\xi)} e^{-(\alpha s + \beta z)}
\end{bmatrix}
\begin{bmatrix}
\dfrac{X_m - Y_m}{4\mu}
\end{bmatrix}
$$

$$
+ \frac{1}{\beta} \left[e^{-\beta(z+s)} + e^{-\beta|z-s|} \right] \begin{bmatrix} \dfrac{X_m + Y_m}{4\mu} \end{bmatrix} , \qquad (3.2.26)
$$

$$
\tilde{u}_{r_m}^{m+1} - i\tilde{u}_{\theta_m}^{m+1} =
\begin{bmatrix}
\dfrac{\xi^2}{\alpha k_s^2}\, e^{-\alpha|z-s|} - \dfrac{\beta}{k_s^2}\, e^{-\beta|z-s|} \\[2em]
-\dfrac{\xi^2}{\alpha k_s^2}\, \dfrac{R^+(\xi)}{R^-(\xi)}\, e^{-\alpha(z+s)} - \dfrac{\beta}{k_s^2}\, \dfrac{R^+(\xi)}{R^-(\xi)}\, e^{-\beta(z+s)} \\[2em]
+\dfrac{4\xi^2\alpha\beta(2\xi^2-k_s^2)}{\alpha k_s^2 R^-(\xi)}\, e^{-(\beta s+\alpha z)} \\[2em]
+\dfrac{4\xi^2\alpha\beta(2\xi^2-k_s^2)}{\alpha k_s^2 R^-(\xi)}\, e^{-(\alpha s+\beta z)}
\end{bmatrix}
\begin{bmatrix}\dfrac{X_m-Y_m}{4\mu}\end{bmatrix}
$$

$$
-\frac{1}{\beta}\left[\, e^{-\beta(z+s)} + e^{-\beta|z-s|}\,\right]\begin{bmatrix}\dfrac{X_m+Y_m}{4\mu}\end{bmatrix}\,, \qquad (3.2.27)
$$

where

$$
X_m = \tilde{P}_m^{\,m-1}(\xi) - i\tilde{Q}_m^{\,m-1}(\xi)\,,
$$
$$
\hspace{8em}(3.2.28)
$$
$$
Y_m = \tilde{P}_m^{\,m+1}(\xi) + i\tilde{Q}_m^{\,m+1}(\xi)\,,
$$

$$
R^\pm(\xi) = (2\xi^2-k_s^2)^2 \pm 4\xi^2\alpha\beta\,. \qquad (3.2.29)
$$

Application of the appropriate Hankel Inversion formulas to (3.2.26) and (3.2.27) will give an integral representation of the Fourier components of the desired Green's function $\hat{u}_1(z,s)$. The Green's functions $\dfrac{\partial\hat{u}_1}{\partial s}(z,s)$ and $\dfrac{\partial^2\hat{u}_1}{\partial s^2}(z,s)$ can be obtained by permissible differentiations of $\hat{u}_1(z,s)$ under the integral sign.

3.3 INTEGRAL REPRESENTATIONS

Up to this point, the cross section of the bar has been left arbitrary. In what follows, attention will be confined to the case of most interest, a bar of circular cross section. Henceforth, the open cross-sectional region Π is taken to be

$$\Pi = \{(x_1,x_2) \mid x_1^2 + x_2^2 < a^2\} \ , \tag{3.3.1}$$

where "a" is the radius of the circular cross section. For a uniformly distributed shear force over Π_s with unit resultant acting in the x_1-direction,

$$\tau_{zr}(r,s^-) - \tau_{zr}(r,s^+) = \frac{1}{\pi a^2} \cos\theta \ , \quad r \leq a \ ,$$

$$\tau_{z\theta}(r,s^-) - \tau_{z\theta}(r,s^+) = -\frac{1}{\pi a^2} \sin\theta \ , \quad r \leq a \ . \tag{3.3.2}$$

From (3.3.2), it follows that

$$P_1(r) = P_{-1}(r) = \begin{cases} \dfrac{1}{2\pi a^2} & , \quad r \leq a \\[2em] 0 & , \quad r > a \end{cases}$$

$$P_m(r) = 0 \quad \text{for all } m \neq \pm 1 \ ,$$

and $\hspace{6cm}$ (3.3.3)

$$Q_1(r) = -Q_{-1}(r) = \begin{cases} i\,\dfrac{1}{2\pi a^2} & , \quad r \leq a \\[2em] 0 & , \quad r > a \end{cases}$$

$$Q_m(r) = 0 \quad \text{for all } m \neq \pm 1 \ .$$

Combining (3.3.3), (3.2.26), (3.2.27) and (3.2.28), and performing the

inverse transforms, one finds

$$u_{r_1}(r,z;s) = u_{r_{-1}}(r,z;s)$$

$$= \frac{1}{4\pi\mu a} \left[\begin{array}{c} \int_0^\infty \gamma_1(z,s,\xi) J_1(\xi a)[J_0(\xi r)-J_2(\xi r)]d\xi \\ \\ + \int_0^\infty \gamma_2(z,s,\xi) J_1(\xi a)[J_0(\xi r)+J_2(\xi r)]d\xi \end{array} \right] , (3.3.4)$$

$$u_{r_m}(r,z;s) = 0 \qquad \text{for all } m \neq \pm 1$$

where

$$\gamma_1(z,s,\xi) = \frac{\xi^2}{\alpha k_s^2} e^{-\alpha|z-s|} - \frac{\beta}{k_s^2} e^{-\beta|z-s|}$$

$$- \frac{\xi^2}{\alpha k_s^2} \frac{R^+(\xi)}{R^-(\xi)} e^{-\alpha(z+s)} - \frac{\beta}{k_s^2} \frac{R^+(\xi)}{R^-(\xi)} e^{-\beta(z+s)}$$

$$+ \frac{4\xi^2\beta}{k_s^2} \frac{(2\xi^2-k_s^2)}{R^-(\xi)} \left[e^{-(\beta s+\alpha z)} + e^{-(\beta z+\alpha s)} \right] , \qquad (3.3.5)$$

$$\gamma_2(z,s,\xi) = \frac{1}{\beta} e^{-\beta|z-s|} + \frac{1}{\beta} e^{-\beta(z+s)} . \qquad (3.3.6)$$

The desired Green's function $\hat{u}_1$ can finally be obtained by substituting (3.3.4) into (3.2.16) and specializing it to r=0. In terms of dimensionless variables $\bar{\omega} = \frac{\omega a}{C_s}$, $\bar{z} = \frac{z}{a}$, $\bar{s} = \frac{s}{a}$ and $k = \frac{k_d}{k_s}$, it can be written as

$$\hat{u}_1(\bar{z},\bar{s}) = \frac{1}{4\pi\mu a} [I_1 - I_2 + I_3 + I_4 - I_5 - I_6 + I_7 + I_8] \quad , \qquad (3.3.7)$$

where

$$I_1(\bar{\omega},\bar{z},\bar{s}) = \int_0^\infty \frac{\tau^2}{(\tau^2-k^2)^{1/2}} \, e^{-\bar{\omega}(\tau^2-k^2)^{1/2}|\bar{z}-\bar{s}|} \, J_1(\bar{\omega}\tau)\,d\tau$$

$$I_2(\bar{\omega},\bar{z},\bar{s}) = \int_0^\infty (\tau^2-1)^{1/2} \, e^{-\bar{\omega}(\tau^2-1)^{1/2}|\bar{z}-\bar{s}|} \, J_1(\bar{\omega}\tau)\,d\tau$$

$$I_3(\bar{\omega},\bar{z},\bar{s}) = \int_0^\infty \frac{1}{(\tau^2-1)^{1/2}} \, e^{-\bar{\omega}(\tau^2-1)^{1/2}|\bar{z}-\bar{s}|} \, J_1(\bar{\omega}\tau)\,d\tau$$

$$I_4(\bar{\omega},\bar{z},\bar{s}) = \int_0^\infty \frac{1}{(\tau^2-1)^{1/2}} \, e^{-\bar{\omega}(\tau^2-1)^{1/2}(\bar{z}+\bar{s})} \, J_1(\bar{\omega}\tau)\,d\tau$$

$$I_5(\bar{\omega},\bar{z},\bar{s}) = \int_0^\infty \frac{\tau^2}{(\tau^2-k^2)^{1/2}} \frac{R^+(\tau)}{R^-(\tau)} \, e^{-\bar{\omega}(\tau^2-k^2)^{1/2}(\bar{z}+\bar{s})} \, J_1(\bar{\omega}\tau)\,d\tau \qquad (3.3.8)$$

$$I_6(\bar{\omega},\bar{z},\bar{s}) = \int_0^\infty \frac{(\tau^2-1)^{1/2}R^+(\tau)}{R^-(\tau)} \, e^{-\bar{\omega}(\tau^2-1)^{1/2}(\bar{z}+\bar{s})} \, J_1(\bar{\omega}\tau)\,d\tau$$

$$I_7(\bar{\omega},\bar{z},\bar{s}) = \int_0^\infty \frac{4\tau^2(\tau^2-1)^{1/2}(2\tau^2-1)}{R^-(\tau)} \, e^{-\bar{\omega}[(\tau^2-1)^{1/2}\bar{s}+(\tau^2-k^2)^{1/2}\bar{z}]} \, J_1(\bar{\omega}\tau)\,d\tau$$

$$I_8(\bar{\omega},\bar{z},\bar{s}) = \int_0^\infty \frac{4\tau^2(\tau^2-1)^{1/2}(2\tau^2-1)}{R^-(\tau)} \, e^{-\bar{\omega}[(\tau^2-1)^{1/2}\bar{z}+(\tau^2-k^2)^{1/2}\bar{s}]} \, J_1(\bar{\omega}\tau)\,d\tau \qquad .$$

Here,

$$R^\pm(\tau) \;=\; (2\tau^2-1)^{\frac{1}{2}} \pm 4\tau^2(\tau^2-1)^{\frac{1}{2}}(\tau^2-k^2)^{\frac{1}{2}} \quad .$$

With the aid of (3.3.7), the Green's function $\dfrac{\partial \hat{u}_1}{\partial \bar{s}}(\bar{z},\bar{s})$ can be derived as

$$\frac{\partial \hat{u}_1}{\partial \bar{s}}(\bar{z},\bar{s}) \;=\; \frac{\bar{\omega}}{4\pi\mu a}\,[(I_1'-I_2'+I_3')\;\mathrm{sgn}\,(\bar{z}-\bar{s}) - I_4'+I_5'+I_6'-I_7'-I_8'] \quad , \qquad (3.3.9)$$

where

$$I_1'(\bar{\omega},\bar{z},\bar{s}) \;=\; \int_0^\infty \tau^2\; e^{-\bar{\omega}(\tau^2-k^2)^{\frac{1}{2}}|\bar{z}-\bar{s}|}\, J_1(\bar{\omega}\tau)\,d\tau$$

$$I_2'(\bar{\omega},\bar{z},\bar{s}) \;=\; \int_0^\infty (\tau^2-1)e^{-\bar{\omega}(\tau^2-1)^{\frac{1}{2}}|\bar{z}-\bar{s}|}\, J_1(\bar{\omega}\tau)\,d\tau$$

$$I_3'(\bar{\omega},\bar{z},\bar{s}) \;=\; \int_0^\infty e^{-\bar{\omega}(\tau^2-1)^{\frac{1}{2}}|\bar{z}-\bar{s}|}\, J_1(\bar{\omega}\tau)\,d\tau$$

$$I_4'(\bar{\omega},\bar{z},\bar{s}) \;=\; \int_0^\infty e^{-\bar{\omega}(\tau^2-1)^{\frac{1}{2}}(\bar{z}+\bar{s})}\, J_1(\bar{\omega}\tau)\,d\tau$$

$$I_5'(\bar{\omega},\bar{z},\bar{s}) \;=\; \int_0^\infty \tau^2\,\frac{R^+(\tau)}{R^-(\tau)}\, e^{-\bar{\omega}(\tau^2-k^2)^{\frac{1}{2}}(\bar{z}+\bar{s})}\, J_1(\bar{\omega}\tau)\,d\tau \qquad (3.3.10)$$

$$I_6'(\bar{\omega},\bar{z},\bar{s}) \;=\; \int_0^\infty (\tau^2-1)\,\frac{R^+(\tau)}{R^-(\tau)}\, e^{-\bar{\omega}(\tau^2-1)^{\frac{1}{2}}(\bar{z}+\bar{s})}\, J_1(\bar{\omega}\tau)\,d\tau$$

$$I_7'(\bar{\omega},\bar{z},\bar{s}) = \int_0^\infty \frac{4\tau^2(\tau^2-1)(2\tau^2-1)}{R^-(\tau)} e^{-\bar{\omega}[(\tau^2-1)^{1/2}\bar{s}+(\tau^2-k^2)^{1/2}\bar{z}]} J_1(\bar{\omega}\tau)\,d\tau$$

$$I_8'(\bar{\omega},\bar{z},\bar{s}) = \int_0^\infty \frac{4\tau^2(\tau^2-1)^{1/2}(\tau^2-k^2)^{1/2}(2\tau^2-1)}{R^-(\tau)} e^{-\bar{\omega}[(\tau^2-1)^{1/2}\bar{z}+(\tau^2-k^2)^{1/2}\bar{s}]} J_1(\bar{\omega}\tau)\,d\tau$$

$$\text{sgn }(\bar{z}-\bar{s}) = \begin{cases} +1 & , \quad \bar{z}>\bar{s} \\ -1 & , \quad \bar{z}<\bar{s} \end{cases} .$$

Likewise, the Green's function $\dfrac{\partial^2 \hat{u}_1}{\partial \bar{s}^2}(\bar{z},\bar{s})$ can be found as

$$\frac{\partial^2 \hat{u}_1}{\partial \bar{s}^2}(\bar{z},\bar{s}) = \frac{\bar{\omega}^2}{4\pi\mu a}\left[I_1'' - I_2'' + I_3'' + I_4'' - I_5'' - I_6'' + I_7'' + I_8'' \right] , \quad (3.3.11)$$

where

$$I_1''(\bar{\omega},\bar{z},\bar{s}) = \int_0^\infty \tau^2(\tau^2-k^2)^{1/2} e^{-\bar{\omega}(\tau^2-k^2)^{1/2}|\bar{z}-\bar{s}|} J_1(\bar{\omega}\tau)\,d\tau$$

$$I_2''(\bar{\omega},\bar{z},\bar{s}) = \int_0^\infty (\tau^2-1)^{\frac{3}{2}} e^{-\bar{\omega}(\tau^2-1)^{1/2}|\bar{z}-\bar{s}|} J_1(\bar{\omega}\tau)\,d\tau$$

$$I_3''(\bar{\omega},\bar{z},\bar{s}) = \int_0^\infty (\tau^2-1)^{1/2} e^{-\bar{\omega}(\tau^2-1)^{1/2}|\bar{z}-\bar{s}|} J_1(\bar{\omega}\tau)\,d\tau$$

$$I_4''(\bar{\omega},\bar{z},\bar{s}) = \int_0^\infty (\tau^2-1)^{1/2} e^{-\bar{\omega}(\tau^2-1)^{1/2}(\bar{z}+\bar{s})} J_1(\bar{\omega}\tau)\,d\tau$$

$$I_5''(\bar{\omega},\bar{z},\bar{s}) = \int_0^\infty \tau^2(\tau^2-k^2)^{1/2} \frac{R^+(\tau)}{R^-(\tau)} e^{-\bar{\omega}(\tau^2-k^2)^{1/2}(\bar{z}+\bar{s})} J_1(\bar{\omega}\tau)\,d\tau \qquad (3.3.12)$$

$$I_6''(\bar{\omega},\bar{z},\bar{s}) = \int_0^\infty (\tau^2-1)^{\frac{3}{2}} \frac{R^+(\tau)}{R^-(\tau)} e^{-\bar{\omega}(\tau^2-1)^{1/2}(\bar{z}+\bar{s})} J_1(\bar{\omega}\tau)\,d\tau$$

$$I_7''(\bar{\omega},\bar{z},\bar{s}) = \int_0^\infty \frac{4\tau^2(\tau^2-1)^{\frac{3}{2}}(2\tau^2-1)}{R^-(\tau)} e^{-\bar{\omega}[(\tau^2-1)^{1/2}\bar{s}+(\tau^2-k^2)^{1/2}\bar{z}]} J_1(\bar{\omega}\tau)\,d\tau$$

$$I_8''(\bar{\omega},\bar{z},\bar{s}) = \int_0^\infty \frac{4\tau^2(\tau^2-1)^{1/2}(\tau^2-k^2)(2\tau^2-1)}{R^-(\tau)} e^{-\bar{\omega}[(\tau^2-1)^{1/2}\bar{z}+(\tau^2-k^2)^{1/2}\bar{s}]} J_1(\bar{\omega}\tau)\,d\tau \quad,$$

respectively. Equations (3.3.7), (3.3.9) and (3.3.11) constitute the set of Green's functions required for the solution of the governing integral equation. Owing to the complexity and importance of these functions, it is appropriate to give a discussion of their general properties and evaluation procedures, which is the subject of the next chapter.

CHAPTER IV

PROPERTIES AND EVALUATION OF THE GREEN'S FUNCTIONS

In Chapter 3 integral representations for the Green's functions $\hat{u}_1(\bar{z},\bar{s})$, $\dfrac{\partial \hat{u}_1}{\partial \bar{s}}(\bar{z},\bar{s})$ and $\dfrac{\partial^2 \hat{u}_1}{\partial \bar{s}^2}(\bar{z},\bar{s})$ were derived analytically. It is

clear, however, from their complicated expressions that a complete

closed-form evaluation of these Green's functions would be extremely

difficult if not impossible. The problem stems mainly from the appear-

ance of the irrational function $\bar{R}(\tau)$ in some of the integrals involved.

$\bar{R}(\tau)$ is commonly called the Rayleigh function, the positive root of

which corresponds to the Rayleigh wave speed. A detailed discussion of

this interesting and yet complicated function may be found in Achenbach

[1]. For those integrals that involve $\bar{R}(\tau)$, there are few alternatives

to evaluating them numerically. In contrast, the rest of the integrals

which do not involve $\bar{R}(\tau)$ can, despite their complexities, be evaluated

in closed form. This is clearly desirable as it reduces the number of

integrals that must be treated numerically. More importantly, however,

it provides the required tools for a direct and systematic approach of

resolving some of the problems encountered in the numerical treatment of

the integrals, as will be discussed later in the chapter.

In what follows, a discussion of the basic properties of the

Green's functions is first given as they are of both theoretical and

practical importance in the later treatment of the governing integral

equation (2.2.16). The subsequent section is devoted to describing the

development of the analytical and numerical procedures employed for the evaluation of the various Green's functions. Typical behaviors of these functions are illustrated in the last section.

4.1 BASIC PROPERTIES OF THE GREEN'S FUNCTIONS

To determine the properties of the Green's functions, it is relevant, as a first step, to examine some of the general features of the integrals involved. An examination of the integrals in (3.3.8), (3.3.10) and (3.3.12) reveals that they all assume a common form

$$I(\bar{\omega},\bar{z},\bar{s}) = \int_0^\infty F(\bar{\omega},\bar{z},\bar{s},\tau) J_\nu(\bar{\omega}\tau) d\tau \qquad (4.1.1)$$

in which

$$F(\bar{\omega},\bar{z},\bar{s},\tau) = f(\tau) e^{-\bar{\omega} g(\tau,\bar{z},\bar{s})} . \qquad (4.1.2)$$

Here, $f(\tau)$ is an algebraic function which may contain irrational expressions and thereby may require definitions of branch cuts; $g(\tau,\bar{z},\bar{s})$ is an increasing function of τ when τ is sufficiently large and is a nondecreasing function of $|\bar{z}-\bar{s}|$; J_ν is the Bessel function of the first kind of order ν.

Owing to the presence of the decaying exponential factor in the integrands, the Green's function $\hat{u}_1(\bar{z},\bar{s})$ can be shown to be twice continuously differentiable with respect to $\bar{z}$ and $\bar{s}$ at all locations except possibly at $\bar{z}=\bar{s}$ or at $\bar{\omega} = 0$. From (3.3.7) and (3.3.11), it can be demonstrated directly that $\hat{u}_1(\bar{z},\bar{s})$ and $\dfrac{\partial^2 \hat{u}_1}{\partial \bar{s}^2}(\bar{z},\bar{s})$. are continuous at

all points including $\bar{z}=\bar{s}$. In contrast, although $\dfrac{\partial \hat{u}_1}{\partial \bar{s}}$ is also continuous

at most locations, it suffers a finite jump-discontinuity at $\bar{z}=\bar{s}$. This

is typical of most Green's functions encountered in mechanics. The

situation is less transparent when either $\bar{\omega}$ or $(\bar{z}+\bar{s})$ is zero, since in

this instance the integrands no longer decay exponentially. Any suspi-

cion of singular behavior can, however, be safely removed via an

asymptotic analysis which indicates that all the aforementioned

properties still hold for the Green's functions in such circumstances.

This should represent no surprise as the corresponding static solution

is believed to be well-behaved. The real difficulty in such situations

lies in the numerical computation of the Green's functions which is the

subject of the next section.

4.2 EVALUATION OF THE GREEN'S FUNCTIONS

To solve the integral equation (2.2.16), numerical values of the

Green's functions $\hat{u}_1(\bar{z},\bar{s})$, $\dfrac{\partial \hat{u}_1}{\partial \bar{s}}(\bar{z},\bar{s})$ and $\dfrac{\partial^2 \hat{u}_1}{\partial \bar{s}^2}(\bar{z},\bar{s})$ must actually be

computed. This requires an accurate determination of the various

integrals involved in (3.3.8), (3.3.10) and (3.3.12). In this section,

the above problem is addressed together with the general objective of

developing an accurate and reliable numerical procedure for the evalua-

tion of integrals of the general form shown in (4.1.1). The availabil-

ity of an effective approach for such a problem is desirable because

that type of integral occurs quite frequently in seismological studies

and wave propagation problems. In view of the similarity in procedures for the evaluation of the three Green's functions, attention will be mainly focused on $\hat{u}_1(\bar{z},\bar{s})$ in this exposition.

As indicated in (3.3.7), the evaluation of $\hat{u}_1(\bar{z},\bar{s})$ requires the computation of eight integrals, I_1 to I_8. Although integrals I_5 to I_8 are difficult to determine analytically owing to the complications of $\bar{R}(\tau)$, integrals I_1 to I_4 can be evaluated in closed form. This is also true of integrals I_1' to I_4' and I_1'' to I_4'' which are involved in $\dfrac{\partial \hat{u}_1}{\partial \bar{s}}(\bar{z},\bar{s})$ and $\dfrac{\partial^2 \hat{u}_1}{\partial \bar{s}^2}(\bar{z},\bar{s})$, respectively. With the branches of $(\tau^2-k^2)^{\frac{1}{2}}$ and $(\tau^2-1)^{\frac{1}{2}}$ chosen as shown in Figure 4.1, it can be shown that

$$I_1(\bar{\omega},\bar{z},\bar{s}) = -i\sqrt{\frac{\pi}{2\bar{\omega}}}\,\frac{k^{3/2}}{(d_1^2+1)^{3/4}}\,H_{3/2}^{(2)}\,[k\bar{\omega}(d_1^2+1)^{\frac{1}{2}}]$$

$$I_2(\bar{\omega},\bar{z},\bar{s}) = i\left[\frac{e^{-i\bar{\omega}d_1}}{\bar{\omega}} + \sqrt{\frac{\pi}{2\bar{\omega}}}\left(\frac{d_1^2}{(d_1^2+1)^{3/4}}\,H_{3/2}^{(2)}\,[\bar{\omega}(d_1^2+1)^{\frac{1}{2}}]\right.\right.$$
$$\left.\left. - \frac{1}{\bar{\omega}(d_1^2+1)^{3/4}}\,H_{1/2}^{(2)}\,[\bar{\omega}(d_1^2+1)^{\frac{1}{2}}]\right)\right]$$

$$I_3(\bar{\omega},\bar{z},\bar{s}) = -i\sqrt{\frac{\pi}{2}}\,J_{1/2}\left[\frac{\bar{\omega}}{2}\,[(d_1^2+1)^{\frac{1}{2}}-d_1]\right]\cdot H_{1/2}^{(2)}\,[\bar{\omega}(d_1^2+1)^{\frac{1}{2}}] \qquad (4.2.1)$$

$$I_4(\bar{\omega},\bar{z},\bar{s}) = -i\sqrt{\frac{\pi}{2}}\,J_{1/2}\left[\frac{\bar{\omega}}{2}\,[(d_2^2+1)^{\frac{1}{2}}-d_2]\right]\cdot H_{1/2}^{(2)}\,[\bar{\omega}(d_2^2+1)^{\frac{1}{2}}]$$

where
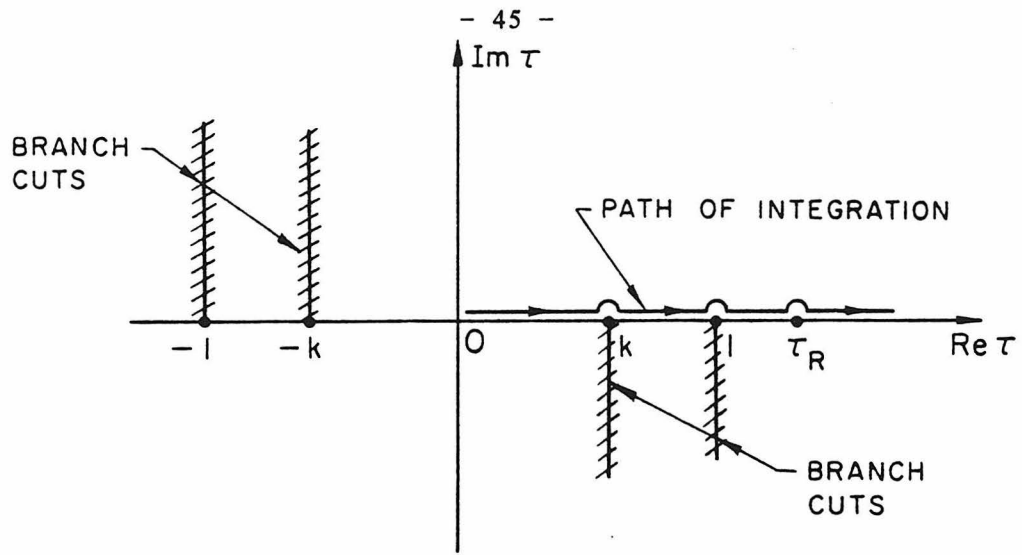
Figure 4.1   Branch Cuts and Path of Integration
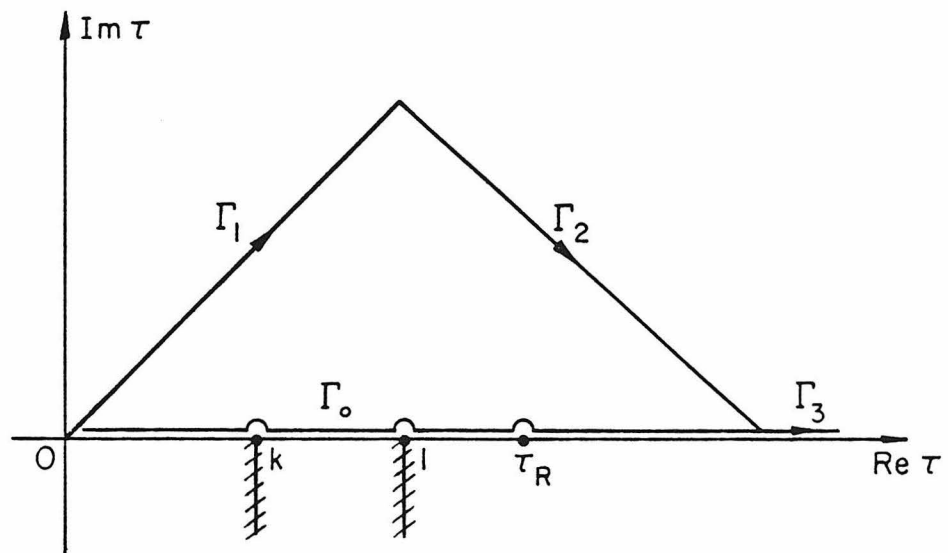
Figure 4.2   Modified Path of Integration

$$d_1 = |\bar{z}-\bar{s}|$$

$$d_2 = \bar{z}+\bar{s}$$

$$J_\nu = \text{Bessel function of the first kind of order } \nu$$

$$H_\nu^{(2)} = \text{Hankel function of the second kind of order } \nu$$

$$\bar{z}, \bar{s} \geq 0 \;.$$

When combined with the time factor $e^{i\omega t}$, I_1 to I_4 in (4.2.1) all represent outward propagating waves, confirming previous assertions in Chapter III on the choice of branches. The Hankel functions involved in (4.2.1) are all of fractional orders and are thus expressible in terms of circular functions. This is a clear advantage since no special numerical algorithms are needed for their evaluation.

For integrals I_5 to I_8, numerical integration represents the logical alternative since closed-form evaluation seems impossible. An examination of the integrals, however, reveals two basic problems in such procedures. The first one concerns the existence of several singularities on the path of integration. There are two branch points at $\tau = 1$ and $\tau = k$, respectively, and a simple pole at $\tau = \tau_R$ which corresponds to the root of the Rayleigh function $R(\tau)$. To overcome this problem, one could use the special procedure suggested by Longman [23] which involves separate integration over subintervals and a special technique to integrate over the pole. The method of branch-line integration, as employed by Ewing et al. [13], represents another

possibility although the choice of contours is not obvious in the
present case. On the other hand, the problem can be totally avoided if
one simply resorts to the Cauchy's theorem in the theory of contour
integration. By the theorem, the original path of integration $\Gamma_0 + \Gamma_3$
can be replaced by a new contour $\Gamma_1 + \Gamma_2 + \Gamma_3$ which is free of any
singularities (see Figure 4.2). On this modified contour, the integral
can be evaluated easily by standard quadrature techniques.

A more serious problem in the numerical computation of the
integrals is concerned with the treatment of the infinite upper limit of
integration. For numerical purposes, the upper limit must be truncated
at a finite value τ_u. This does not present great difficulties in most
cases owing to the strong decay of the integrand induced by the exponen-
tial factor. However, this is no longer true when either ω or $(\bar{z}+\bar{s})$ is
small or vanishing because in these cases the exponential decay will
become vanishingly small or nonexistent. As some of the functions $f(\tau)$
involved in (3.3.8) are of order τ^n, $n \geq 1$ as $\tau \to \infty$, numerical integra-
tion with a truncated upper limit on such an occasion may lead to
grossly inaccurate results; the procedure may even be divergent. The
situation is particularly serious in the case of $\dfrac{\partial^2 \hat{u}_1}{\partial \bar{s}^2} (\bar{z},\bar{s})$.

A remedy for the problem is suggested by the following observation:
as $\bar{\omega}$ or $(\bar{z} + \bar{s})$ tends to zero, the contribution of the integrands at
large values of τ apparently becomes increasingly important. Prompted
by this observation, an asymptotic analysis of the integrands at large τ
is performed. It is at this point that the knowledge of I_1 to I_4, I'_1

to I'_4 and I''_1 to I''_4 becomes helpful. Using the integrands of these integrals as the basic asymptotic sequence where appropriate, an asymptotic expansion $F_{asym}(\bar{\omega},\bar{z},\bar{s},\tau)$ of the original integrand $F(\bar{\omega},\bar{z},\bar{s},\tau)$ can be found with the property that the difference between F and F_{asym} decreases rapidly as τ increases, e.g., $|F-F_{asym}| \sim 0(\frac{1}{\tau^2})$ as $\tau \to \infty$. With this result, the integral (4.1.1) can be written as

$$I(\bar{\omega},\bar{z},\bar{s}) = \int_0^\infty F_r(\bar{\omega},\bar{z},\bar{s},\tau) J_\nu(\bar{\omega}\tau)d\tau$$

$$+ \int_0^\infty F_{asym}(\bar{\omega},\bar{z},\bar{s},\tau) J_\nu(\bar{\omega}\tau)d\tau \qquad (4.2.2)$$

where

$$F_r(\bar{\omega},\bar{z},\bar{s},\tau) = F(\bar{\omega},\bar{z},\bar{s},\tau) - F_{asym}(\bar{\omega},\bar{z},\bar{s},\tau)d\tau \quad . \qquad (4.2.3)$$

With F_{asym} determined as described above, F_r, the residual integrand, will decay to zero very rapidly in τ. As a consequence, the first integral in (4.2.2) can always be determined with negligible error regardless of the values of $\bar{\omega}$, $\bar{z}$ and $\bar{s}$, provided the upper limit is truncated at a reasonable finite value. On the other hand, the second integral in (4.2.2) can be evaluated exactly in closed form, on the basis of the analytical results such as those shown in (4.2.1). An error bound for this method of integration by asymptotic decomposition can be established rigorously once the upper limit τ_u is specified and vice-versa.

For high frequencies or very deep locations, accurate results can also be obtained economically by applying standard asymptotic techniques, e.g., the method of steepest descent, to the integral representations of the Green's functions. It is, however, necessary in such procedures to derive terms to at least second order before the result is meaningful.

4.3 NUMERICAL RESULTS

By the procedure described in the previous section, the Green's functions $\hat{u}_1(\bar{z},\bar{s})$, $\dfrac{\partial \hat{u}_1}{\partial \bar{s}^2}(\bar{z},\bar{s})$ and $\dfrac{\partial^2 \hat{u}_1}{\partial \bar{s}^2}(\bar{z},\bar{s})$ can be computed accurately. Representative results are shown in Figure 4.3 to 4.8 wherein $\overset{o}{u}_1(\bar{z},\bar{s})$, defined as $4\pi\mu a \hat{u}_1(\bar{z},\bar{s})$, is a non-dimensional form of the Green's function.

In an integral equation, the most important quantity is undoubtedly the kernel function. For the equation under consideration, the kernel, as it appears in (2.2.17), involves both $\overset{o}{u}_1(\bar{z},\bar{s})$ and $\dfrac{\partial^2 \overset{o}{u}_1}{\partial \bar{s}^2}(\bar{z},\bar{s})$. The variations of $\dfrac{\partial^2 \overset{o}{u}_1}{\partial \bar{s}^2}(\bar{z},\bar{s})$ in $\bar{z}$ and $\bar{s}$ are shown in Figures 4.3 and 4.4, respectively. As can be seen from the figures, $\dfrac{\partial^2 \overset{o}{u}_1}{\partial \bar{s}^2}(\bar{z},\bar{s})$ is a very localized function with most of its significant variations confined to the vicinity of the point $\bar{z}=\bar{s}$. This characteristic has some important consequences in the eventual numerical solution of the integral equation

Figure 4.3 :
Green's Function
$\frac{\partial^2 \overset{o}{u_1}(\bar{z},\bar{s})}{\partial \bar{s}^2}$ at $\bar{s}=20$

$\bar{\omega} = 0.5$
$\nu = 0.25$

Re ——
Im ----
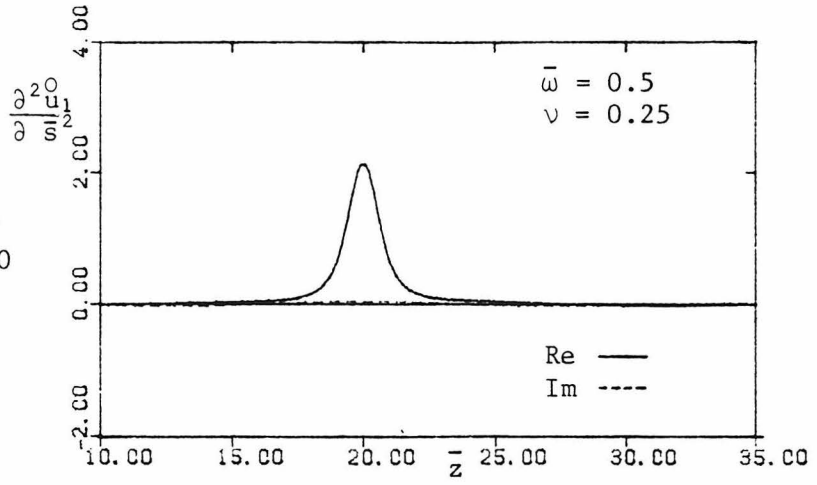
Figure 4.4 :
Green's Function
$\frac{\partial^2 \overset{o}{u_1}(\bar{z},\bar{s})}{\partial \bar{s}^2}$ at $\bar{z}=20$

$\bar{\omega} = 0.5$
$\nu = 0.25$

Re ——
Im ----
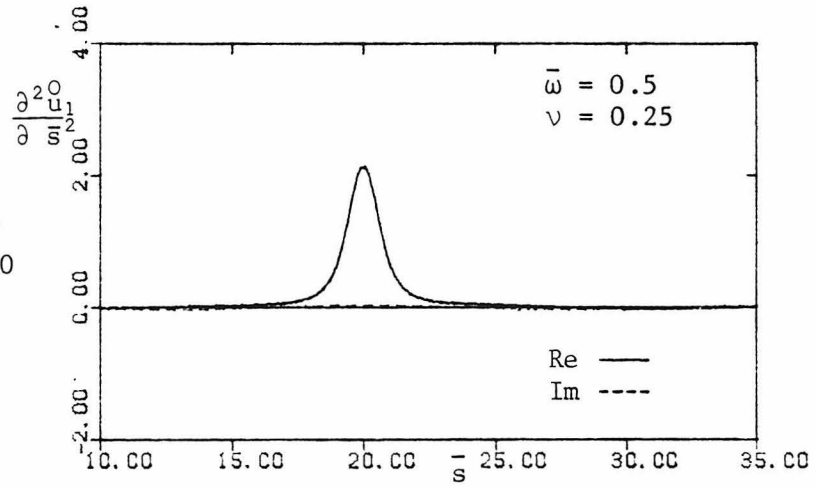
Figure 4.5 :
Green's Function
$\overset{o}{u_1}(\bar{z},\bar{s})$ at $\bar{z}=20$

$\bar{\omega} = 0.5$
$\nu = 0.25$

Re ——
Im ----
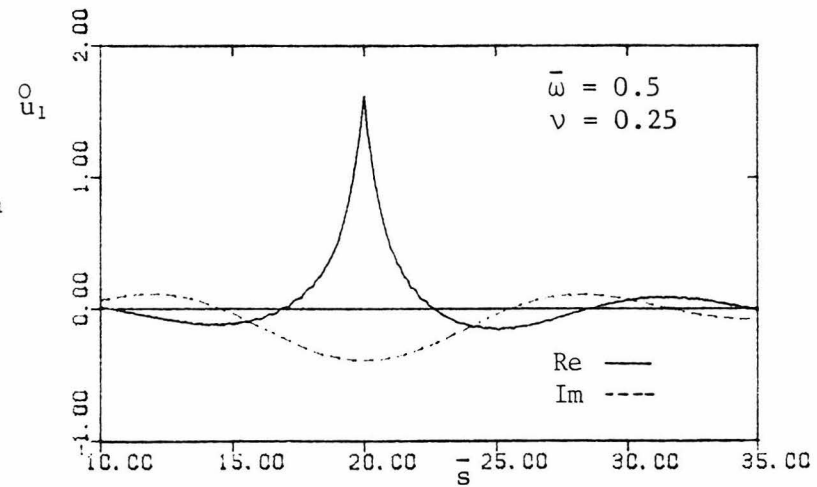
as will be discussed in the next chapter. The oscillatory nature of
this Green's function is also visible although it is grossly masked by
the strong decay of the function. Other properties of the Green func-
tion such as smoothness and continuity are visually apparent, supple-
menting the discussion in Section 4.1.

Similar comments can be made in regard to the Green's function
$\overset{o}{u}_1(\bar{z},\bar{s})$ whose variation in $\bar{s}$ is illustrated in Figure 4.5. The varia-
tion of $\overset{o}{u}_1(\bar{z},\bar{s})$ in $\bar{z}$ is not presented because the function is symmetri-
cal in $\bar{z}$ and $\bar{s}$, as can be deduced from its expression in (3.3.7) and
(3.3.8). This property is in accord with the reciprocity theorem in
elasticity [12]. The oscillatory behavior of $\overset{o}{u}_1(\bar{z},\bar{s})$ is, in contrast to
that of $\dfrac{\partial^2 \overset{o}{u}_1}{\partial \bar{s}^2}(\bar{z},\bar{s})$, quite distinct. It could be noticed from the figure
that the smoothness of the real and imaginary part of $\overset{o}{u}_1(\bar{z},\bar{s})$ is quite
different at the point $\bar{z}=\bar{s}$. While the imaginary part of $\overset{o}{u}_1(\bar{z},\bar{s})$ is very
smooth at that point, the real part of $\overset{o}{u}_1(\bar{z},\bar{s})$ has a sharp cusp. This
interesting feature can, however, be readily explained if the suppressed
time factor $e^{i\omega t}$ in the analysis is invoked. With the time factor in
place, it can be easily seen that the real part of $\overset{o}{u}_1(\bar{z},\bar{s})$ represents
the response of the half-space at the instant the buried body-force
field reaches its maximum strength, e.g., at t = 0. Since the size of
stress-discontinuity at the plane $\bar{z} = \bar{s}$ is directly proportional to the
magnitude of the force field as described by Equation (3.2.11), the lack
of smoothness in $\overset{o}{u}_1(\bar{z},\bar{s})$ at such a point is expected. Likewise, the
imaginary part of $\overset{o}{u}_1(\bar{z},\bar{s})$ can be interpreted as the response of the

half-space at the instants when the buried body-force field vanishes. In this case, however, (3.2.11) implies that the stress-discontinuity at $\bar{z} = \bar{s}$ would disappear. With the only discontinuity eliminated, the observed smoothness in the response is a logical consequence.

A measure of the sharpness of the cusp in the $\overset{o}{u}_1(\bar{z},\bar{s})$ at $\bar{z} = \bar{s}$ is the value of the jump in slope at that point; i.e., $\left[\dfrac{\partial \overset{o}{u}_1}{\partial \bar{s}} (\bar{z},\bar{s}) \right]_{\bar{s}=\bar{z}^-}^{\bar{z}^+}$. This quantity is also related to the coefficient $A(z)$ in the integral equation (2.2.16). By the analytical results in (4.2.1), it can be shown that $\left[\dfrac{\partial \overset{o}{u}_1}{\partial \bar{s}} (\bar{z},\bar{s}) \right]_{\bar{s}=\bar{z}^-}^{\bar{z}^+}$ takes on the value of $-\dfrac{1}{\pi\mu a}$. The fact that it is a constant helps to ensure that the Fredholm integral equation is regular for all frequencies including $\bar{\omega} = 0$. With this result, it can also be shown that equations (2.2.13) and (2.2.14) are actually deducible from (2.2.12), as asserted in Chapter II.

The behavior of $\dfrac{\partial^2 \overset{o}{u}_1}{\partial \bar{s}^2} (\bar{z},\bar{s})$ and $\overset{o}{u}_1(\bar{z},\bar{s})$ when the source is at the surface of the half-space is illustrated in Figures 4.6 and 4.7. Compared with Figures 4.4 and 4.5 wherein the source is located at depth, the figures indicate that the maximum value of the functions is significantly higher and there is a stronger decay when the source is at or near the free surface. The function $\dfrac{\partial \overset{o}{u}_1}{\partial \bar{s}} (\bar{z},0)$, which constitutes one of the inhomogeneous terms of the integral equation, is shown in Figure 4.8. The nature of this function is generally similar to that of $\overset{o}{u}_1(\bar{z},0)$ and hence will not be described further.

$\dfrac{\partial^2 \overset{O}{u_1}}{\partial \, \bar{s}^2}$

$\bar{\omega} = 0.5$
$\nu = 0.25$

Re ———
Im - - - -

Figure 4.6 :
Green's Function
$\dfrac{\partial^2 \overset{O}{u_1}(\bar{z}, \bar{s})}{\partial \, \bar{s}^2}$ at $\bar{s}=0$

$\overset{O}{u_1}$

$\bar{\omega} = 0.5$
$\nu = 0.25$

Re ———
Im - - - -
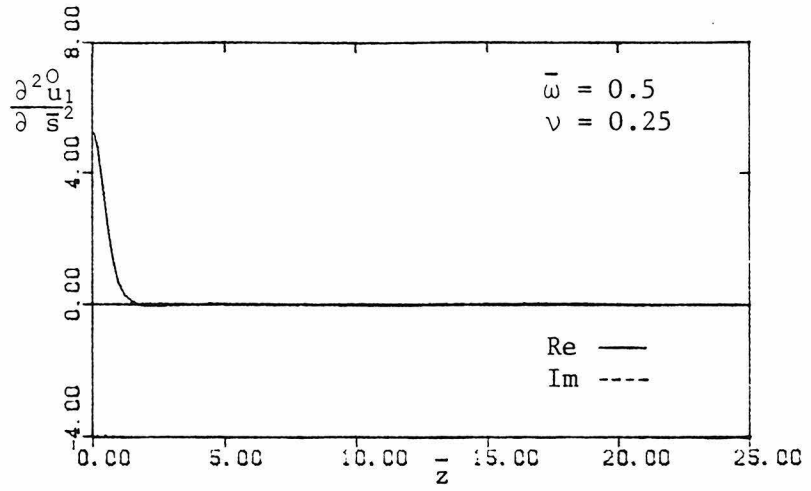
Figure 4.7 :
Green's Function
$\overset{O}{u_1}(\bar{z}, \bar{s})$ at $\bar{s}=0$

$\dfrac{\partial \overset{O}{u_1}}{\partial \bar{s}}$

$\bar{\omega} = 0.5$
$\nu = 0.25$

Re ———
Im - - - -
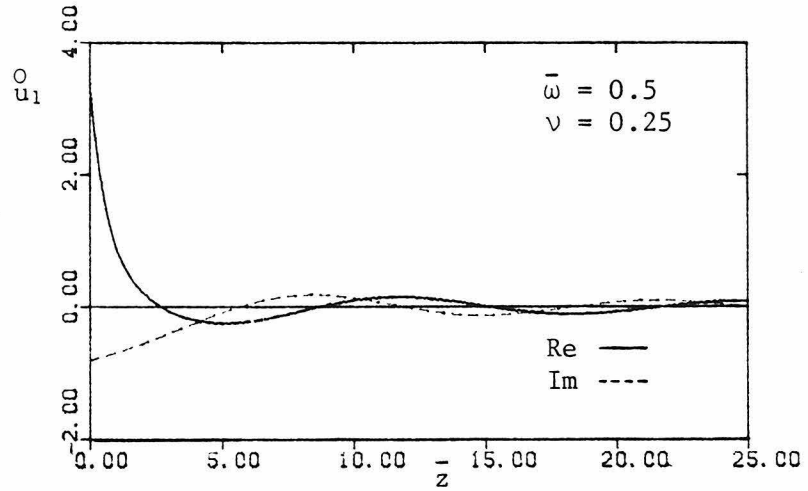
Figure 4.8 :
Green's Function
$\dfrac{\partial \overset{O}{u_1}(\bar{z}, \bar{s})}{\partial \bar{s}}$ at $\bar{s}=0$
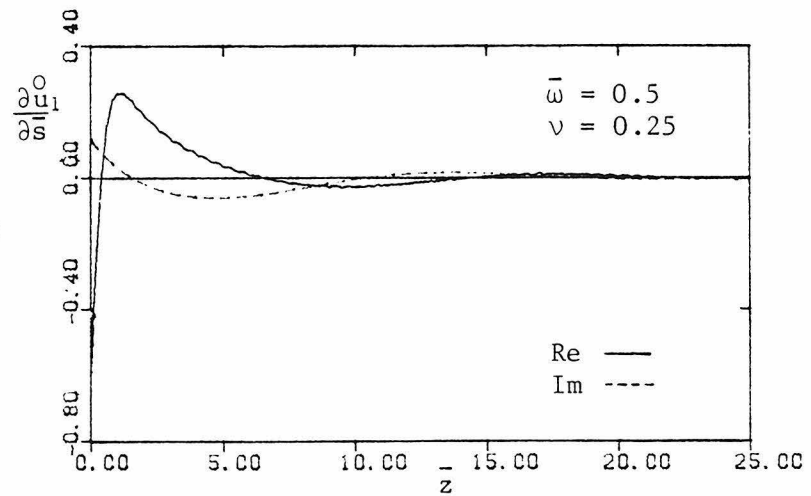
This concludes the discussion of the basic characteristics of the Green's functions. In addition to its intrinsic interests, this information is necessary for the development of an accurate and effective scheme for the solution of the governing integral equation.

CHAPTER V

SOLUTION OF THE FREDHOLM INTEGRAL EQUATION

A reading of the literature [5] indicates that techniques for solving Fredholm integral equations of the second kind can be classified into five broad categories: (1) analytical and semi-analytical methods, (2) kernel approximation methods, (3) projection methods, (4) quadrature methods, and (5) Volterra and initial value methods. Each technique has its own merits and disadvantages in different circumstances, and it is beyond the scope of this presentation to discuss them in general. Interested readers may refer to [17] for more details. However, it is fair to say that in practical applications, projection and quadrature are usually the preferred techniques because of their conceptual simplicity and their ease in computer implementation. Since an understanding of the ideas behind these two methods is helpful for the subsequent development of the solution scheme for the integral equation (2.2.16), a brief exposition of the relevant concepts is given in the following section.

5.1 CONCEPTS IN QUADRATURE AND PROJECTION METHODS

5.1.1 Quadrature Methods

The idea underlying quadrature methods is perhaps the most natural one, whereupon the integral in the equation is approximated by a numerical quadrature. Thus, the Fredholm integral equation of the second kind

$$y(t) - \int_a^b K(t,s)y(s)ds = g(t) \qquad (5.1.1)$$

is approximated by

$$y(t) - \sum_{k=1}^{n} w_k K(t,s_k)y(s_k) \simeq g(t) \qquad (5.1.2)$$

where $\{w_k\}_{k=1}^{n}$ and $\{s_k\}_{k=1}^{n}$ are the weights and nodes of a quadrature rule Q_n, respectively. If $y_n(t)$ is defined as the solution to

$$y_n(t) = \sum_{k=1}^{n} w_k K(t,s_k)y_n(s_k) + g(t) \quad , \qquad (5.1.3)$$

then evaluating $y_n(t)$ at $t=t_j$, $j=1,2,\ldots,n$ gives the following set of algebraic equations for $\{y_n(t_j)\}_{j=1}^{n}$:

$$y_n(t_j) = \sum_{k=1}^{n} w_k K(t_j,s_k)y_n(s_k) + g(t_j) \quad , \quad j=1,\ldots,n \quad . \quad (5.1.4)$$

If (5.1.4) has a unique solution for sufficiently large n, then (5.1.3) provides a natural interpolation formula for obtaining $y_n(t)$ for $t \in [a,b]$. A general convergence proof for the method can be found in [17] where it is also established that the solution error is directly proportional to the quadrature error.

5.1.2 Projection Methods

Projection methods include such techniques as collocation, the method of moments, Galerkin's method and least-square procedures. Collocation is generally the most efficient method since the numerical computation needed to generate the algebraic system of equations is minimized as only single, rather than multiple, integrals need be computed. This is particularly crucial, in terms of both efficiency and accuracy, when the evaluation of the kernel requires a significant amount of numerical effort. Since this is the case in the problem under consideration, the present discussion of projection techniques is specialized to collocation methods. The description of the technique, however, is cast in a fairly general setting so that the procedures for other projection methods will follow essentially the same development with only a few redefinitions.

For the economy of further development, the Fredholm integral equation (5.1.1) may be written in operator form as

$$y(t) - Ky(t) = g(t) \tag{5.1.5}$$

where the operator $K : X \to X$ is defined by

$$Ky(t) = \int_a^b K(t,s)y(s)ds \quad . \tag{5.1.6}$$

Here, X is the Banach space in which the solution is sought. Typically, it is taken to be the space of continuous functions with the norm $\|.\|_\infty$. In this setting, one attempts to approximate the solution y by

a sequence $\{y_n\}_{n=1}^{\infty}$, such that $y_n \in X_n$ where $\{X_n\}_{n=1}^{\infty}$ is taken to be a sequence of finite dimensional subspaces of X. Let P_n denote a projection operator that maps a function f in X onto a function f_n in X_n which interpolates to it on the set of points $\{t_k\}_{k=1}^{n}$. Mathematically, this can be written as

$$f_n(t) \equiv P_n f(t) = \sum_{k=1}^{n} f(t_k) \phi_k(t) \qquad (5.1.7)$$

where $\{\phi_k(t)\}_{k=1}^{n}$ is a set of interpolation functions with the property that $\phi_k(t_j) = \delta_{kj}$, δ_{kj} being the Kronecker delta. Some common choices of $\{\phi_k\}$ are Lagrange interpolation functions and Chebyshev polynomials. Taking $\tilde{y}_n$ as an approximation to y and substituting it into the integral equation, one obtains

$$\tilde{y}_n - K\tilde{y}_n - g = R_n(\tilde{y}_n) \qquad (5.1.8)$$

where $R_n(\tilde{y}_n)$ is the residual which will be zero if $\tilde{y}_n$ is equal to y. Since this will not be true in general, one seeks to select y_n such that $R_n(\tilde{y}_n)$ is minimized. This is accomplished by making the projection of R_n onto X_n equal to zero; i.e.,

$$P_n\tilde{y}_n - P_n K\tilde{y}_n - P_n g = 0 \quad . \qquad (5.1.9)$$

With the definition of P_n as in (5.1.7) and the property that $P_n\phi_k = \phi_k$, (5.1.9) gives

$$\sum_{k=1}^{n} \tilde{y}(t_k) \phi_k(t) - \sum_{j=1}^{n} \tilde{y}(t_j) \int_a^b K(t_k,s) \phi_j(s) ds \; \phi_k(t)$$

$$= \sum_{k=1}^{n} g(t_k) \phi_k(t) \quad . \tag{5.1.10}$$

By evaluating both sides of (5.1.10) at t_j and using the fact that $\phi_k(t_j) = \delta_{kj}$, equation (5.1.10) leads to

$$\tilde{y}(t_j) - \sum_{k=1}^{n} \tilde{y}(t_k) \int_a^b K(t_j,s) \phi_k(s) ds = g(t_j) \quad , \; j=1,2,\ldots,n \quad . \tag{5.1.11}$$

This is a system of linear algebraic equations, the solution of which together with (5.1.7) furnishes an approximation $y_n(t)$ to the exact solution. A convergence proof for this method is given in [5], on the conditions that (i) $||K_n - K|| \to 0$ where $K_n = P_n K$, and (ii) $P_n g \to g$ as n approaches infinity. If the operator K is compact, then it is sufficient that $P_n f \to f$ for all $f \in X$ and $||P_n|| \leq M$ for $n \geq 1$ where M is a positive constant [6].

Several comments are warranted at this point. If K(t,s) and y(t) are smooth functions, both quadrature and collocation will generally perform satisfactorily. However, if K(t,s) has rapid variations or is very localized, quadrature methods will usually be inaccurate unless n, the number of nodes, is taken to be very large which is often impractical. Collocation methods usually perform better on such occasions, although the choice of collocation points can sometimes be critical for

the success. For example, it is well known that polynomial collocation using equally spaced nodes is generally divergent.

In the following section, a numerical scheme which contains the essence of both the quadrature and collocation techniques is developed for the solution of the integral equation (2.2.16). The possible interpretation of the procedure as an improved quadrature method, as will be discussed later, should make it appealing to engineers who demand accurate but simple solution methodology.

5.2 PROPOSED NUMERICAL SCHEME

It is convenient for further consideration that the governing Fredholm integral equation be put into a dimensionless form. To this end, the following dimensionless parameters are defined:

$$\overline{u}_*(\overline{z}) = \frac{u(z)}{a}$$

$$\overline{M}_*(\overline{z}) = \frac{M(z)}{4\pi\mu_s a^3}$$

$$\overline{M}_0 = \frac{M_0}{4\pi\mu_s a^3}$$

$$\overline{V}_0 = \frac{V_0}{4\pi\mu_s a^2} \qquad (5.2.1)$$

$$RM = \frac{\rho_*}{\rho_s}$$

$$RS = \frac{16\mu_s}{E_*}$$

$$\bar{\rho} = \frac{\rho_b}{\rho_s}$$

$$\bar{E} = \frac{E_b}{E_s} \quad .$$

Here, RM and RS are functions of the relative mass ratio $\bar{\rho}$ and the relative stiffness ratio $\bar{E}$, respectively. In terms of these parameters, the integral equation (2.2.16) can be written as:

$$\overset{o}{A}(\bar{z})\bar{M}_*(\bar{z}) + \overset{o}{B}(\bar{z})\bar{u}_*(0) + \overset{o}{C}(\bar{z})\bar{u}_*(\bar{\ell}) + \int_0^{\bar{\ell}} \overset{o}{K}(\bar{z},\bar{s})\bar{M}_*(\bar{s})d\bar{s}$$

$$= \bar{V}_0 \overset{o}{u}_1(\bar{z},0) - \bar{M}_0 \frac{\partial \overset{o}{u}_1}{\partial \bar{s}}(\bar{z},0) \quad , \tag{5.2.2}$$

where

$$\overset{o}{A}(\bar{z}) = 4\pi\mu_s a^2 \left[\frac{\partial \overset{o}{u}_1}{\partial \bar{s}}(\bar{z},\bar{s}) \right]_{\bar{z}^-}^{\bar{z}^+}$$

$$\overset{o}{B}(\bar{z}) = \left(1 - \frac{\bar{z}}{\bar{\ell}}\right) - \bar{\omega}^2 \frac{RM}{4} \int_0^{\bar{\ell}} \left(1 - \frac{\bar{s}}{\bar{\ell}}\right) \overset{o}{u}_1(\bar{z},\bar{s})d\bar{s}$$

$$\overset{o}{C}(\bar{z}) \;=\; \left(\frac{\bar{z}}{\bar{l}}\right) \;-\; \bar{\omega}^2 \, \frac{RM}{4} \int_0^{\bar{l}} \left(\frac{\bar{s}}{\bar{l}}\right) \overset{o}{u}_1(\bar{z},\bar{s}) d\bar{s} \qquad\qquad (5.2.3)$$

$$\overset{o}{u}_1(\bar{z},\bar{s}) \;=\; \frac{1}{4\pi\mu a} \, \hat{u}_1(\bar{z},\bar{s})$$

$$\overset{o}{G}(\bar{z},\bar{s}) \;=\; RS \begin{cases} \left(1 - \dfrac{\bar{s}}{\bar{l}}\right) \bar{z} & , \quad \bar{z} < \bar{s} \\[2em] \left(1 - \dfrac{\bar{z}}{\bar{l}}\right) \bar{s} & , \quad \bar{z} > \bar{s} \end{cases}$$

$$\overset{o}{K}(\bar{z},\bar{s}) \;=\; \frac{\partial^2 \overset{o}{u}_1(\bar{z},\bar{s})}{\partial \bar{s}^2} \;-\; \overset{o}{G}(\bar{z},\bar{s}) \;+\; \bar{\omega}^2 \, \frac{RM}{4} \int_0^{\bar{l}} \overset{o}{G}(\bar{\eta},\bar{s}) \overset{o}{u}_1(\bar{z},\bar{\eta}) d\bar{\eta} \quad .$$

Because of the linearity of the Fredholm integral equation, the inhomogeneous terms on the right-hand side of (5.2.2) arising from the applied shear $\bar{V}_0$ and the applied moment $\bar{M}_0$ may be considered separately in the solution process.

In solving equation (5.2.2), the following set of approximate integral operators $\{K_n\}_{n=1}^{\infty}$ is employed:

$$K_n f(x) \;=\; \sum_{k=1}^{n} f(x_j) \int_0^{\bar{l}} \overset{o}{K}(x,s) \, \phi_j(s) ds \qquad , \quad n \geq 2 \qquad (5.2.4)$$

where $\{x_j\}_{j=1}^{n}$ is a set of nodal points with $x_1 = 0$ and $x_n = \bar{l}$, and $\{\phi_j\}_{j=1}^{n}$ is a set of pyramid functions defined by

$$\phi_1(x) \;=\; \begin{cases} \dfrac{(x_2-x)}{(x_2-x_1)} & x \in [0,x_2] \\[4mm] 0 & \text{otherwise} \end{cases}$$

$$\phi_j(x) \;=\; \begin{cases} \dfrac{(x-x_{j-1})}{(x_j-x_{j-1})} & x \in [x_{j-1},x_j] \\[4mm] \dfrac{(x_{j+1}-x)}{(x_{j+1}-x_j)} & x \in [x_j,x_{j+1}] \\[4mm] 0 & \text{otherwise} \end{cases} \qquad (5.2.5)$$

$$\phi_n(x) \;=\; \begin{cases} \dfrac{(x-x_{n-1})}{(x_n-x_{n-1})} & x \in [x_{n-1},x_n] \\[4mm] 0 & \text{otherwise} \;. \end{cases}$$

The functions $\{\phi_j\}_{j=1}^n$ are illustrated in Figure 5.1. It can be shown that they form an independent set and that the corresponding approximation subspaces $\{X_n\}$ have the property that $U_{n=1}^{\infty} X_n$ is dense in $C[0,\bar{l}]$. The latter condition ensures that the approximation subspaces can eventually cover the class of functions in which the solution is sought. Upon replacing the integral operator by the approximate one and evaluating it at the set of nodal points $\{x_j\}_{j=1}^n$, equation (5.2.2) gives

$$a_i\bar{M}_i + b_i\bar{u}_*(0) + c_i\bar{u}_*(\bar{l}) + \sum_{j=1}^n K_{ij}\bar{M}_j = \bar{f}_i \qquad (5.2.6)$$

where
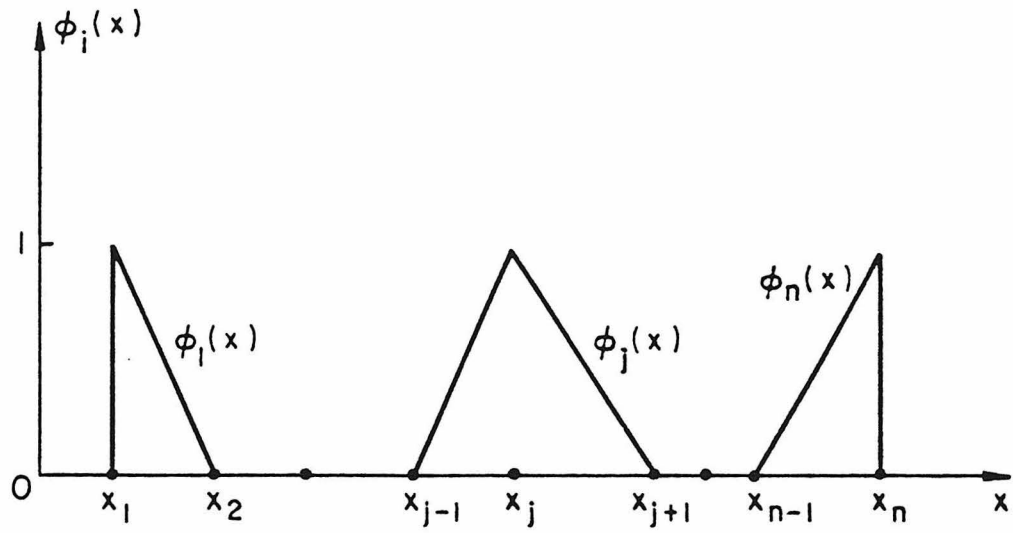
Figure 5.1   The Pyramid Functions $\{\phi_i\}$

$$\overline{M}_i = \overline{M}_*(x_i)$$

$$a_i = \overset{o}{A}(x_i)$$

$$b_i = \overset{o}{B}(x_i)$$

$$c_i = \overset{o}{C}(x_i) \hspace{3cm} (5.2.7)$$

$$K_{ij} = \int_0^{\overline{\ell}} \overset{o}{K}(x_i,s)\phi_j(s)ds$$

$$\overline{f}_i = \overline{V}_0 \overset{o}{u}_i(x_i,0) \quad \text{or} \quad -\overline{M}_0 \frac{\partial \overset{o}{u}_i}{\partial \overline{s}}(x_i,0) \quad .$$

In matrix form, (5.2.6) is equivalent to

$$[\widetilde{K}]\{\overline{M}\} + \overline{u}_*(0)\{b\} + \overline{u}_*(\overline{\ell})\{c\} = \{\overline{f}\} \hspace{2cm} (5.2.8)$$

where $\widetilde{K}_{ij} = K_{ij} - a_i\delta_{ij}$. Since $\overline{M}_1$ and $\overline{M}_n$ are already specified by the boundary conditions and take on the values $\overline{M}_0$ and zero, respectively, while $\overline{u}_*(0)$ and $\overline{u}_*(\overline{\ell})$ are a pair of extra unknowns, the system of equations in (5.2.8) can be arranged into

$$[K']\{\overline{M}'\} = \{\overline{f}'\} \hspace{3cm} (5.2.9)$$

where

$$[K'] \quad = \quad \left[\left[\left[b\right]\right]\left[\begin{array}{ccc} \tilde{K}_{1,2} & \cdots & \tilde{K}_{1,n-1} \\ \cdot & & \\ \cdot & & \\ \tilde{K}_{n,2} & & \tilde{K}_{n,n-1} \end{array}\right]\left[\left[c\right]\right]\right]$$

$$\overline{M}' \quad = \quad \left[\begin{array}{c} \overline{u}_*(0) \\ \overline{M}_2 \\ \cdot \\ \cdot \\ \overline{M}_{n-1} \\ \overline{u}_*(\overline{l}) \end{array}\right] \qquad\qquad (5.2.10)$$

$$\overline{f}' \quad = \quad \left[\,\overline{f}\,\right] - \overline{M}_0 \left[\begin{array}{c} \tilde{K}_{1,1} \\ \cdot \\ \cdot \\ \cdot \\ \tilde{K}_{n,1} \end{array}\right] .$$

Equation (5.2.9) represents a set of linear algebraic equations for the n unknowns $\overline{M}'_i$. The solution of this system can be obtained readily on a digital computer. Together with the known values of $\overline{M}_1$ and $\overline{M}_n$, it furnishes the complete bending moment profile and the top and bottom displacements of the bar.

Note that if the projection operator which appeared in the description of collocation methods is defined as

$$P_n u(t) = \sum_{k=1}^{n} u(t_k) \, \phi_k(t) \qquad (5.2.11)$$

where $\{\phi_k\}$ is the set of pyramid functions defined by (5.2.5), the method proposed above can be formally considered as a collocation method. The kernel $\overset{o}{K}(\bar{z}, \bar{s})$ of the integral equation, defined in (5.2.3), is composed of three continuous functions and is thus also continuous. With this property, it can be shown that the integral operator associated with $\overset{o}{K}$ is compact. Since the projection operator defined in (5.2.11) represents nothing more than a linear interpolation between nodal values, the convergence of $P_n f$ to f for $f \in C$ is guaranteed. As $\|P_n\|$ can easily be shown to be bounded, the convergence theorem in [6] guarantees that the scheme will converge to the exact solution uniformly on $[0, \bar{l}]$ as $n \to \infty$.

An interesting alternative interpretation of the solution scheme is also possible because, in practice, the term K_{ij} defined in (5.2.7) will be determined by quadrature, e.g., by Simpson's rule. It follows then that $K(x,s)$ will be sampled at more points over s than just at the nodal locations. Recall that in standard quadrature methods (i) only the nodal values of $K(x,s)$ and $u(x)$ are computed, and (ii) the solution error depends on the error in integrating $K(x,s)u(s)$. Hence, even if $u(x)$ is smooth, the solution accuracy can still be very poor if $K(x,s)$

varies very rapidly in s, e.g., within one or two nodal spacings. One remedy, of course, is to increase the number of nodes. This approach, however, is usually impractical when the cost of evaluating the kernel is high, because the number of sample points of $K(x,s)$ increases quadratically with n. Furthermore, it also fails to utilize the possible smoothness of the solution to the best advantage in the numerics. In practical terms, if a function is smooth, then the knowledge of its value over a fine mesh is unnecessary as a few nodal values would have been sufficient to define its full characteristics. A logical way to resolve the dilemma is to try to improve the quadrature accuracy by sampling the rapidly varying function $K(x,s)$ at more locations than $u(x)$. This is one of the original motivations of the proposed scheme. The fact that the pyramid functions all have local support and are linear between the nodes permits the scheme to be interpreted as a quadrature method where the quadrature error is reduced by a "secondary" integration over nodal spacings. Note that if m^2 is the number of sample points of $K(x,s)$ required to achieve the desired level of accuracy by standard quadrature methods in the case of a smooth $u(x)$ and an unsmooth $K(x,s)$, the corresponding number required by the proposed method is usually of the order of $m*n$ where $n \ll m$. This will represent substantial savings particularly when m is large and the cost of evaluating the kernel is high. As the use of a very large m in quadrature methods for rapidly varying kernels is usually necessary but typically infeasible, the proposed method can, in most cases, provide a solution of an accuracy that is unobtainable by quadrature. Since the Green's

functions involved in many mechanics problems exhibit the same characteristics as those under consideration, it is hoped that the numerical scheme developed in this chapter would prove to be a simple and effective tool in the solution of other engineering problems by the integral equation approach.

5.3 DETERMINATION OF THE SLOPE AND DISPLACEMENT

The solution of equation (5.2.9) provides the bending moment profile and the top and bottom displacements of the embedded bar. Theoretically, according to the constitutive law $E_*Iu_*'' = M_*$, an integration of $M_*(z)/E_*I$ will give the slope $u_*'(z)$, and a double integration will furnish the displacement $u_*(z)$ of the bar. Practically, however, this approach may not give the most accurate result as it is well known that double numerical integration is usually far less accurate than single numerical quadrature due to accumulation of errors. This problem of uneven accuracy in the determination of u_*' and u_* can be resolved by means of the integral representation of u_* in terms of M_* as it appears in (2.2.15). In dimensionless form, (2.2.15) can be written as:

$$\bar{u}_*(\bar{z}) = -\int_0^{\bar{\ell}} \overset{o}{G}(\bar{z},\bar{s})\bar{M}_*(\bar{s})d\bar{s} + \bar{u}_*(0)\left(1 - \frac{\bar{z}}{\bar{\ell}}\right) + \bar{u}_*(\bar{\ell})\left(\frac{\bar{z}}{\bar{\ell}}\right) \quad (5.3.1)$$

where $\overset{o}{G}(\bar{z},\bar{s})$ is defined in (5.2.3). As is apparent from (5.3.1), once $\bar{M}_*(\bar{z})$ is known, $\bar{u}_*(\bar{z})$ can be obtained from it by any acceptable quadrature rule (e.g., trapezoidal or Simpson's rule). More

importantly, however, (5.3.1) can be differentiated and thereby
generates an integral representation of u'_* as well:

$$\overline{u}'_*(\overline{z}) = -\int_0^{\overline{l}} \frac{\partial \overset{o}{G}}{\partial \overline{z}}(\overline{z},\overline{s}).\overline{M}_*(\overline{s})d\overline{s} + \frac{[\overline{u}(\overline{l})-\overline{u}(0)]}{\overline{l}} \qquad (5.3.2)$$

where

$$\frac{\partial \overset{o}{G}}{\partial \overline{z}}(\overline{z},\overline{s}) = -RS * \begin{cases} \left(1 - \dfrac{\overline{s}}{\overline{l}}\right) & , \quad \overline{z}<\overline{s} \\[2em] \left(\dfrac{\overline{s}}{\overline{l}}\right) & , \quad \overline{z}>\overline{s} \ . \end{cases} \qquad (5.3.3)$$

Thus, $\overline{u}'_*(\overline{z})$ can also be obtained by a single integration of $\overline{M}_*(\overline{z})$. This
illustrates one further advantage of employing integral representations.

5.4 PERFORMANCE

By means of the method outlined in the previous sections, the dis-
placement, slope, and bending moment of the bar can be determined. To
obtain the best performance, the following basic criteria should be
observed: (i) the nodal points should be distributed in such a way that
the characteristics of the inhomogeneous terms and, to a certain extent,
the kernel function of the integral equation are represented adequately.
As an example, this criterion suggests that there should be more nodes
near the top end as the inhomogeneous terms vary rapidly at that
locality (see Figure 4.6 and 4.7).
(ii) Suitable choices of nodal spacings and numerical quadratures which

take into account the special nature of the kernel should be employed to
ensure an accurate evaluation of the matrix [K]. For instance, it was
considered important in most cases to perform refined (composite)
quadratures for the tridiagonal terms of [K] because of the localized
nature of the kernel in the present problem.

With these basic considerations, the numerical scheme was found to
perform extremely well; fast and stable convergence was demonstrated in
all cases being examined. For a bar length of 50 radii, a value chosen
for illustration purposes, the use of 20 to 30 nodes was found to be
adequate for the frequency range of interest ($\bar{\omega}$ = 0.0 to 0.5). Details
of the solutions are presented in Chapter VI.

CHAPTER VI

ILLUSTRATIVE NUMERICAL RESULTS

By the method described in Chapter V, the Fredholm integral equation associated with the dynamic interaction problem can be solved accurately. The numerical solution of the equation furnishes the bending moment profile and the top and bottom displacements of the bar, which, in turn, render the response of the bar and the embedding medium fully determinate. In this chapter, selected results of the analysis are presented to illustrate some of the basic features of the solution. Because of the large number of parameters involved in this problem, attention is focused primarily on those that strongly influence the behavior of the solution. Consistent with general engineering interests and the initial intention of the formulation, results are presented for the low-frequency range ($\bar{\omega}$=0.0 to 0.5) only although validity of the theory in a wider range is expected.

6.1 ZERO-FREQUENCY (STATIC) RESPONSE

Before proceeding to the discussion of the dynamic behavior, it is relevant to examine first the response of the embedded bar under static lateral loadings. In addition to its intrinsic interests, the static solution provides a basis of comparison for the more complicated dynamic response.

Although the formulation of the problem is inherently based on dynamic considerations, the static solution can be obtained from it by

letting $\bar{\omega} \rightarrow 0$. Results for a wide range of flexibilities under shear-loading-only and moment-loading-only conditions are displayed in Figures 6.1 to 6.3 and 6.4 to 6.6, respectively. As can be observed from the figures, all the curves represent functions that are very smooth throughout their interval of definition $0 \leq z/a \leq \ell/a$. The bending moment of the bar under the shear-loading condition (see Figure 6.1) typically reaches its peak value within the top half of the bar depending on the bar/medium stiffness ratio $\bar{E}$. In contrast, the maximum bending moment always occurs at the top of the bar for the moment-loading condition as is evident from Figure 6.4. Although it is probably more apparent in the moment-loading case because of scaling, one common feature for these two types of bending moment profile is a definite reversal of sign at some depth for bars that are not too rigid. This is particularly interesting in view of the absence of such a characteristic in some of the currently accepted numerical treatments of this static problem, e.g., Poulos and Davis [40].

The slopes of the bar for the two loading conditions are shown in Figures 6.2 and 6.5 while the corresponding deflection profiles are illustrated in Figures 6.3 and 6.6, respectively. In accord with the reciprocity theorem in elastostatics, the top rotation due to horizontal force is found to be equal to the top displacement due to applied moment with negligible errors for the whole range of stiffness ratios.
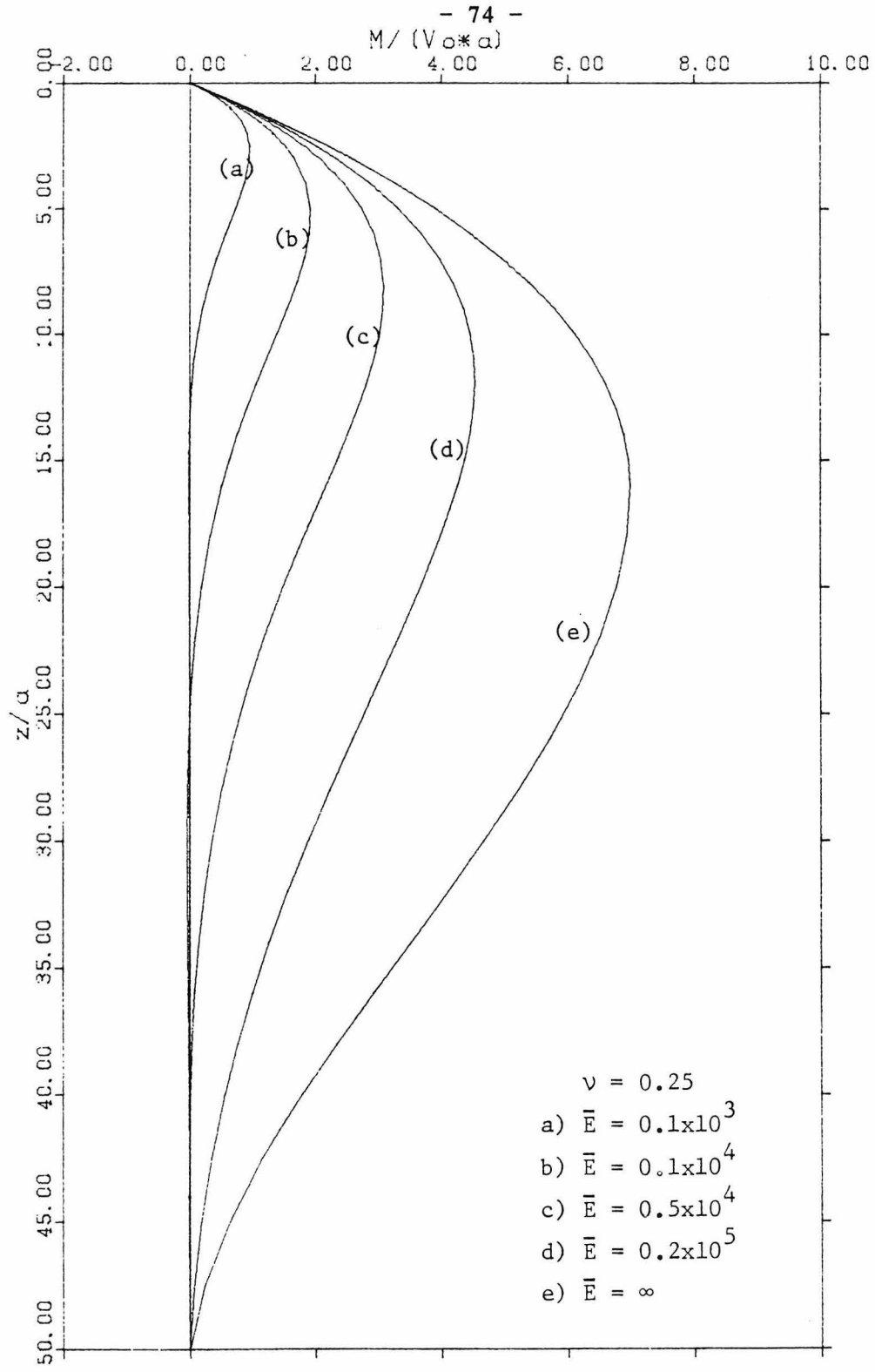
Figure 6.1   Static Solutions under Unit Shear $\overline{V}_0$:
Bending Moment Profiles ($\overline{\ell}$ = 50)
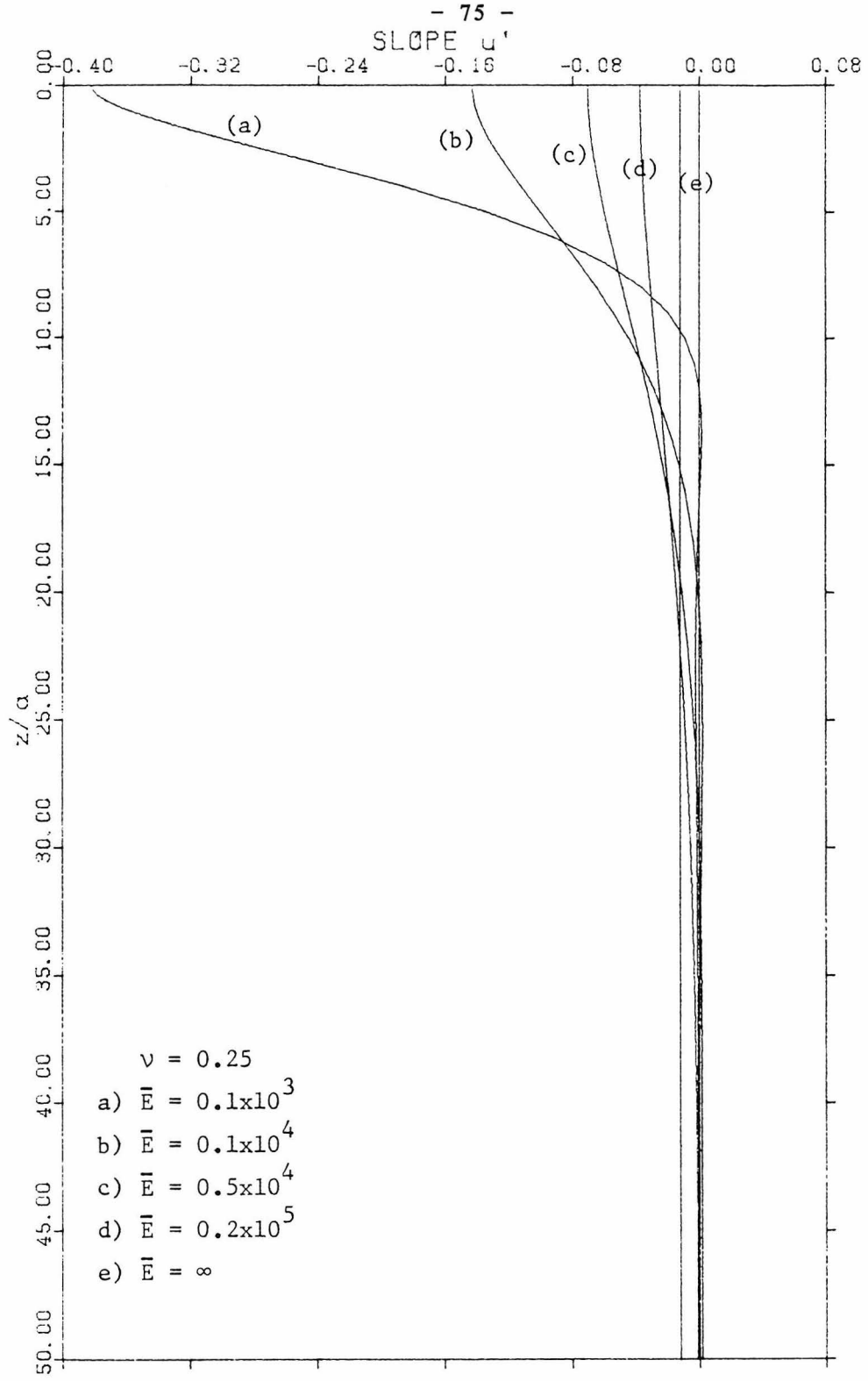
Figure 6.2   Static Solutions under Unit Shear $\overline{V}_0$:
              Slope Profiles ($\overline{\ell}$ = 50)
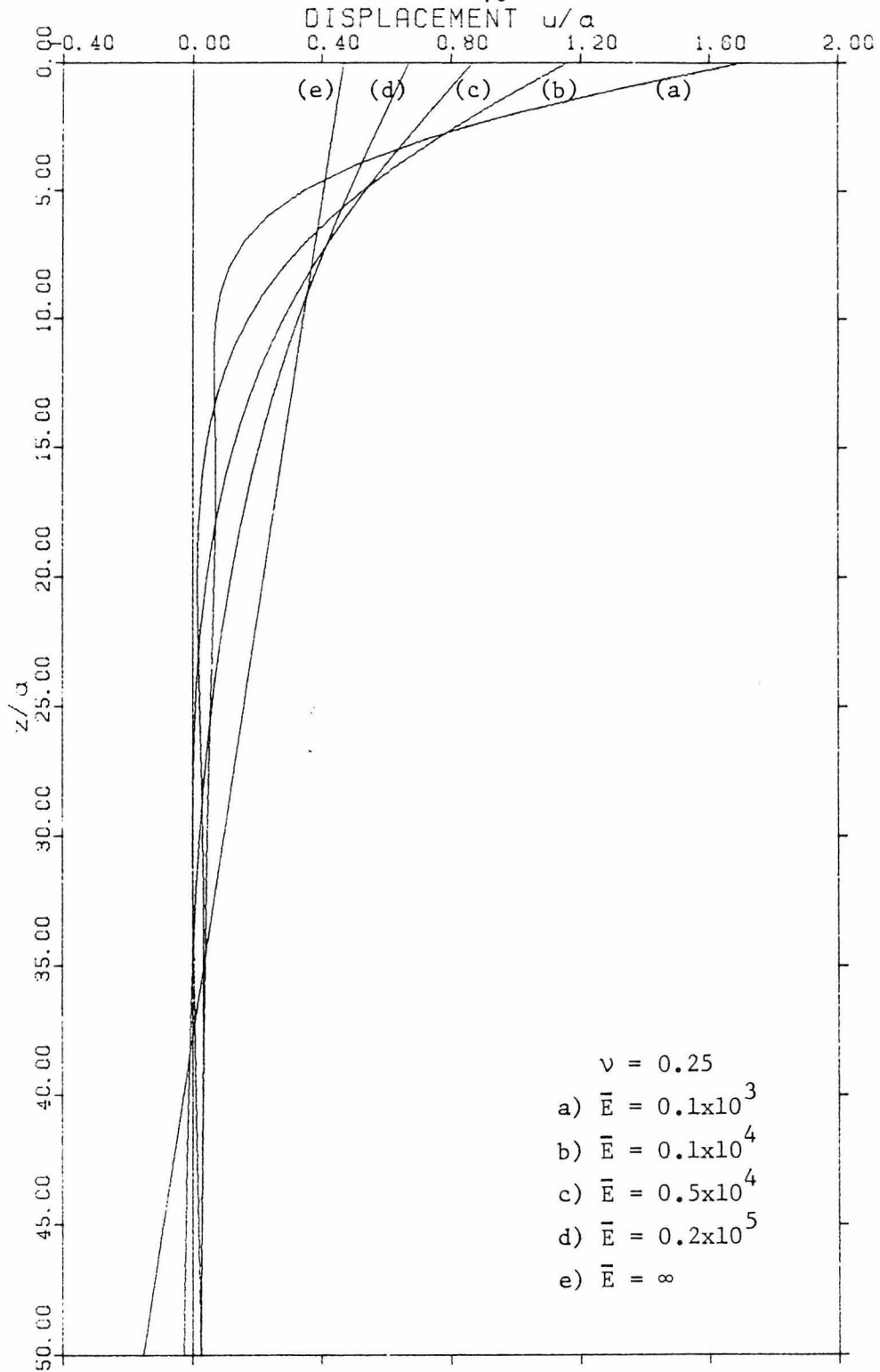
Figure 6.3   Static Solutions under Unit Shear $\overline{V}_0$:
Displacement Profiles ($\overline{\ell}$ = 50)
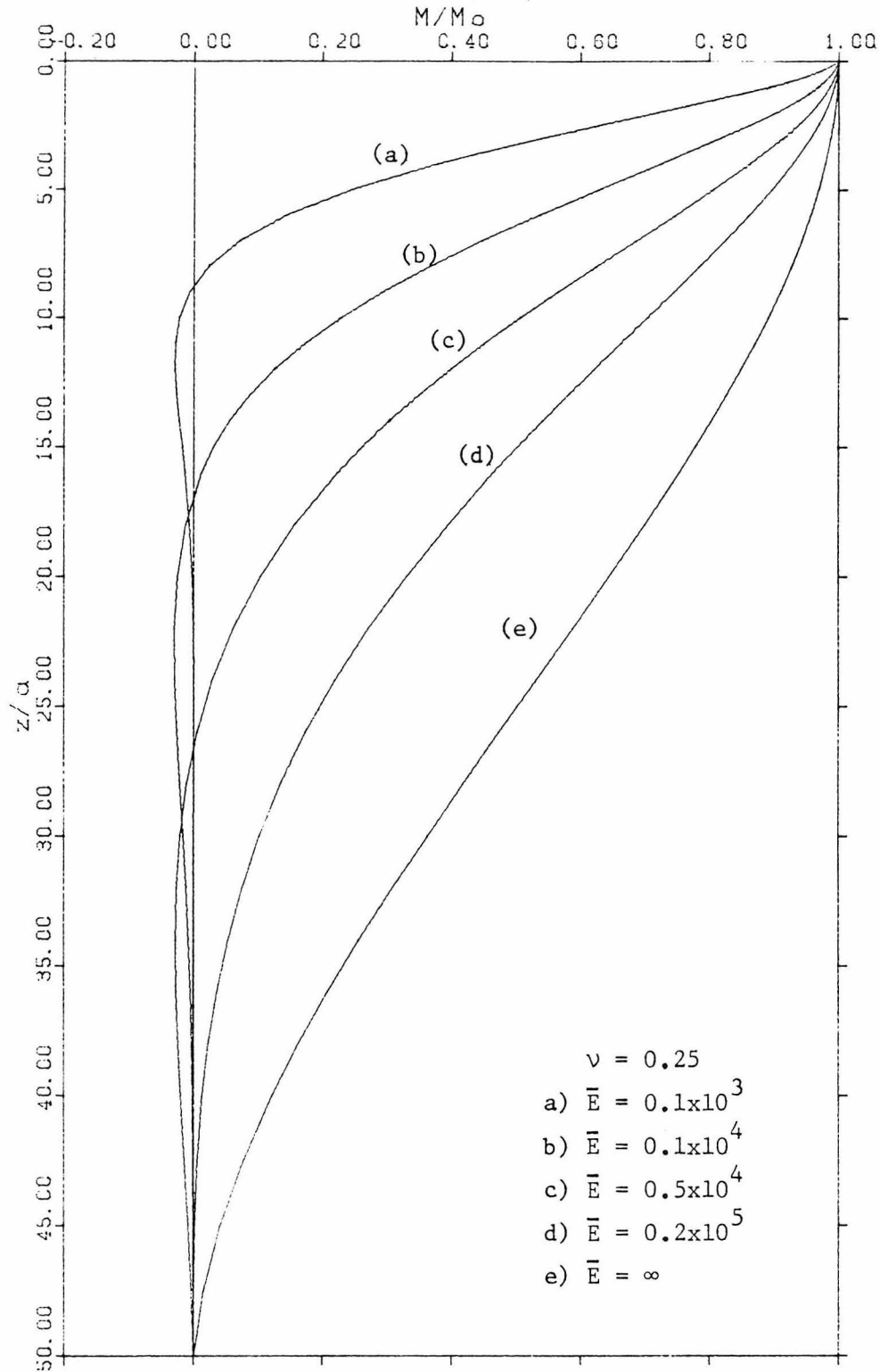
Figure 6.4   Static Solutions under Unit Moment $\overline{M}_0$:
Bending Moment Profiles ($\overline{\ell}$ = 50)
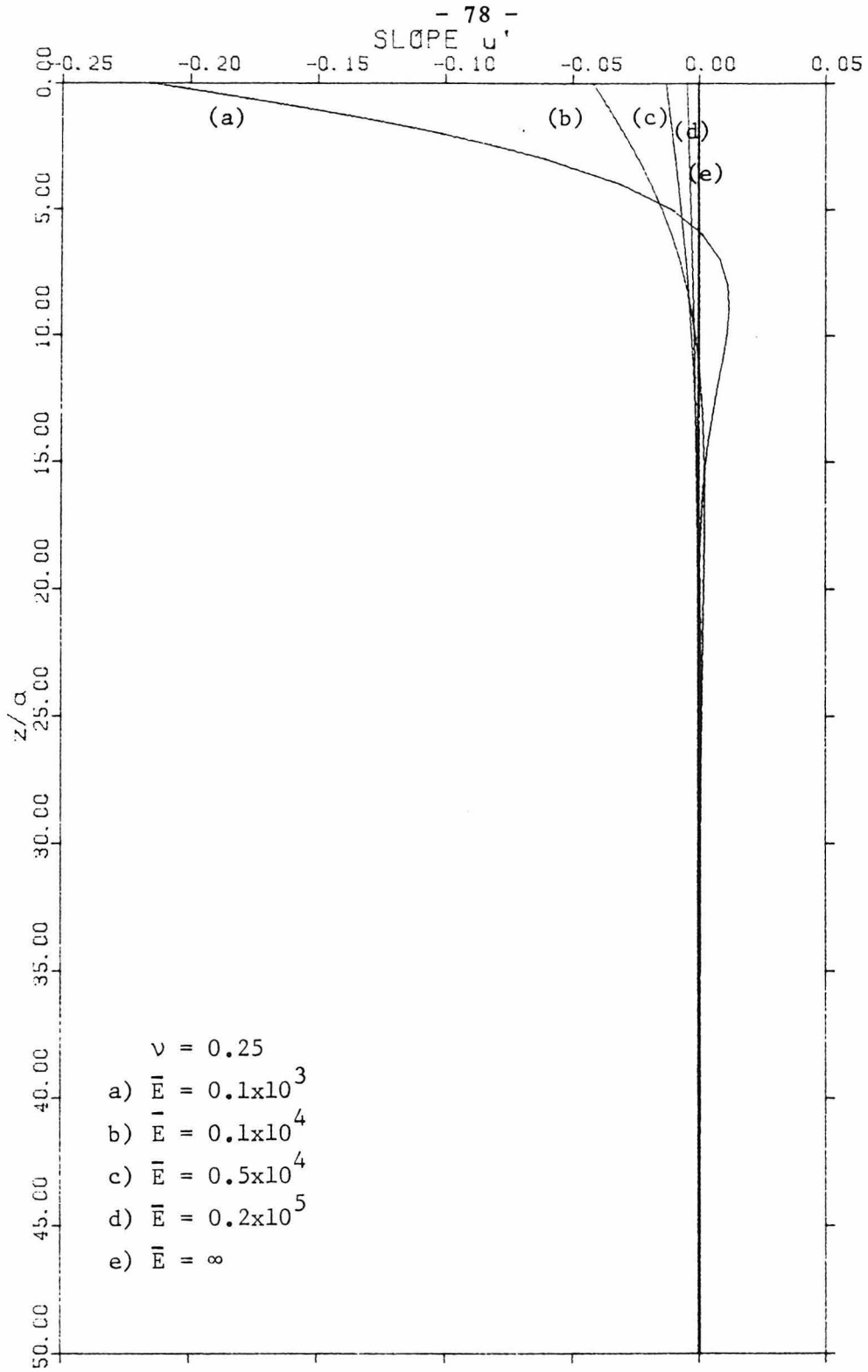
Figure 6.5   Static Solutions under Unit Moment $\overline{M}_0$:
Slope Profiles ($\overline{\ell}$ = 50)
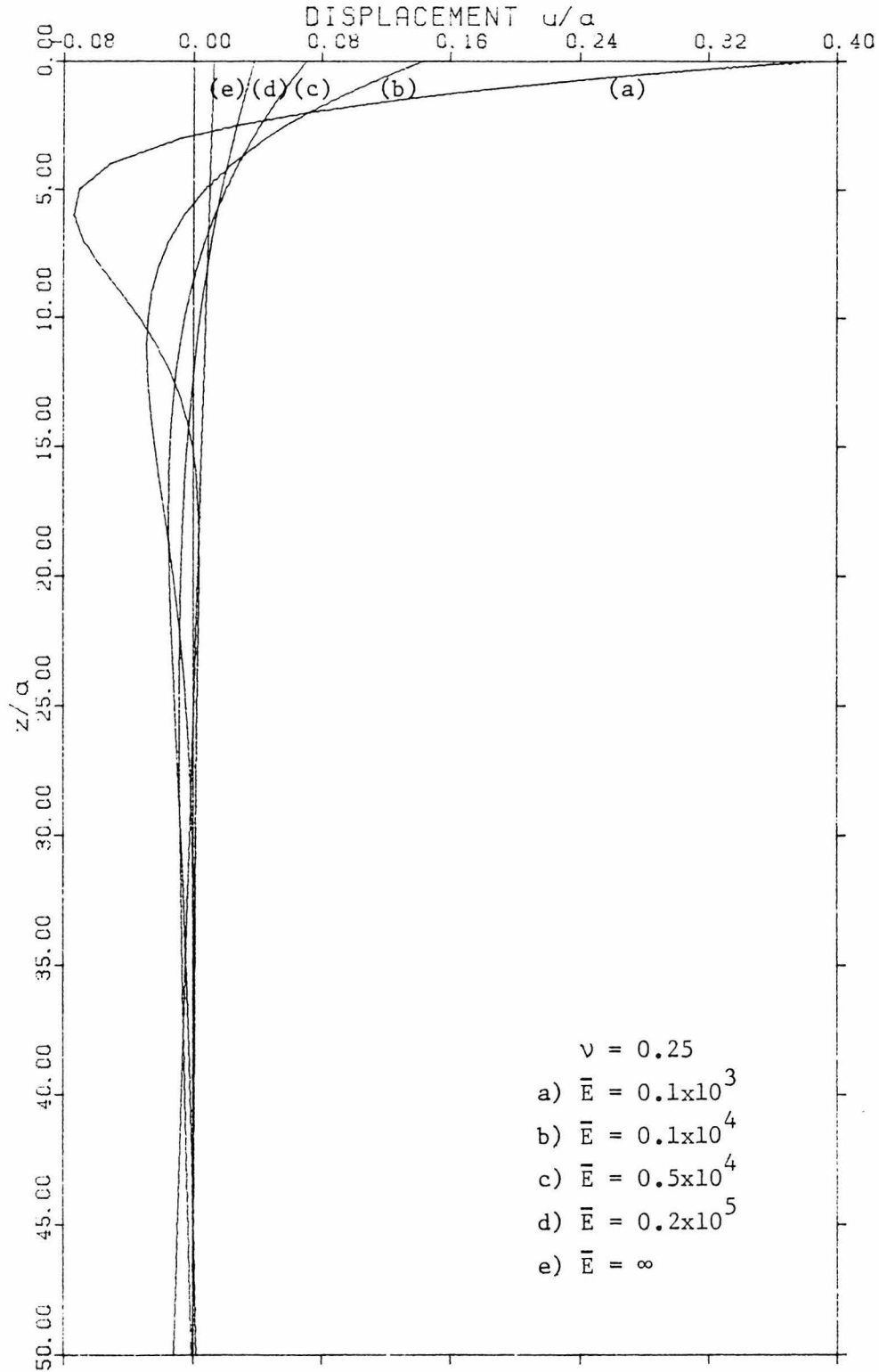
Figure 6.6   Static Solutions under Unit Moment $\overline{M}_0$:
Displacement Profiles ($\overline{\ell}$ = 50)

6.2 DYNAMIC RESPONSE

Following the preceding discussion of the static behavior, atten-
tion will now be focused on the dynamic response of the bar under
harmonic excitations. As illustrations, the responses of the embedded
bar at two excitation frequencies, $\bar{\omega}$ = 0.2 and 0.5 are displayed in Fig-
ures 6.7 to 6.12 and Figures 6.13 to 6.18, respectively, for a typical
set of physical parameters. Since the excitation and the response are
out-of-phase in general, all response quantities are represented in
complex notation, with the real and imaginary parts representing the in-
phase and 90°-out-of-phase components, respectively.

A comparison of the figures with the results in the last section
reveals that the real parts of the dynamic solutions are very similar to
the corresponding static solutions, at least for the range of frequency
under consideration. It is, however, apparent that the oscillatory
nature has become more pronounced and frequency-dependent in the dynamic
case. As can be deduced from the figures, the characteristic wavelength
of the oscillation is, in general, an increasing function of stiffness
ratio $\bar{E}$ and a decreasing function of the excitation frequency $\bar{\omega}$. These
trends are probably more apparent in the imaginary part of the response
which has zero static bias; i.e., the imaginary part is identically zero
when $\bar{\omega}$ = 0.

The effect of embedment on the response is illustrated in Figures
6.19 and 6.20 wherein bars of different lengths ($\bar{l}$ = 30, 40 and 50) are
considered. As is evident from the figures, there is a definite reduc-
tion in deflection and rotation as $\bar{l}$ is increased from 30 to 40 for the
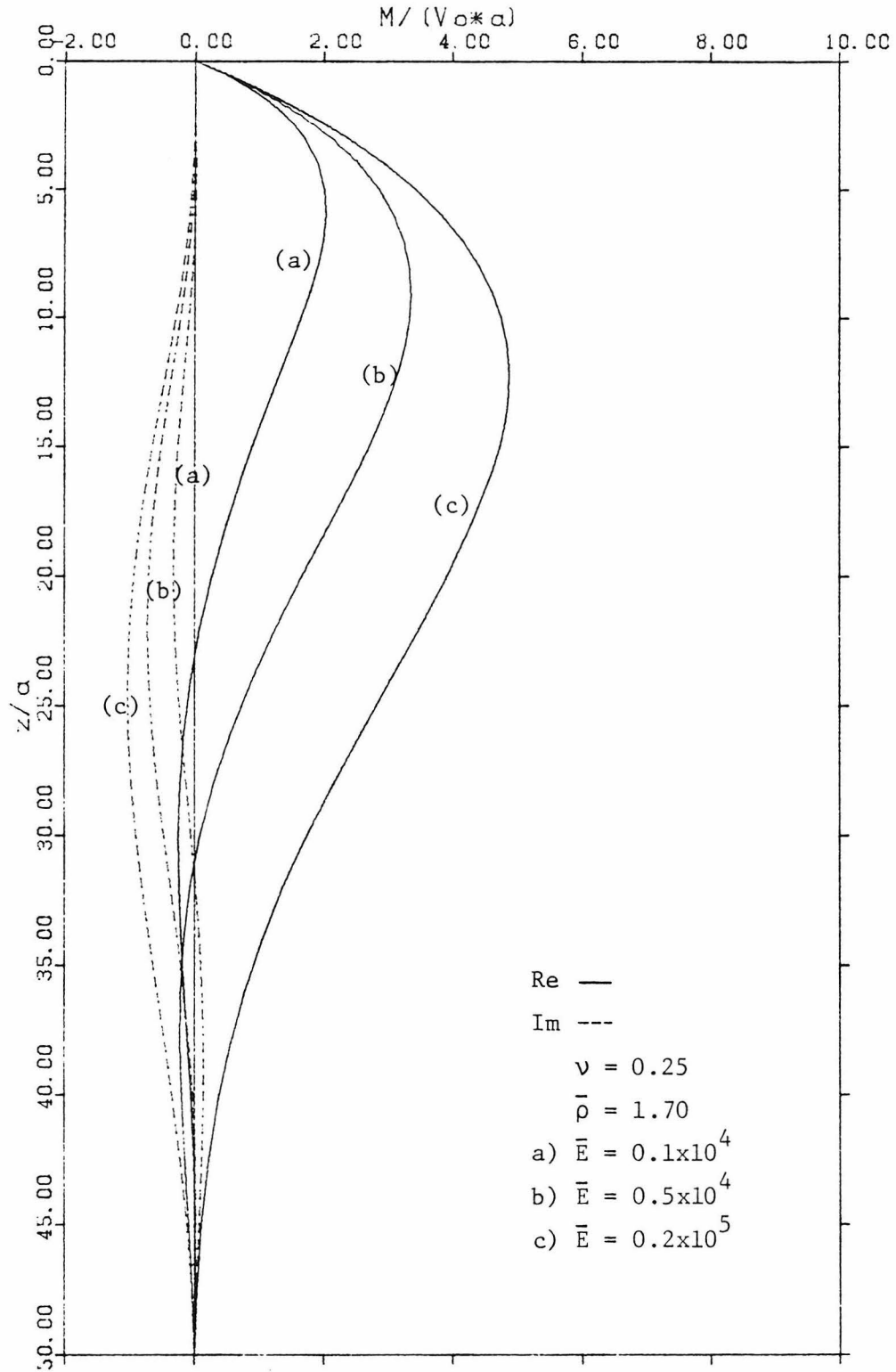
Figure 6.7   Dynamic Solutions under Unit Shear $\bar{V}_0$ at $\bar{\omega}=0.2$:
Bending Moment Profiles ($\bar{\ell} = 50$)

Figure 6.8 Dynamic Solutions under Unit Shear $\bar{V}_0$ at $\bar{\omega}$=0.2: Slope Profiles ($\bar{\ell}$ = 50)
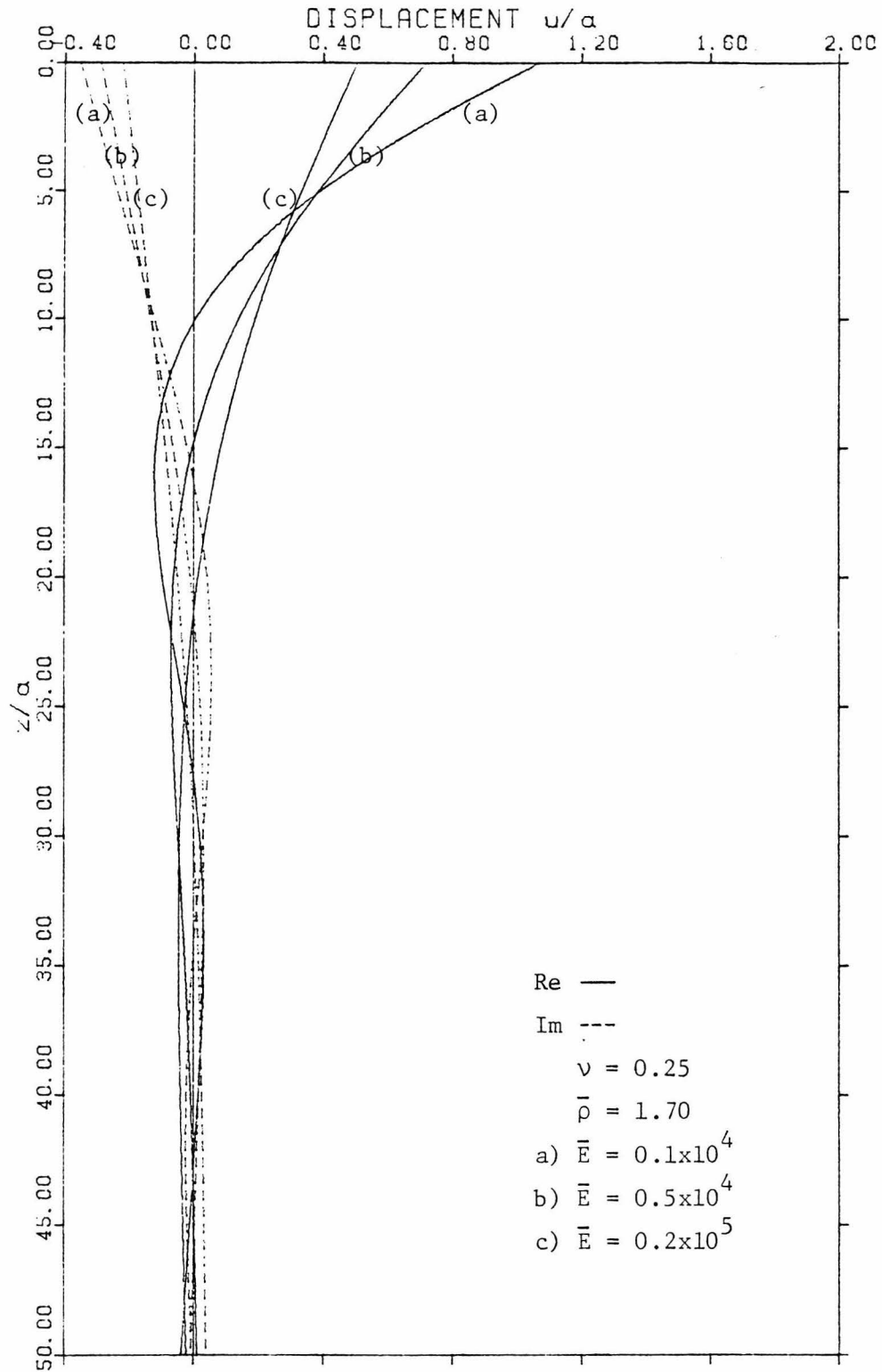
Figure 6.9   Dynamic Solutions under Unit Shear $\bar{V}_0$ at $\bar{\omega}=0.2$:
Displacement Profiles ($\bar{\ell}$ = 50)
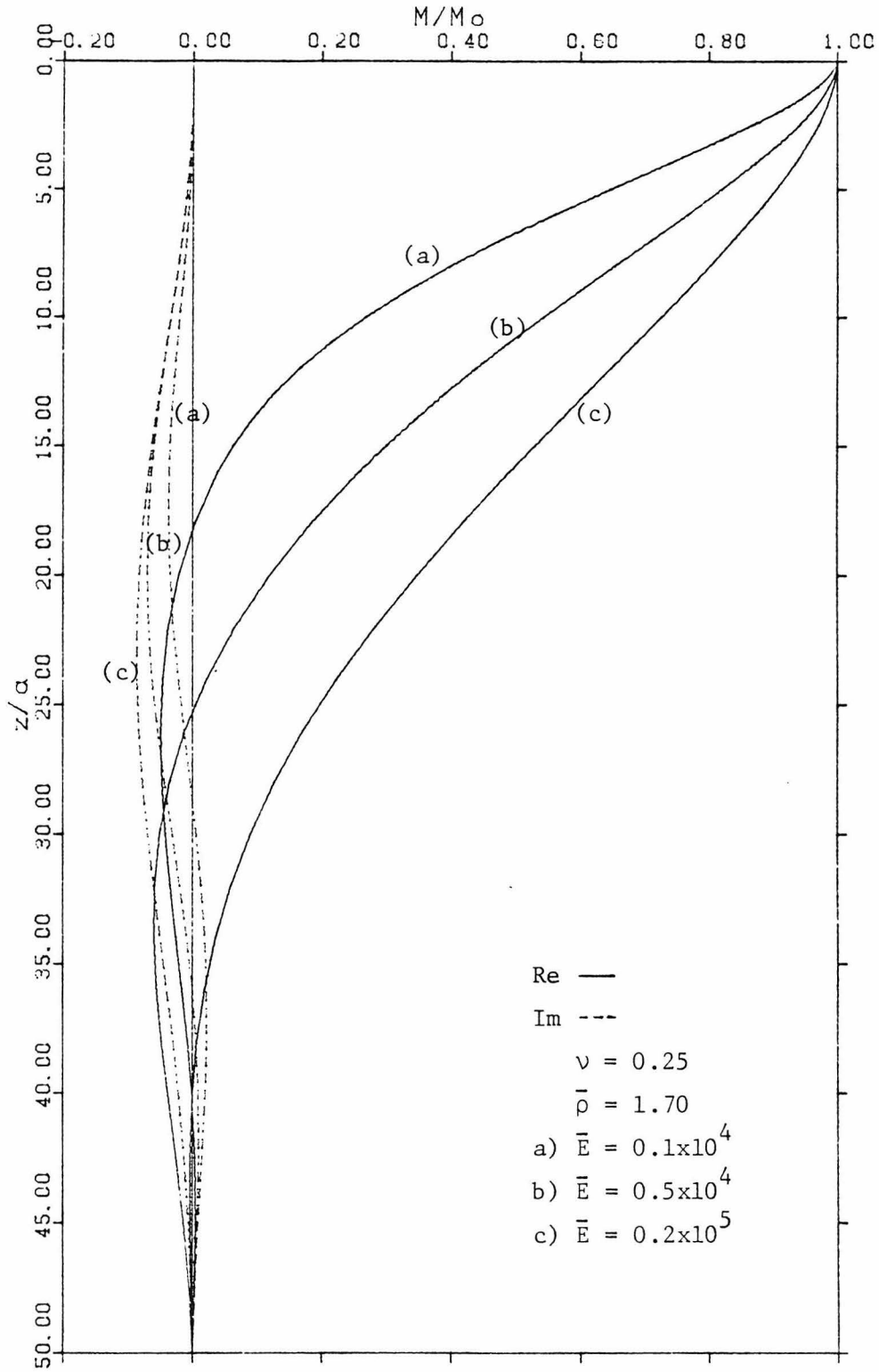
Figure 6.10 Dynamic Solutions under Unit Moment $\bar{M}_0$ at $\bar{\omega}$=0.2
Bending Moment Profiles ($\bar{\ell}$ = 50)
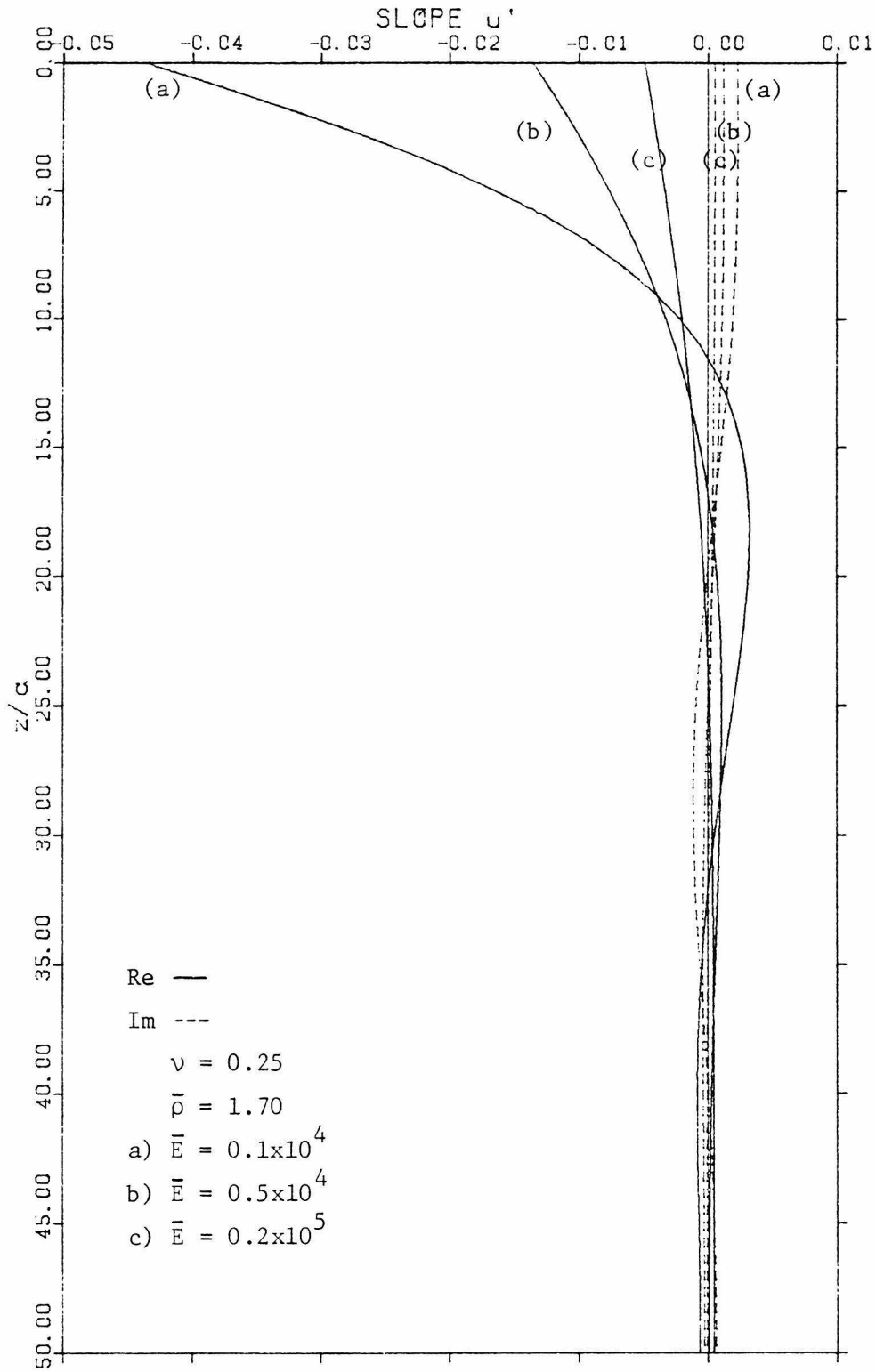
Figure 6.11 Dynamic Solutions under Unit Moment $\bar{M}_0$ at $\bar{\omega}$=0.2:
Slope Profiles ($\bar{\ell}$ = 50)
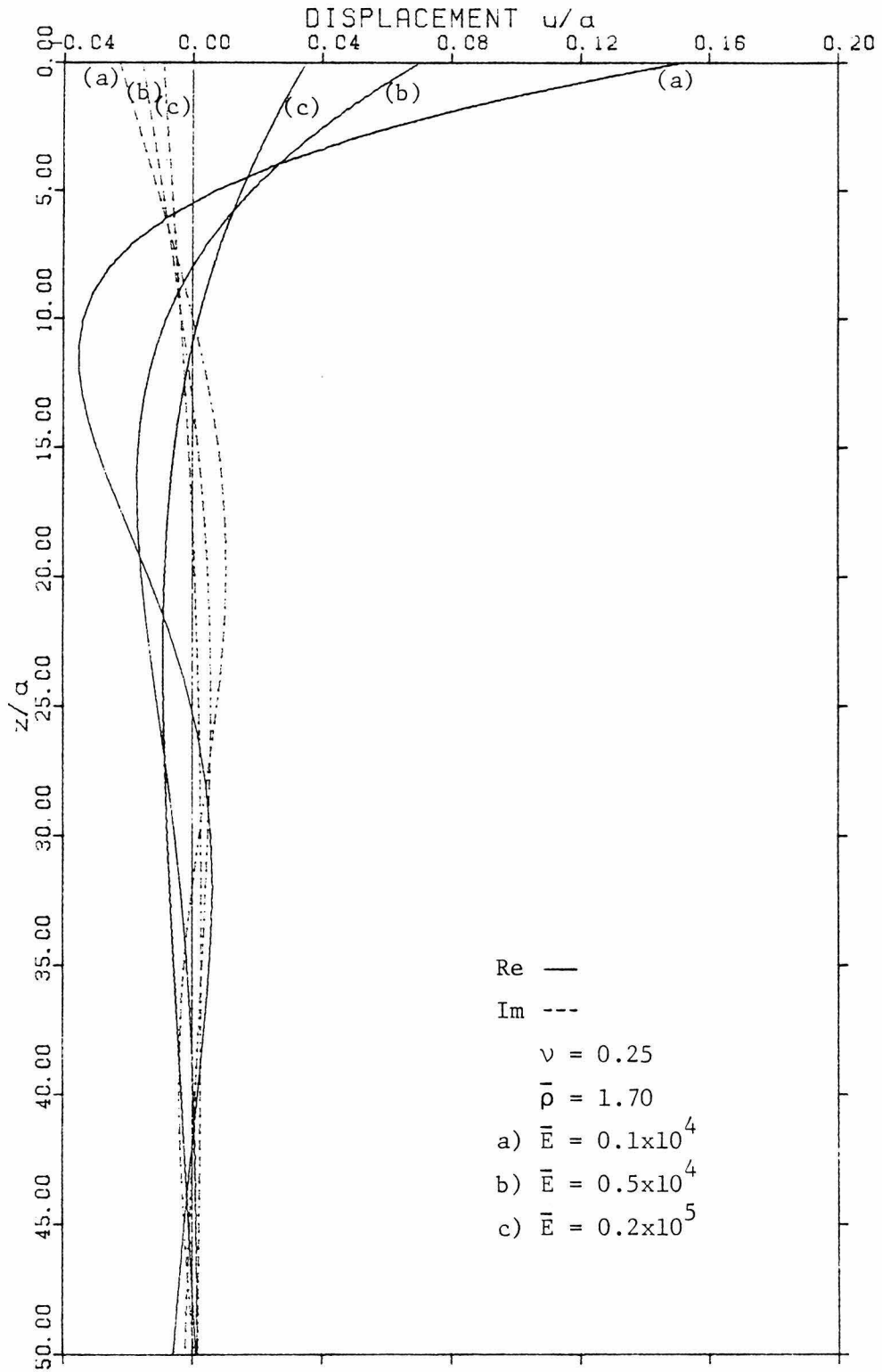
Figure 6.12   Dynamic Solutions under Unit Moment $\bar{M}_0$ at $\bar{\omega}=0.2$:
Displacement Profiles ($\bar{\ell}$ = 50)
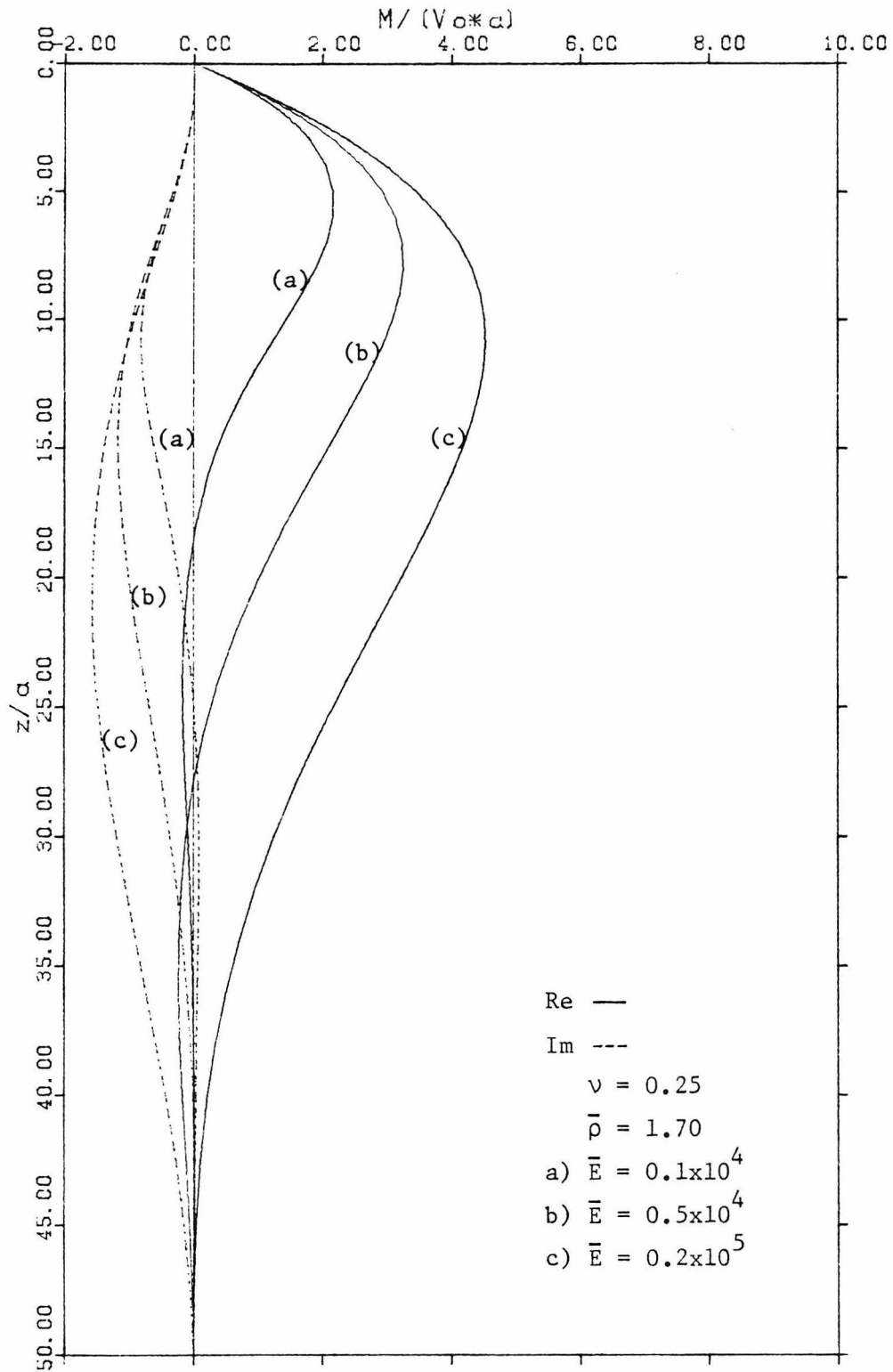
Figure 6.13 Dynamic Solutions under Unit Shear $\bar{V}_0$ at $\bar{\omega}=0.5$:
Bending Moment Profiles ($\bar{\ell} = 50$)
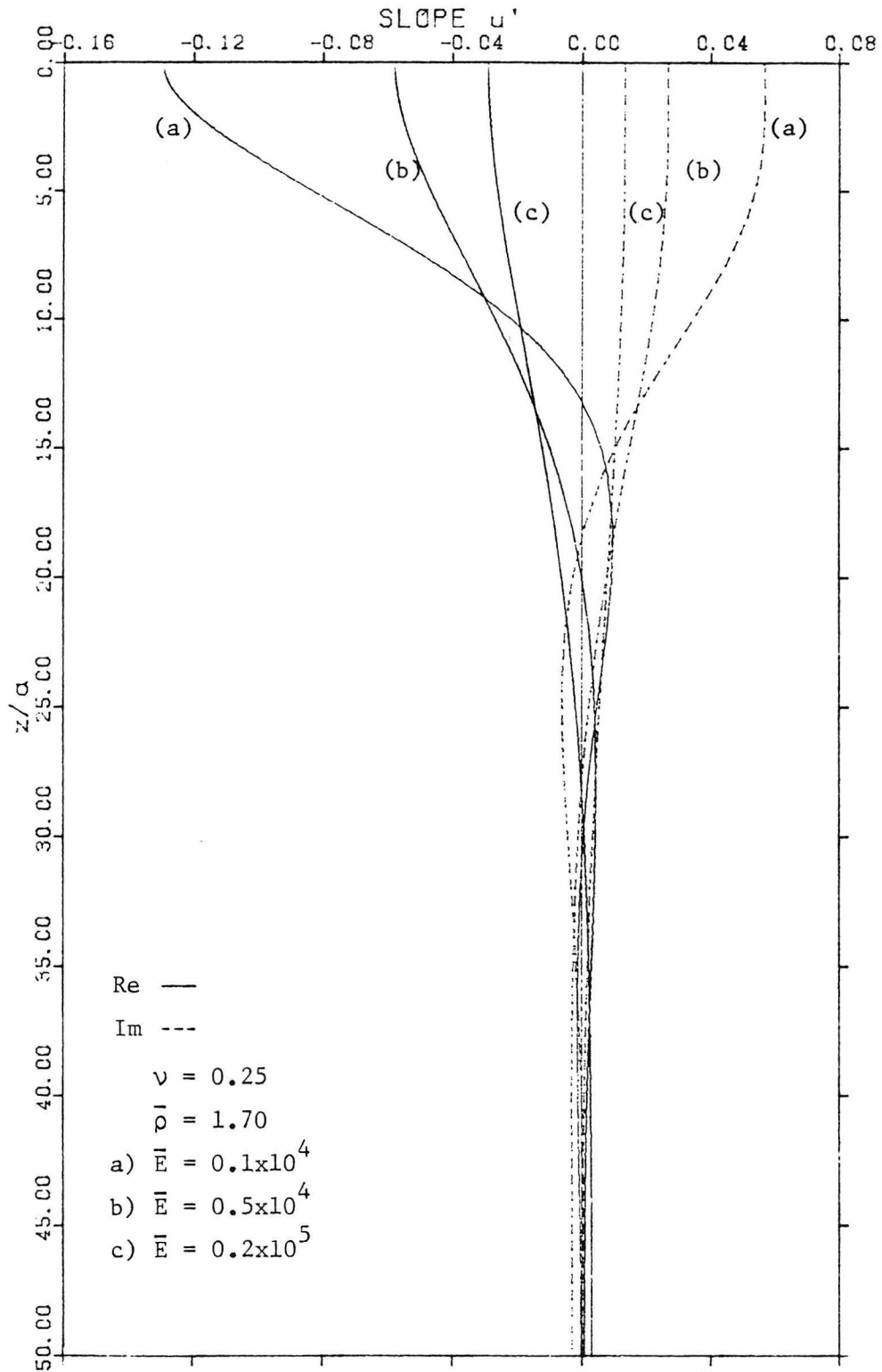
Figure 6.14 Dynamic Solutions under Unit Shear $\bar{V}_0$ at $\bar{\omega}$=0.5 :
Slope Profiles ($\bar{\ell}$ = 50)
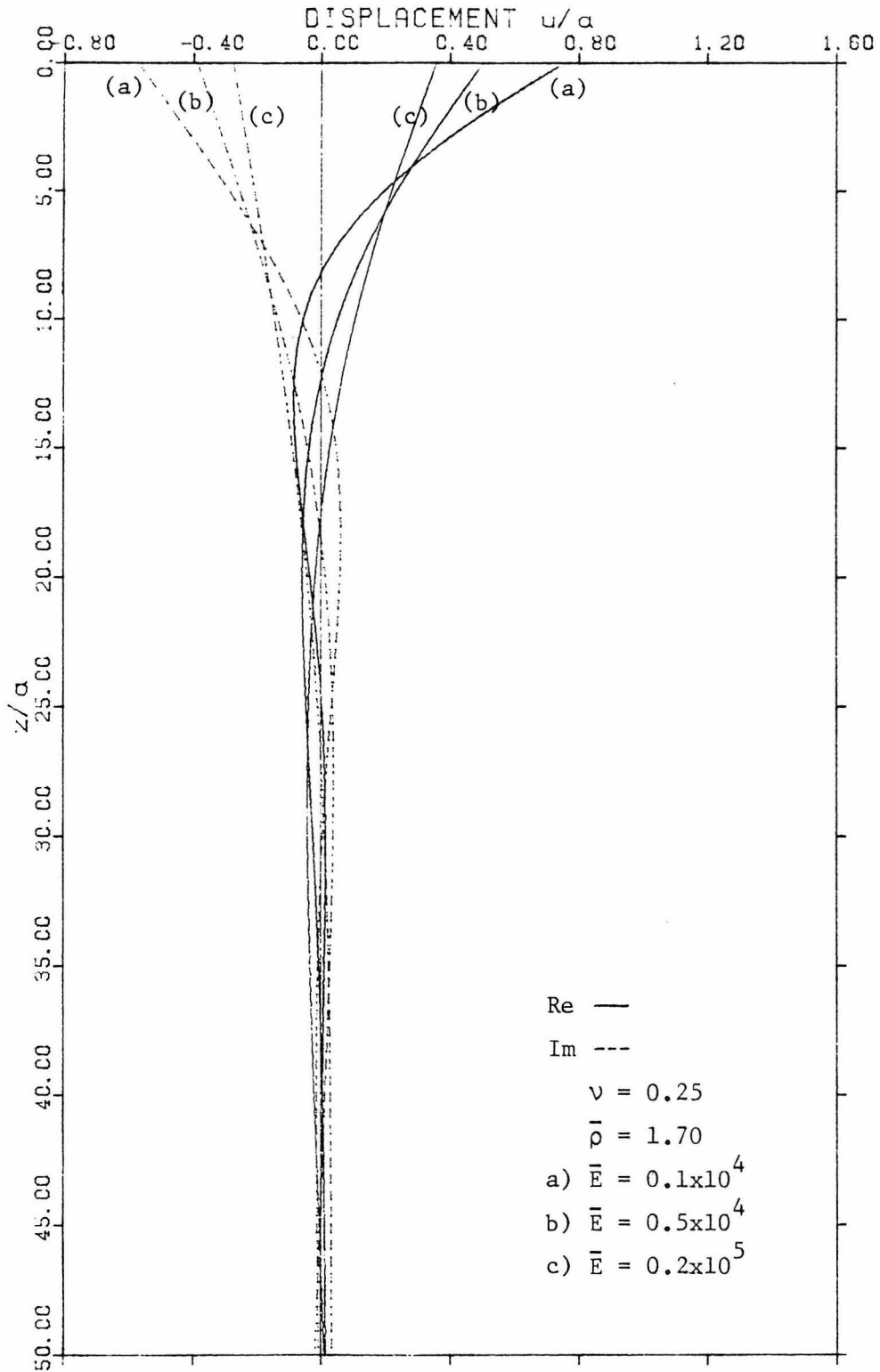
Figure 6.15 Dynamic Solutions under Unit Shear $\bar{V}_0$ at $\bar{\omega}=0.5$:
Displacement Profiles ($\bar{\ell} = 50$)
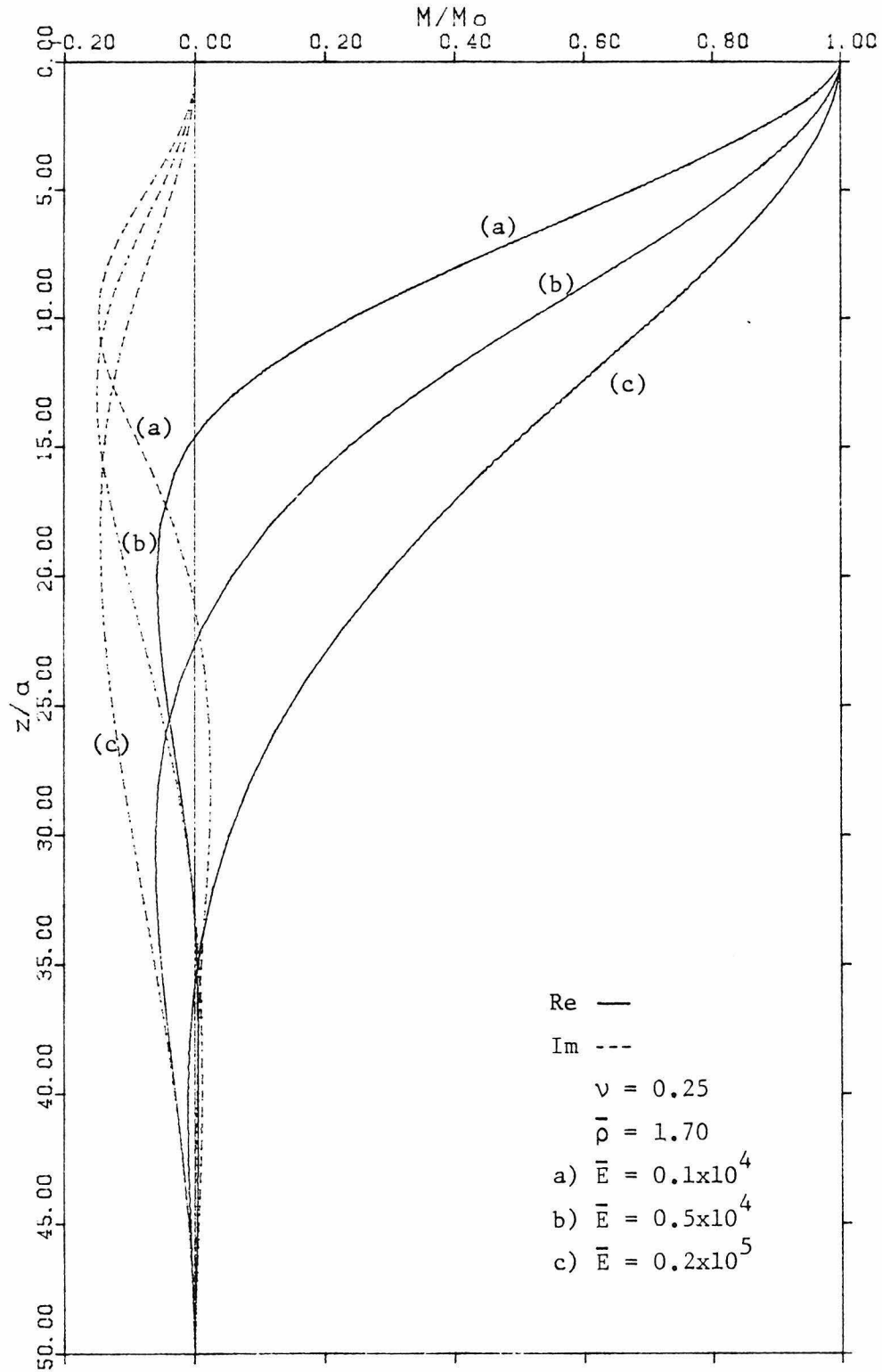
Figure 6.16   Dynamic Solutions under Unit Moment $\bar{M}_0$ at $\bar{\omega}=0.5$:
Bending Moment Profiles ($\bar{\ell} = 50$)
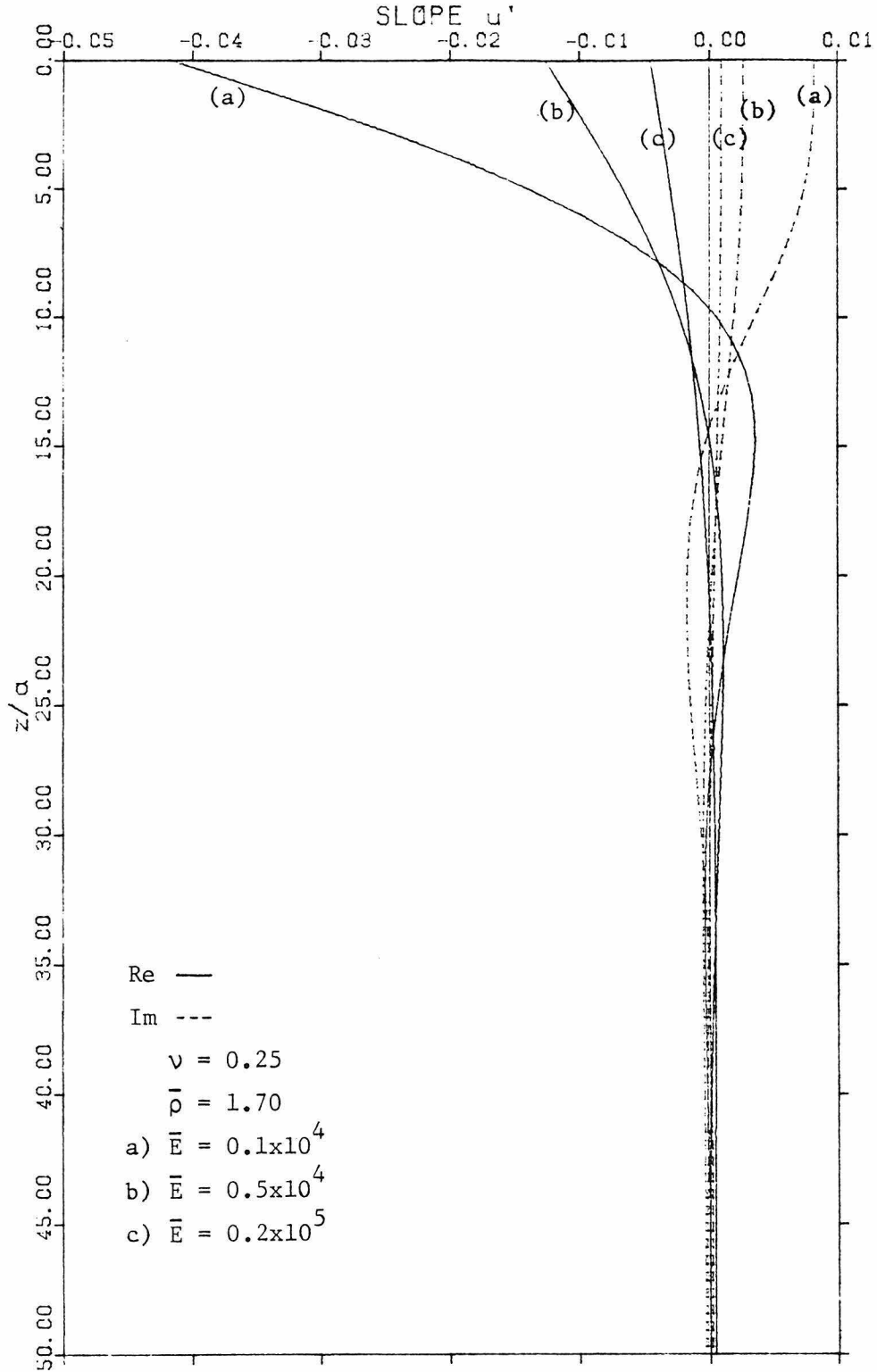
Figure 6.17   Dynamic Solutions under Unit Moment $\bar{M}_0$ at $\bar{\omega}=0.5$:
Slope Profiles ($\bar{\ell}$ = 50)
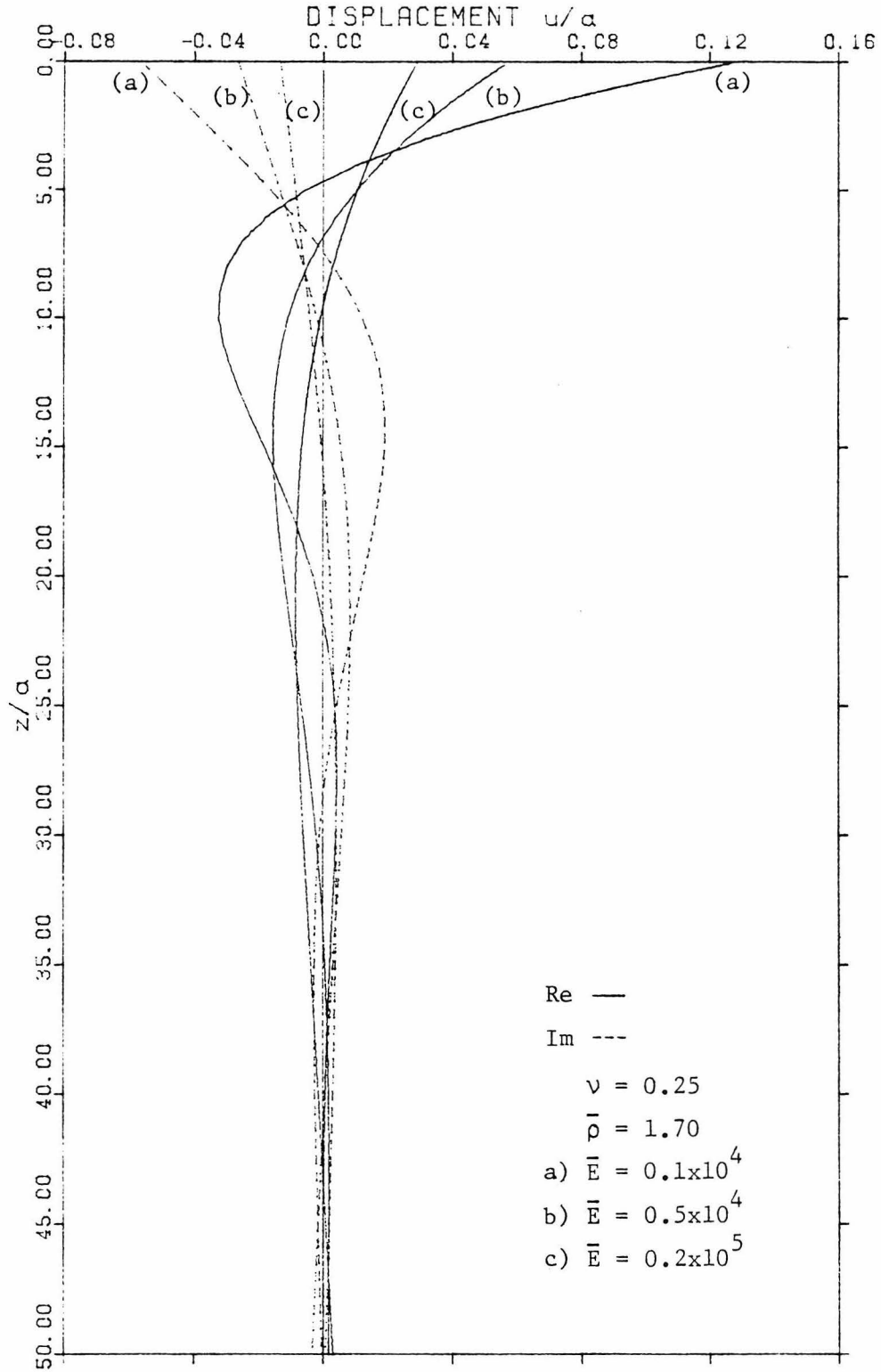
Figure 6.18   Dynamic Solutions under Unit Moment $\bar{M}_0$ at $\bar{\omega}$=0.5: Displacement Profiles ($\bar{\ell}$ = 50)
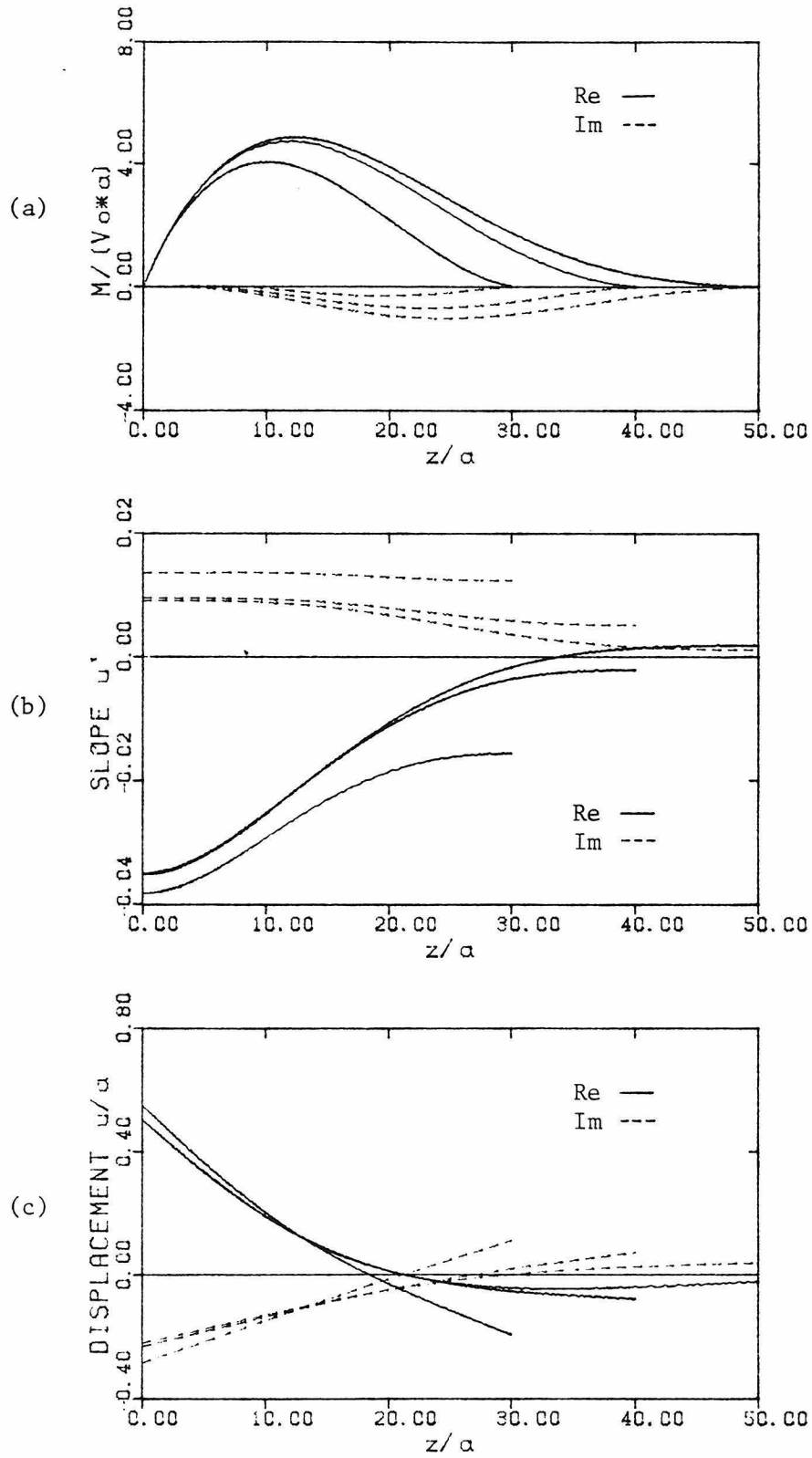
Figure 6.19   Dynamic Response due to Shear $\bar{V}_0$ for Bars of
Length $\bar{\ell}=30,40,50$ ($\bar{\omega}=0.5,\bar{E}=.2\times10^5,\bar{\rho}=1.7,\nu=.25$)
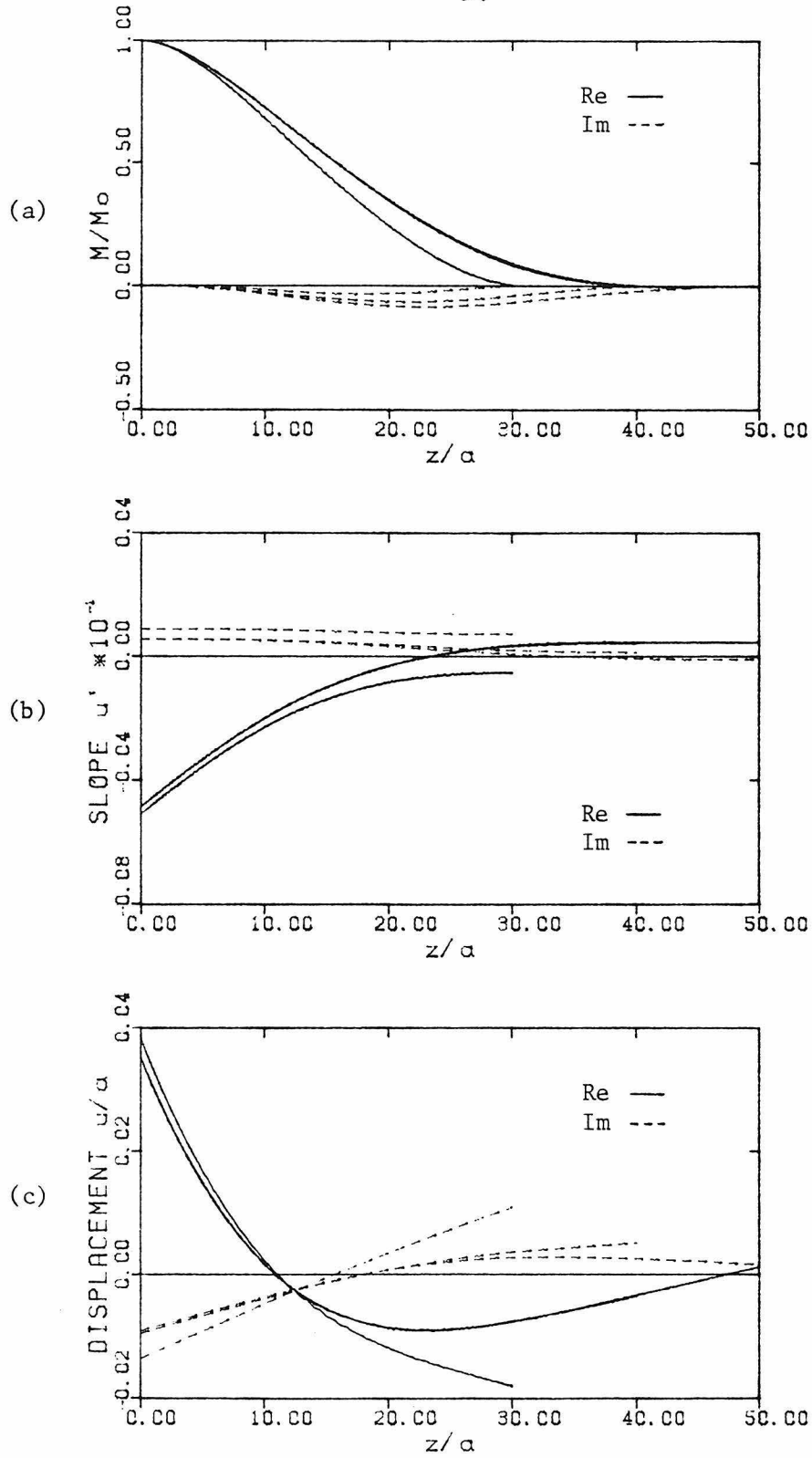
Figure 6.20   Dynamic Response due to Moment $\bar{M}_0$ for Bars of Length $\bar{\ell}$=30,40,50 ($\bar{\omega}$=0.5, $\bar{E}$=.2x10^5, $\bar{\rho}$=1.7, ν=.25)

chosen set of parameters. The change, however, becomes minimal for the top region of the bar when $\bar{l}$ is further increased to 50. This confirms the intuitive idea of a 'limiting length' beyond which further embedment will result in no significant change in the top response of the bar. It is interesting to note that the 'limiting length' appears to be dependent, in addition to the bar/medium parameters and configurations, on the loading conditions; in the example cited, the solutions for $\bar{l}$ = 40 and 50 apparently lie closer to each other under the moment-loading condition than under the shear-loading condition.

The influence of mass ratio $\bar{\rho}$ and Poisson's ratio ν on the response has also been examined. As expected, the inertia contribution of the bar was found to be of minor importance for low-frequency excitations such as those under consideration. Nevertheless, it is noteworthy that its influence is mostly on the 90° out-of-phase components of response; depending on the frequency and the mass ratio, an increase of 15% in response values (relative to that of a massless bar) has been observed. At higher frequencies, however, it is expected that the mass ratio will play a much more important role in the solution than what has been indicated. In regard to the effect of Poisson's ratio, it was found that an increase in its value tends to reduce the deflection and rota-tion of the bar while causes an increase in the bending moment. As the choices of mass ratio and Poisson's ratio do not lead to any significant qualitative change in response, the details of their effects are not presented here.

6.3 DYNAMIC COMPLIANCES

In many engineering applications, the item of primary interest is the relationship between the top response of the bar and the applied lateral loadings. This information, which is furnished by the present theory, can be expressed compactly, as

$$
\begin{bmatrix} \Delta \\ \theta \end{bmatrix} = \begin{bmatrix} C_{vv} & C_{vm} \\ C_{mv} & C_{mm} \end{bmatrix} \begin{bmatrix} \overline{V}_0 \\ \overline{M}_0 \end{bmatrix}
\tag{6.1}
$$

where

$$
\begin{aligned}
\Delta &= \overline{u}(0) \\
\theta &= \overline{u}'(0) \\
\overline{V}_0 &= V_0/4\pi\mu a^2 \\
\overline{M}_0 &= M_0/4\pi\mu a^3 \quad .
\end{aligned}
\tag{6.2}
$$

The matrix appearing in (6.1) is usually called the 'lateral compliance matrix' for the system under consideration. Normalized by their corresponding static values, the elements of the matrix for a typical set of physical parameters are shown in Figures 6.21 to 6.24. Comparing Figure 6.22 to Figure 6.24, one can readily see that C_{vm} is identical to C_{mv}, a demonstration of the reciprocity theorem in elastodynamics [12]. It is interesting to note, however, that the nature of C_{vv} is considerably different from that of C_{mv} or C_{mm} in regard to both the real and imaginary parts. This is not totally surprising in view of the influence of loading conditions on the response characteristics as discussed
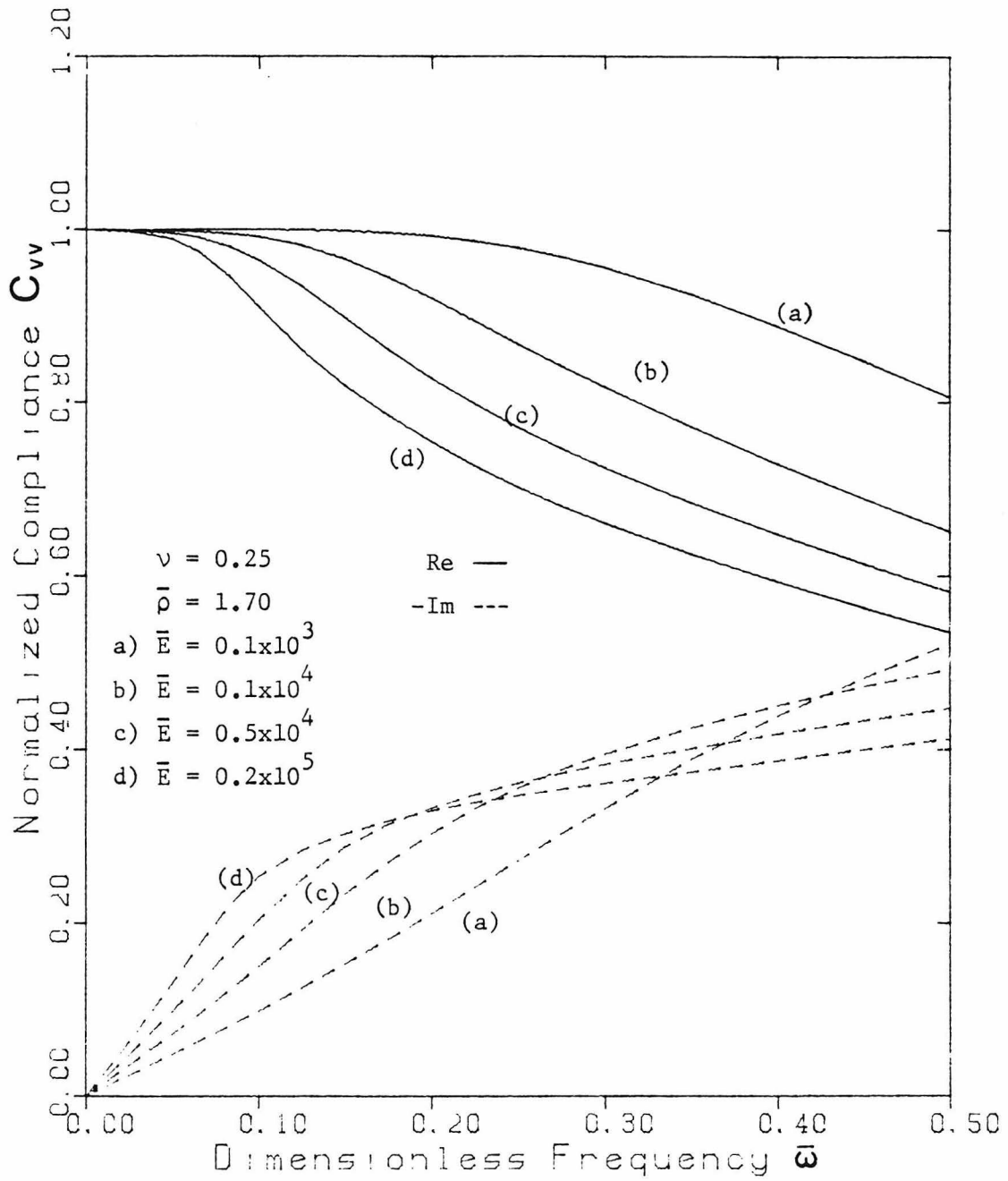
Figure 6.21 Normalized Compliance Function C_{vv} ($\bar{\ell}=50$)
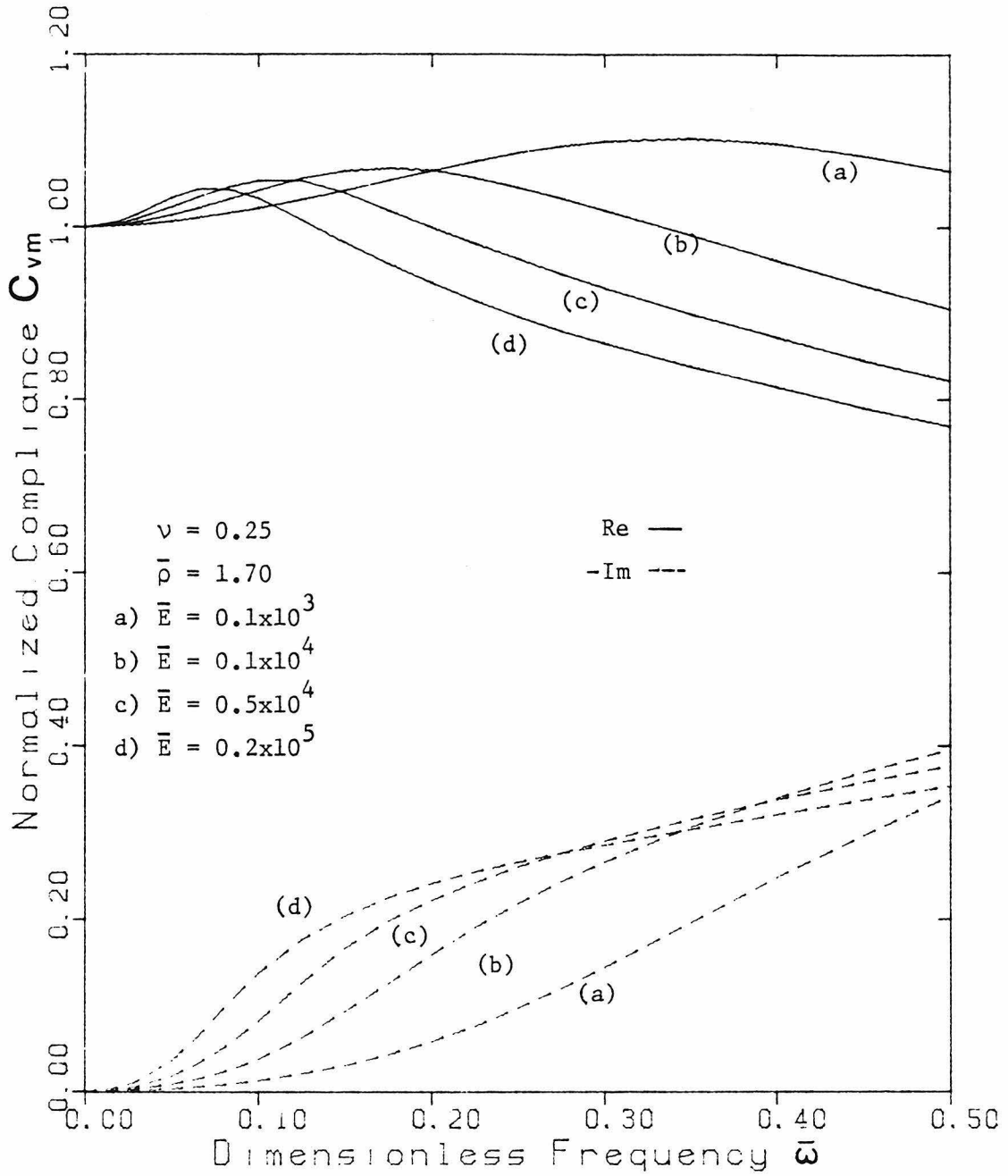
Figure 6.22 Normalized Compliance Function C_{vm} ($\bar{\ell}=50$)
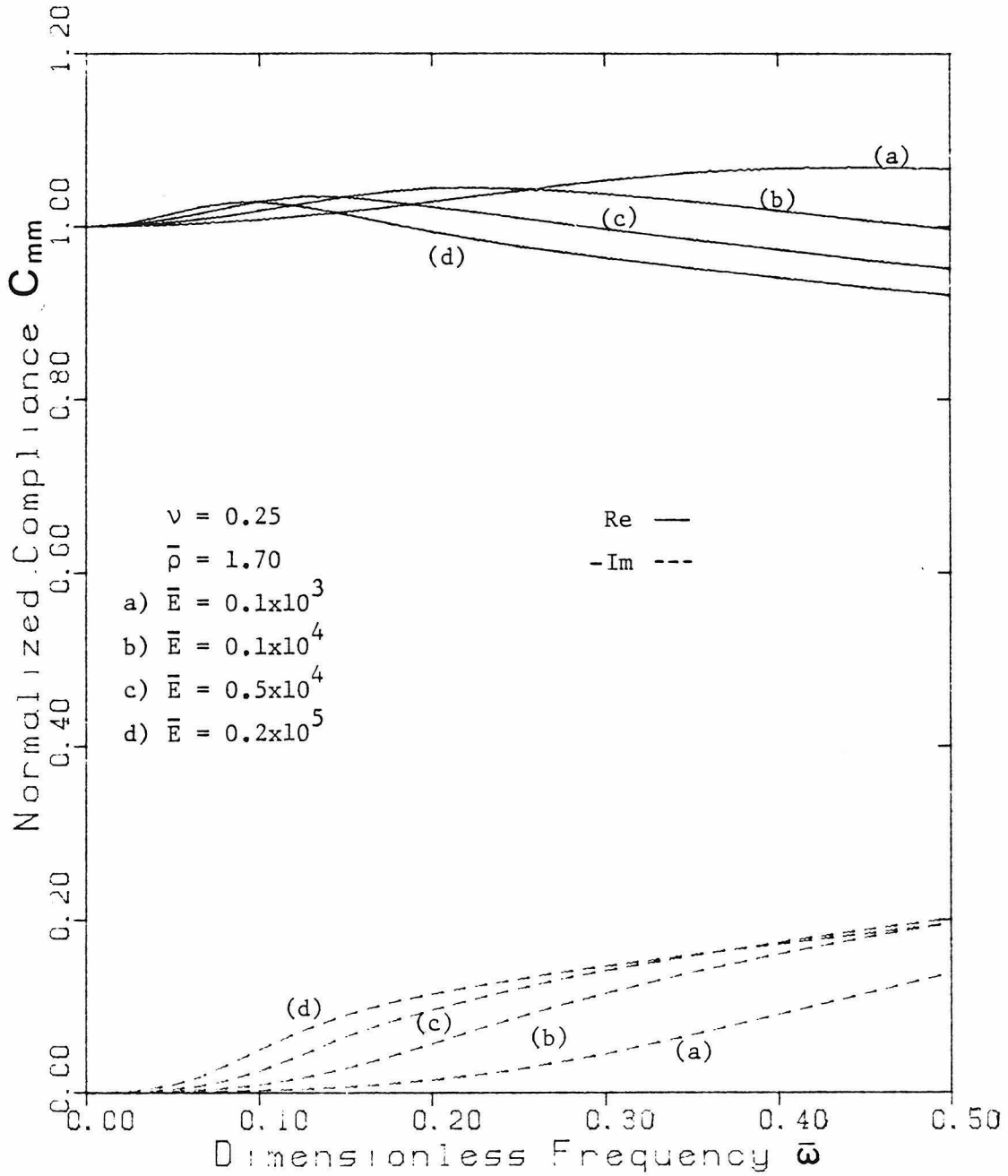
Figure 6.23 Normalized Compliance Function C_{mm} ($\bar{\ell}=50$)
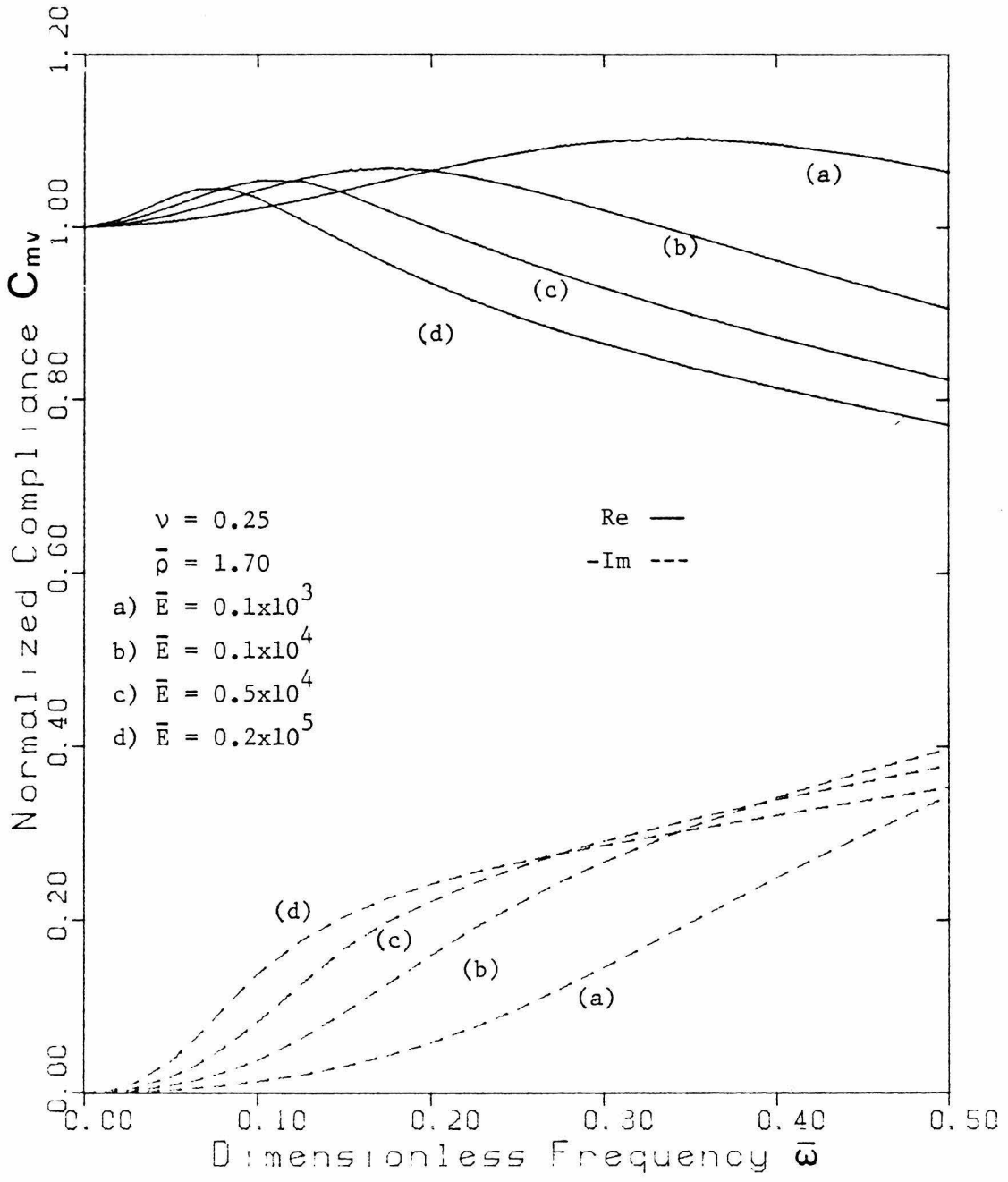
Figure 6.24 Normalized Compliance Function C_{mv} ($\bar{\ell}$=50)

earlier.

To provide further insight into the results, the normalized amplitudes of the compliances are plotted in Figures 6.25 to 6.27. From the figures, it is evident that there are indeed 'resonance frequencies' at which the responses are greater than their corresponding static values. Nevertheless, the size of amplification can be seen to be generally small although it does tend to increase with decreasing stiffness ratios.

Compliance functions are useful tools in studies of soil-structure interaction by both analytical and numerical approaches. Examples of their applications can be found in References [41], [15] and [9].
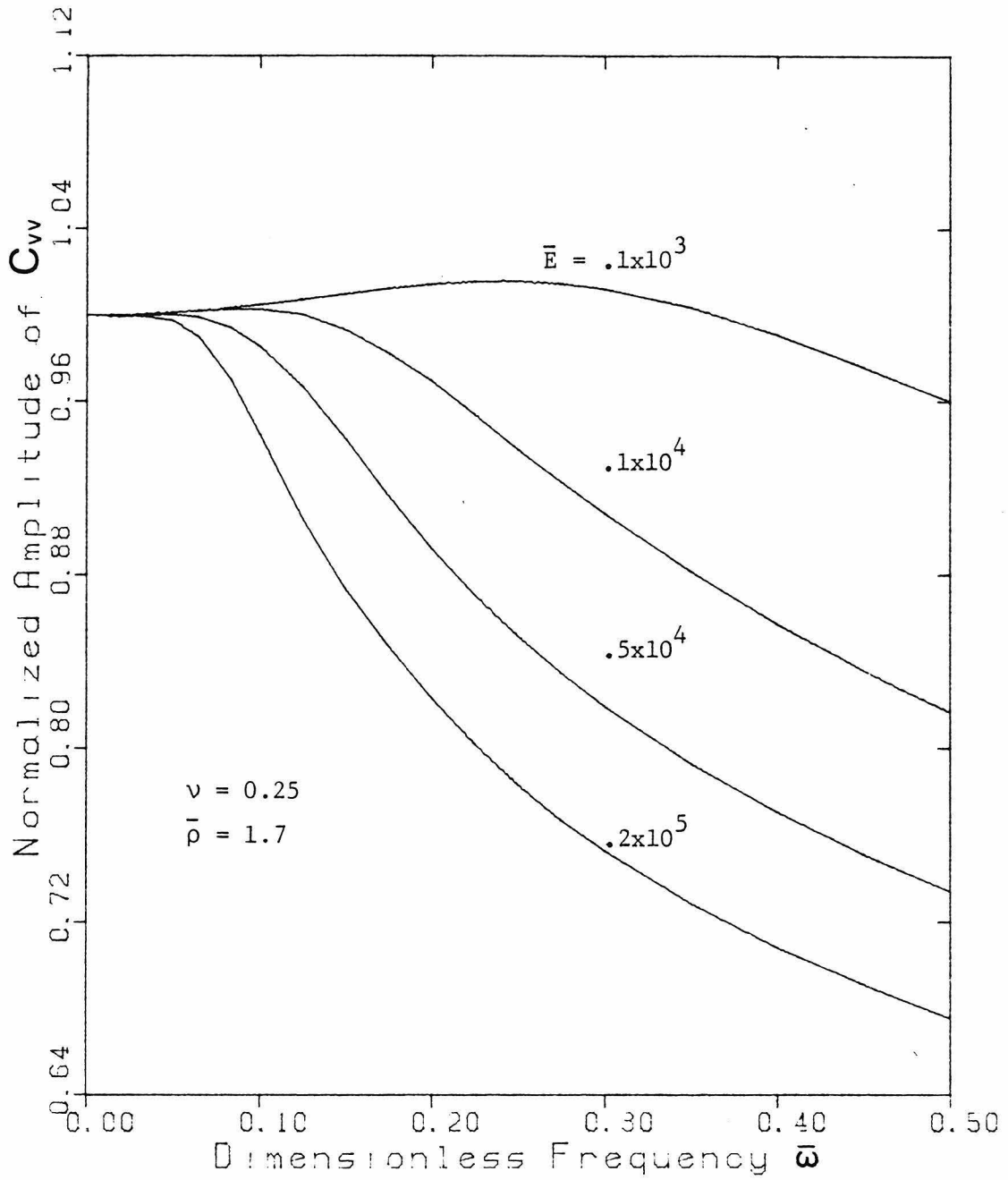
Figure 6.25   Normalized Amplitude of C_{vv} ($\bar{\ell}$=50)
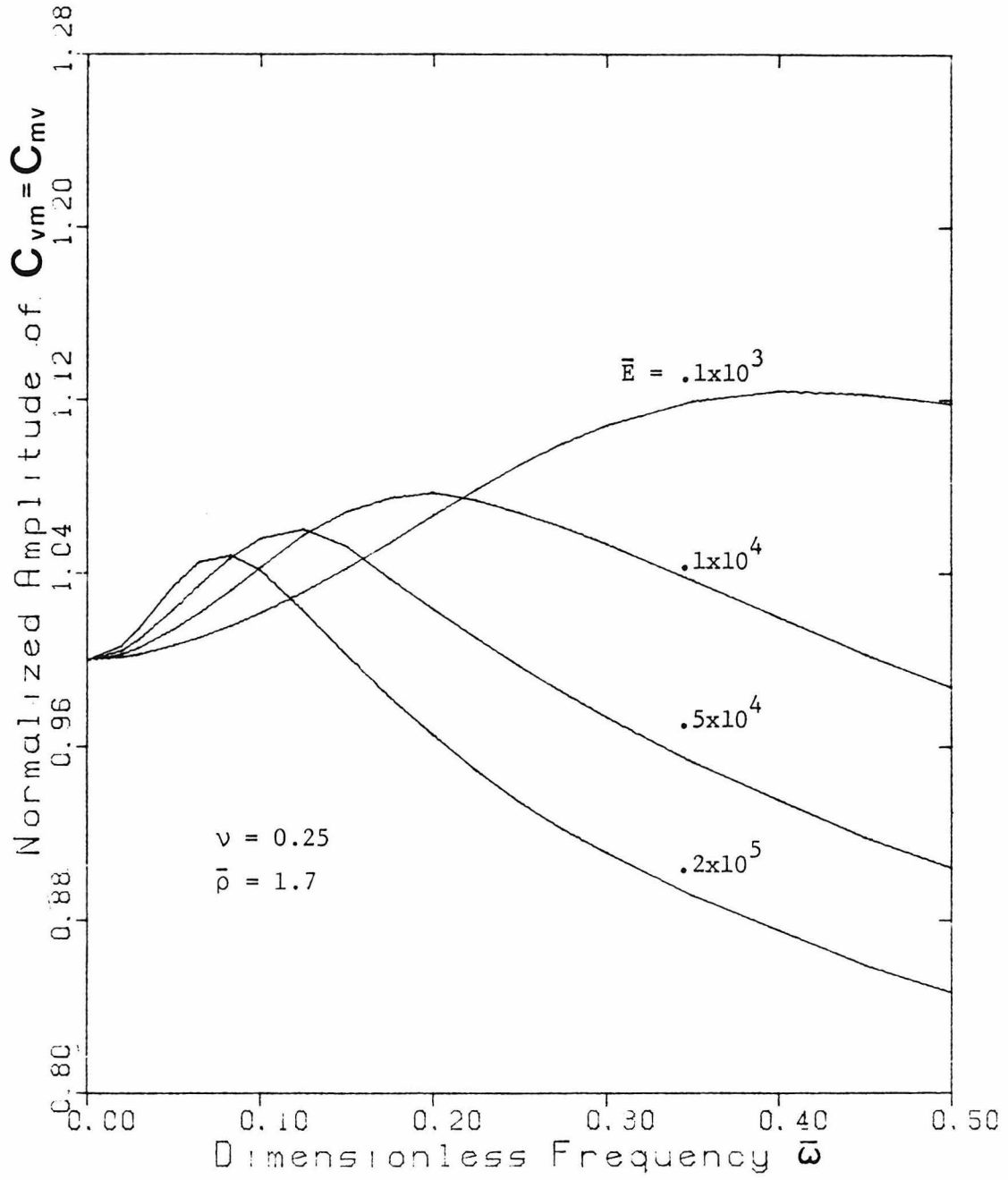
Figure 6.26 Normalized Amplitiude of C_{vm} & C_{mv} ($\bar{\ell}=50$)
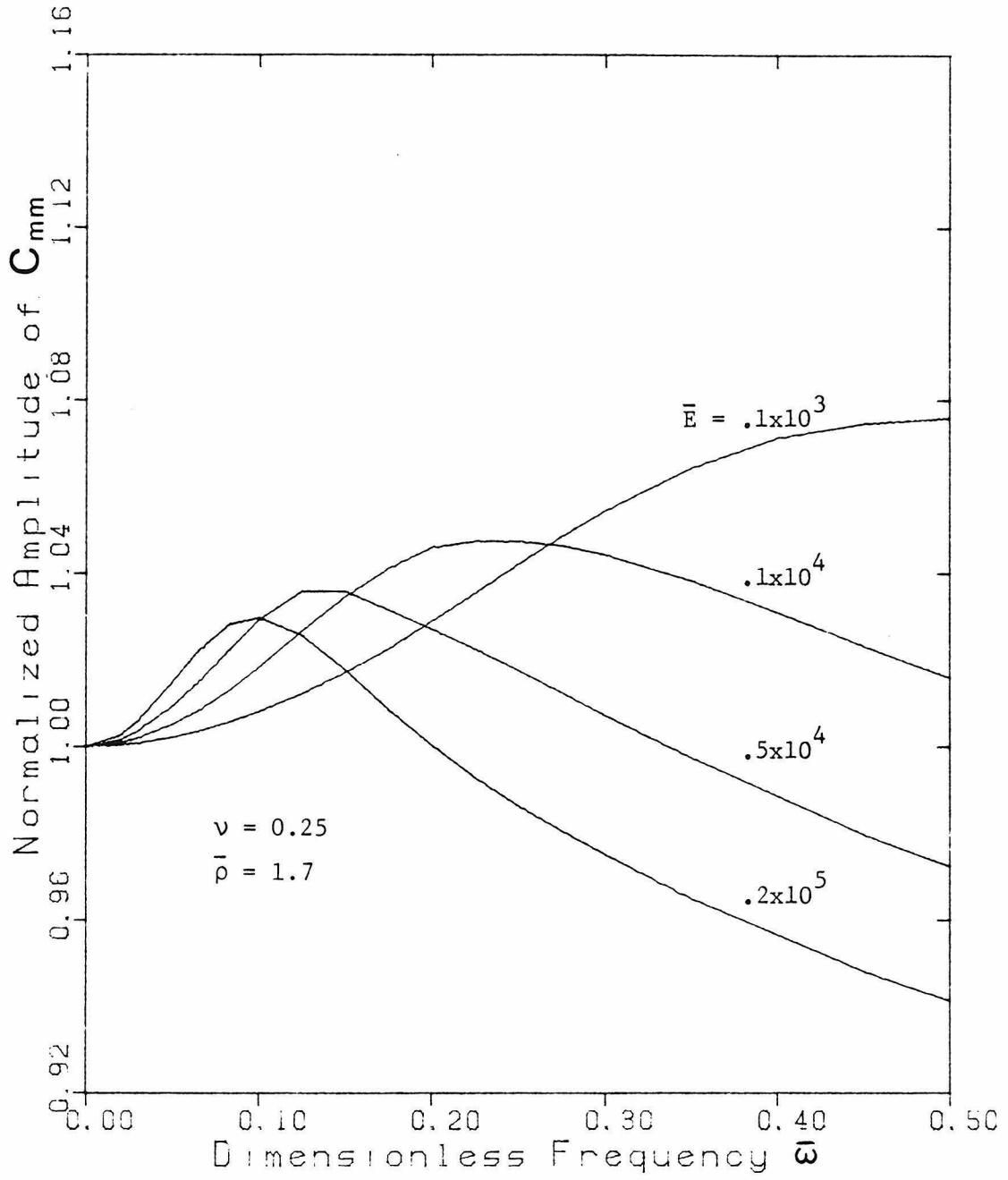
Figure 6.27 Normalized Amplitude of C_{mm} ($\bar{\ell}$=50)

CHAPTER VII

SUMMARY AND CONCLUSIONS

In this dissertation, the dynamic response of a partially embedded bar under transverse excitations was examined theoretically. For applications in soil-structure interaction, the problem serves well as a fundamental idealization for the dynamic analysis of piles or other embedded foundations whose flexibilities are not negligible. The investigation involved several relatively distinct phases of work which are summarized as follows:

I) **Mathematical Formulation**

A formulation was proposed whereby the bar was regarded essentially as a one-dimensional structure and the embedding half-space as a three-dimensional elastic contimuum. The finite lateral dimensions of the bar were accounted for by effecting its load transfer to the medium at any depth over an area which corresponds to the cross section of the bar. With the aid of several Green's functions, the interaction problem was reduced to a Fredholm integral equation of the second kind.

II) **Derivation of the Green's Function**

The Green's functions required in the proposed formulation are concerned with the response of an elastic half-space to a finite, distributed, buried source which acts in the lateral direction. A technique of solution for this class of three-dimensional asymmetric wave propagation problems was developed which utilizes displacement-potential representations and features, in particular, relatively simple

transformed stress and displacement potential relations. Specializing
the method to the problem under consideration, the required Green's
functions were derived as integral representations.

III) <u>Numerical Evaluation of the Green's Function</u>

The Green's functions are expressed in terms of several semi-
infinite Hankel-type integrals. Some of the integrals could be
evaluated in closed form but the rest, due to the involvement of the
Rayleigh function in their integrands, had to be evaluated numerically.
By the incorporation of asymptotic techniques, a numerical procedure was
developed which is free of the basic difficulties commonly encountered
in such problems. Error bounds for the method could be established
quite readily.

IV) <u>Development of a Numerical Scheme for the Integral Equation</u>

Not atypical in mechanics problems, the kernel function of the
governing Fredholm integral equation, which is composed of various
Green's functions, was found to be very localized in nature. In view of
this characteristic, numerical solution by the commonly employed
quadrature methods was considered as inefficient as very fine subdivi-
sions would be required to achieve accurate results. Without resorting
to complicated procedures, a simple numerical method containing the
essence of both the quadrature and collocation techniques was developed
and applied to the equation under consideration.

With the development described above, the dynamic interaction
problem was solved. Selected results were presented to illustrate vari-
ous basic features of the solution under lateral shear and moment

loading conditions. In general, the following observations can be made:

(1) Definite characteristic oscillations were found to exist in the solutions of the time-independent problem, contrary to the findings of some of the currently accepted numerical treatments.

(2) As the frequency of excitation increases, the oscillatory nature of the solution becomes more pronounced. The characteristic wavelength appears to be an increasing function of stiffness ratio and a decreasing function of frequency.

(3) The results demonstrate the existence of a limiting length beyond which further embedment of the bar does not alter the top response significantly. The limiting length is dependent, in addition to the bar/medium parameters, on the loading conditions.

(4) The response tends to decrease slightly when the mass of the bar is ignored; the difference in response, however, lies mainly in the 90°-out-of-phase component.

(5) The slope and deflection tend to decrease with increasing Poisson's ratio of the medium. The trend is, however, opposite for the bending moment.

(6) The lateral compliance matrix obtained from the solution shows strong dependence on $\bar{E}$ and $\bar{\omega}$. The variation of the compliance C_{vv} appears to be distinctly different from C_{vm} or C_{mm}.

(7) Despite the absence of large amplifications, distinct 'resonance' frequencies were observable in most of the compliance functions.

REFERENCES

[1] Achenbach, J.D., <u>Wave Propagation in Elastic Solids</u>, North-Holland
Publishing Company, Amsterdam, 1973.

[2] Anselone, P.M., <u>Collectively Compact Operator Approximation Theory
and Applications to Integral Equations</u>, Prentice-Hall, Inc., New
Jersey, 1971.

[3] Arnold, R.N., Bycroft, G.N. and Warburton, G.B., "Forced Vibra-
tions of a Body on an Infinite Elastic Solid," <u>J. Appl. Mech.</u>,
ASME, 22, pp. 391-400, 1955.

[4] Apsel, R.J. and Luco, J.E., "Torsional Response of a Rigid Embed-
ded Foundation," <u>J. Engrg. Mech. Div.</u>, ASCE, 102, EM6, pp. 957-
970, 1976.

[5] Atkinson, K.E., <u>A Survey of Numerical Methods for the Solution of
Fredholm Integral Equations of the Second Kind</u>, Soc. Indust. Appl.
Math., Philadelphia, Pennsylvania, 1976.

[6] Baker, C.T.H., <u>The Numerical Treatment of Integral Equations</u>,
Cambridge University Press, Oxford, England, 1977.

[7] Baranov, V.A., "On the Calculation of Excited Vibrations of an
Embedded Foundation," (in Russian), Voprosy Dynamiki i Prochnocti,
No. 14, Polytechnical Institute of Riga, pp. 195-209, 1967.

[8] Chao, C.C., "Dynamic Response of an Elastic Half-Space to Tangen-
tial Surface Loading," <u>J. Appl. Mech.</u>, ASME, 27, pp. 559-567,
1960.

[9] Chopra, A.K. and Gutierrez, J.A., "Earthquake Response Analysis of Multistory Buildings Including Foundation Interaction," Int. J. Earthq. Struct. Dyn., 3, pp. 65-77, 1974.

[10] Cohen, M., "Silent Boundary Methods for Transient Wave Analysis," Report EERL 80-09, Earthq. Engrg. Research Laboratory, California Institute of Technology, Pasadena, California, 1980.

[11] Dravinsky, M. and Thau, S.A., "Multiple Diffractions of Elastic Waves by a Rigid Rectangular Foundation: Plane-Strain Model," J. Applied Mech., ASME, 43, pp. 291-294, 1976.

[12] Eringen, A.C. and Suhubi, E.S., Elastodynamics Volume 2, Academic Press, New York, 1975.

[13] Ewing, W.M., Jardetsky, W.S. and Press, F., Elastic Waves in Layered Media, McGraw-Hill, New York, 1957.

[14] Fowler, G.F. and Sinclair, G.B., "The Longitudinal Harmonic Excitation of a Circular Bar Embedded in an Elastic Half-Space," Int. J. Solids Struct., 14, pp. 999-1012, 1978.

[15] Gazetas, G., "Analysis of Machine Foundation Vibrations: State of the Art," Soil. Dyn. Earthq. Engrg., 2, pp. 2-42, 1983.

[16] Gladwell, G.M.L., "Forced Tangential and Rotary Vibration of a Rigid Circular Disc on a Semi-Infinite Solid," Int. J. Engrg. Sci., 6, pp. 591-607, 1968.

[17] Goldberg, M.A., Solution Methods for Integral Equations; Theory and Applications, Plenum Press, New York, 1978.

[18] Harding, J.W. and Sneddon, I.N., "The Elastic Stresses Produced by the Indentation of the Plane Surface of a Semi-Infinite Elastic Solid by a Rigid Punch," Prod. Cambridge Phil. Soc., 41, pp. 16-26, 1945.

[19] Israel, M. and Kovach, R.L., "Near-Field Motions from a Propagating Strike-Slip Fault in an Elastic Half-Space," Bull. Seism. Soc. Am., 67, pp. 977-994, 1977.

[20] Johnson, L.R., "Green's Function for Lamb's Problem," Geophys. J., 37, pp. 99-131, 1974.

[21] Lamb, H., "On the Propagation of Tremors over the Surface of an Elastic Solid," Phil. Trans. Royal Soc. London, Ser. A, 203, pp. 1-42, 1904.

[22] Lee, V.M. and Trifunac, M.D., "Response of Tunnels to SH-Waves," J. Engrg. Mech. Div., ASCE, 105, EM4, pp. 643-659, 1979.

[23] Longman, I.M., "On the Numerical Evaluation of Cauchy Principal Values of Integrals," Math. Tables and Other Aids to Computation, Vol. 12, pp. 205-207, 1958.

[24] Luco, J.E., "Dynamic Interaction of a Shear Wall with Soil," J. Engrg. Mech. Div., ASCE, 95, EM2, pp. 333-346, 1969.

[25] Luco, J.E. and Westmann, R.A., "Dynamic Response of a Rigid Footing Bonded to an Elastic Half Space," J. Appl. Mech., ASME, 39, pp. 527-534, 1972.

[26] Luco, J.E., "Torsional Response of Structures for SH Wave: the Case of Hemispherical Foundations," Bull. Seism. Soc. Am., 66, 1, pp. 109-124, 1976.

[27] Luco, J.E., "Linear Soil-Structure Interaction: a Review," *Earthq. Ground Motion and Its Effects on Structures*, AMD-Vol. 53, ASME, 1982.

[28] Maiti, N.C. and Mitra, M. "Wave Propagation from Extended Asymmetric Surface Sources in an Elastic Half-Space," *Bull. Seism. Soc. Am.*, 69, pp. 713-735, 1979.

[29] Miklowitz, J., *The Theory of Elastic Waves and Waveguides*, North-Holland Publishing Company, Amsterdam, 1978.

[30] Morse, P.M. and Feshbach, H., *Methods of Theoretical Physics Part I and II*, McGraw-Hill, New York, pp. 1762-1767, 1953.

[31] Muki, R., "Asymmetric Problems of the Theory of Elasticity for a Semi-Infinite Solid and a Thick Plate," *Progress in Solid Mech.*, Vol. 1, North-Holland Publishing Company, Amsterdam, 1960.

[32] Muki, R. and Sternberg, E., "On the Diffusion of Load from a Transverse Tension Bar into a Semi-Infinite Elastic Sheet," *J. Appl. Mech.*, ASME, 35, pp. 737-746, 1968.

[33] Muki, R. and Sternberg, E., "On the Diffusion of an Axial Load from an Infinite Cylindrical Bar Embedded in an Elastic Medium," *Int. J. Solids Struct.*, 5, pp. 587-605, 1969.

[34] Muki, R. and Sternberg, E., "Elastostatic Load-Transfer to a Half-Space from a Partially Embedded Axially Loaded Rod," *Int. J. Solids Struct.*, pp. 69-90, 1970.

[35] Novak, M. and Nogami, T., "Soil-Pile Interaction in Horizontal Vibration," *Earthq. Engrg. Struct. Dyn.*, 5, pp. 263-281, 1977.

[36] Novak, M., "Vertical Vibration of Floating Piles," <u>J. Engrg. Mech. Div.</u> , ASCE, 103, EM1, pp. 153-167, 1977.

[37] Novak, M. and Beredugo, Y.O., "Vertical Vibration of Embedded Footings," <u>Soil Mech. Fdn. Div.</u>, ASCE, 98, SM12, pp. 1291-1310, 1972.

[38] Pekeris, C.L. and Longman, I., "The Motion of the Surface of a Uniform Elastic Half-Space Produced by a Buried Torque Pulse," <u>Geophys. J.</u>, 1, pp. 146-153, 1955.

[39] Poulos, H.G., "Behavior of Lateral Loaded Piles: I-Single Piles," <u>J. Soil Mech. Fdn. Div.</u>, ASCE, 97, SM5, pp. 711-731, 1971.

[40] Poulos, H.G. and Davis, E.H., <u>Pile Foundation Analysis and Design</u>, John Wiley and Sons, New York, pp. 188, 1980.

[41] Richart, F.E., Hall, J.R. Jr. and Woods, R.D., <u>Vibrations of Soils and Foundations</u>, Prentice-Hall, Inc., New Jersey, 1970.

[42] Tajimi, H., "Dynamic Analysis of a Structure Embedded in an Elastic Stratum," <u>Proc. 4th World Conf. Earthq. Engrg.</u>, Santiago, Chile, 1969.

[43] Thau, S.A., "Motion of a Finite Strip in an Elastic Half Space Subjected to Blast Wave Loading," <u>Int. J. Solids Struct.</u>, 7, pp. 193-211, 1971.

[44] Thau, S.A. and Umek, A., "Transient Response of a Buried Foundation to Anti-Plane Shear Waves," <u>J. Appl. Mech.</u>, ASME, 40, pp. 1041-1066, 1973.

[45] Thau, S.A. and Umek, A., "Coupled Rocking and Translating Vibrations of Buried Foundations," J. Appl. Mech., ASME, 41, pp. 697-702, 1974.

[46] Thiruvenkatachar, V.R., "Stress Waves Produced in a Semi-Infinite Elastic Solid by Impulse Applied over a Circular Area of the Plane Face," Proc. Congr. Theoret. Appl. Mech., India, 1st, Kharagpur, pp. 181-188, 1955.

[47] Thomson, W.T. and Kobori, T., "Dynamical Compliance of Rectangular Foundations on an Elastic Half-Space," J. Appl. Mech., ASME, 30, pp. 579-584, 1963.

[48] Wolf, J.P. and Darbre, G.R., "Dynamic-Stiffness of Embedded and Pile Foundations by Indirect Boundary-Element Method," Trans. 7th Inst. Mech. in Reactor Tech., Chicago, Illinois, 1983.

[49] Wong, H.L., "Dynamic Soil-Structure Interaction," Report EERL 75-01, Earthq. Engrg. Research Lab, California Institute of Technology, Pasadena, California, 1975.

[50] Wong, H.L. and Luco, J.E., "Dynamic Response of Rigid Foundations of Arbitrary Shape," Earthq. Engrg. Struct. Dyn., 4, pp. 579-587, 1976.

[51] Wong, H.L. and Trifunac, M.D., "Interaction of a Shear Wall with the Soil for Incident Plane SH Waves: Elliptical Rigid Foundation," Bull. Seism. Soc. Am., 64, pp. 1825-1842, 1974.